Master of Science Thesis

Sustainable Microgrid for charging electric vehicles from on-road contactless power transfer systems

Theodora-Elli Stamati

Supervisor: Dr. Ir. P. Bauer

November 2012

Sustainable Microgrid for charging electric vehicles from on-road contactless power transfer systems

by

Theodora-Elli Stamati

Thesis submitted to the faculty of Electrical Engineering, Mathematics and Computer Science (EEMCS) group of Electrical Power Processing (EPP) in partial fulfillment of the requirements for the degree of

Master of Science
in
Sustainable Energy Technology

Thesis committee:
Prof. Dr. Eng. J.A. Ferreira
Dr. ir. P. Bauer
Dr. ir. M. Gibescu

November 2012
Delft, the Netherlands

Faculty of Electrical Engineering, Mathematics and Computer Science (EEMCS)
Electrical Power Engineering (EPE) department
Electrical Power Processing (EPP) group

Visiting address
Mekelweg 4
2628 CD Delft

Postal address
P.O. Box 5031
2600 GA Delft
The Netherlands
http://www.ewi.tudelft.nl

Author
Theodora-Elli Stamati
Student number 4120205
E-mail T.E.Stamati@student.tudelft.nl

Abstract

A sustainable microgrid for supplying power to electric vehicles (EVs) is investigated in this thesis. The energy produced by the microgrid would be directly transferred to the electric vehicles via on-road charging systems. The proposed sustainable microgrid is located on the roadside and consists of wind turbines, solar panels and a stationary storage system. The optimum sizing, the topology and the power management are discussed. Both the grid-connected and the stand-alone options are investigated.

The on-road chargers consist of Contactless Power Transfer (CPT) systems for powering electric vehicles without any physical interconnection. The concept of CPT systems is similar to an air-cored transformer, where the primary winding is installed on the road and the secondary winding below the vehicle's chassis. The implementation of such on-road charging systems for EV driving range extension and EV battery size decrease is also investigated within this thesis.

Acknowledgements

This master thesis was completed in the Electrical Power Processing group of the Electrical Power Engineering department as a part of the two years MSc program in 'Sustainable Energy Technology'.

Through my acknowledgements, I would like first to thank my supervisor, Pavol Bauer, for giving me the opportunity to work on this topic and for his guidance throughout this project.

I would like to thank everyone in the student room (JK, Prasanth, Gyorgy, Behtzua, Vangelis, Stijn) for sharing our thoughts and concerns these past few months. Sometimes, just to see them work hard was a great encouragement! I want also to acknowledge Arne Kaas who helped me in the beginning of my thesis by sharing his views, his ideas and his model.

I would like to take the opportunity to deeply thank Kostas, Angeliki [2] and Diana for supporting me and cheering me up when needed, during my work on this project. My life in Delft is full of nice memories and they are a great part of them.

Of course, I would like to thank my parents and my sister for always being there for me. They are supporting and motivating me even when they are miles away!

Contents

List of Figures

List of Tables

List of Abbreviations

CPT system	Contactless Power Transfer system
EV	Electric Vehicle
RES	Renewable Energy System
PV system	Photovoltaic system
MPPT	Maximum Power Point Tracking
WT	Wind Turbine
BAT	Battery storage system
SoC	State of Charge of Battery
DoD	Depth of Discharge of Battery
p.u.	per unit
LCOE	Levelized Cost of Electricity
LOS	Level Of Service (Highways)

Introduction

The future in energy production is renewable energy sources. There is an effort worldwide for the implementation of environmental friendly energy sources, such as solar and wind power. The trend in transport nowadays is a transition from petrol-fueled mobility to electric mobility. A combination of the two aforementioned trends could lead to an electric mobility system powered by green energy. This could be realized by installing wind turbines and photovoltaic systems along the roadside and use the produced energy to power/charge the electric vehicles (EVs) passing-by. The power could be transferred to the EVs via Contactless Power Transfer systems. This concept introduces a real sustainable solution which minimizes the CO_2 footprint of road transport.

The main drawbacks that electric vehicles have in comparison with conventional cars are the limited driving range and the high cost, which are both related to the technology and the specifications of today's batteries. Batteries used in electric vehicles are expensive, have a limited capacity, a short lifetime and a high cost. With an extensive implementation of on-road charging systems based on Contactless Power Transfer, a driving range extension and/or a battery size decrease is possible. Therefore, such systems provide a way to overcome the aforementioned bottlenecks of electric mobility.

In this thesis, a sustainable power system for charging EVs while driving will be investigated. In the beginning, a discussion on the on-road charging systems, as far as the technology and their implementation will be conducted. Then, the total power demand of the EVs passing-by would be estimated on which the sizing of the microgrid will be based on. A further discussion on the microgrid and its components will be included and conclusions will be drawn concerning the sizing, the topology and the power management of this sustainable microgrid.

More specifically, in Chapter 1 an introduction to the theory of contactless power transfer will be presented. First, the air-cored transformer will be described and next the implementation of such transformers on EV charging applications will be explained. The two main ways of using CPT systems for powering electric vehicles, while the EV is driving or on idle state, will be compared. Some design considerations of the system specifications are listed and analyzed.

The implementation of CPT systems for charging-while-driving becomes more efficient if it is implemented on roads with heavy traffic. Therefore, in Chapter 2 an overview of the road system infrastructure and the Dutch driving pattern will be presented. In this way the extensive implementation of CPT systems in the Netherlands can be investigated.

In Chapter 3, the implementation of CPT systems on highways will be studied. First, the model used to simulate an electric vehicle driving on a highway with CPT system installed will be presented. Then, from the simulation results, conclusions can be drawn on the specifications of the on-road charging system depending on the EV driving range and the EV battery size.

In Chapter 4, the microgrid consisting of solar, wind energy and storage, which will supply power to the electric vehicles via the contactless power transfer system, will be studied. A brief overview of the existing microgrid systems will be presented, as well as some information about different topologies. The data for the power demand of the electric vehicle, the solar irradiance and the wind speed will be presented. A discussion on the operation, the power and the cost of each component will follow. The main models for finding the optimum sizing of the microgrid will be introduced.

As mentioned before, a microgrid can be stand-alone or grid-connected. In Chapter 5, the stand-alone operation mode will be studied, in order to investigate the optimum configuration and the optimum sizing of the system as far as the wind power, the solar power and the storage are concerned. The power management strategy of the stand-alone operation will be presented and the results will be discussed.

In Chapter 6, the grid-connected microgrid will be investigated. In case a grid connection is established, the microgrid components might decrease in size. The excess renewable power produced could be also sold to the grid, providing revenues to the system.

Finally, in Chapter 7 the conclusions derived from the previous analysis, concerning the on-road CPT systems powered by sustainable energy sources will be discussed. The main results that have been found will be outlined and in Chapter 8 some recommendations for future work will be mentioned.

1 Contactless Power Transfer System

In this chapter an introduction to the theory of contactless power transfer will be outlined. First, the air-cored transformer will be described and next the implementation of such transformers for charging electric vehicles will be discussed. The two main ways of using CPT systems for power electric vehicles - while driving or being on idle state- will be compared. Some design considerations of the system specifications are also listed and analyzed.

1.1 Contactless Power Transformer

A Contactless Power Transfer System (CPT) refers to a system where power can be transferred magnetically with no physical contact over an air gap. The system consists basically of two windings, the primary and the secondary. The secondary is also referred to as the pick-up coil. The principle of operation can be compared to that of an air-cored transformer; however, the main difference is that the transformer of the CPT system operates at high frequencies with resonant mode coupling [1], [2], [3].

Just like an iron-cored transformer, the circuit consists of leakage inductances of the primary and the secondary windings, as well as the mutual inductance. The main difference in this case is for the CPT transformer the leakage inductances are much larger and greater than the mutual inductance. This is due to the large air gap between the two windings. As a result, the overall efficiency of the CPT transformer is much lower.

The schematic diagram of the CPT transformer is represented in the figure below.

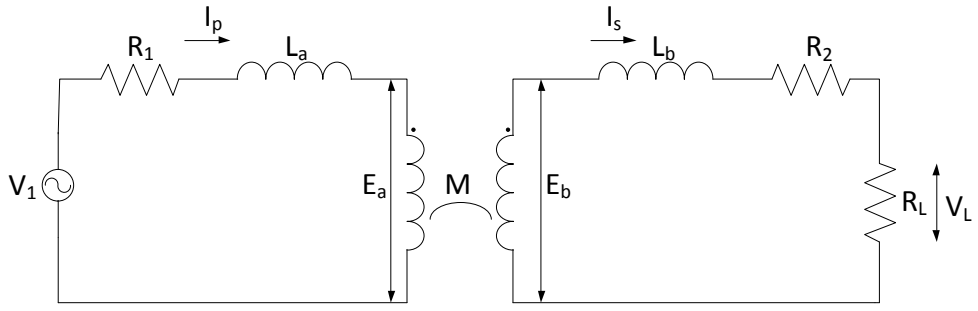

Figure 1.1 - Schematic diagram of CPT transformer [4]

If the primary winding is excited and the two coils are magnetically coupled, according to the theory of coupled inductors, the self-inductance of the primary winding results in a mutual inductance and a series inductance, as well as the secondary self-inductance results in a series inductance and a mutual inductance. So, the equivalent circuit of the CPT transformer is as shown below, where R_L is the load resistance, M is the mutual inductance, R_1 and L_a is the series resistance and inductance of the primary and R_2 and L_b is the series resistance and inductance of the secondary.

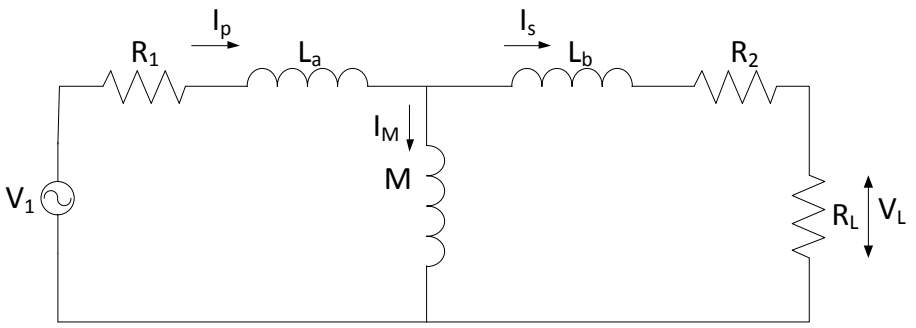

Figure 1.2 - Equivalent circuit of CPT transformer [4]

As observed in literature, the efficiency of such a transformer depends on the parameters of the primary and the secondary winding, but also on the load and the operating frequency. We can see that the fact for iron-cored transformers that the voltage and current in the primary and secondary depend only on the number of turns of these windings is not valid in this case.

In order to transfer power efficiently the operating frequency should be within the VLF range (3kHz-30kHz) or the LF range (30kHz-300kHz). The efficiency depends also on the load and the system specifications. At very high frequencies (higher that the resonant frequency) the efficiency may become independent of the load. On the other hand, at high frequencies the skin effect becomes significant and one way to deal with it is by using Litz wire for the windings. The proposed operating frequency in [4] is 100 kHz.

Another way to increase the efficiency of a CPT system is to reduce the value of the leakage inductances by compensating them with capacitances [1], [2]. Several configurations of parallel or series compensation have been investigated in literature, where various advantages and disadvantages have been mentioned for these techniques. The efficiency that can be achieved from each technique depends on the level of operating frequency, voltage and current.

1.2 Contactless Power Transfer for charging electric vehicles

Charging the battery of the electric vehicles is done traditionally by conductive charging. During conductive charging the car should be connected to the charging station. The charging time depends on the charging level of the particular station. The different modes of conductive charging are:

- Slow charging (1-phase AC power of 3.3 kW, 230 V, 16 A)
- Semi-fast charging (AC power of 7 to 22 kW, 1-phase 32A outlet or a 3-phase 16A outlet)
- Fast-charging (DC power of about 50kW)

It is known that to achieve a full charge at home a charging time of about 8 hours is needed. However, there is also the possibility of fast charging which takes less than one hour, but requires special infrastructure and the high charging current is harmful for the battery.

Electric vehicles can be charged also via Contactless Power Transfer System, if they have pick-up coils installed below the chassis and are aligned with a primary winding connected to a power source. The two windings form the CPT transformer described previously.

One advantage of this type of charging is that it is automated, meaning that in this case the user does not need to manually start the charging process. Apart from convenience, also the risk to the user is reduced especially during wet and damp conditions. In addition, CPT systems have no movable parts and require low maintenance.

Contactless power transfer is possible when the car is idle or even when the car is on the move. This creates another major advantage, as in this case the car can be charged while in use, increasing the driving range. This could be a solution to the long charging time of conductive charging which causes great inconvenience to EV users.

CPT systems can be installed at private areas (e.g. parking areas) or under the road at traffic lights, if the system is for cars being on idle. For this case, the system consists of a primary coil installed under the ground which has size more or less comparable with a car and the secondary pick-up coil, which is installed at the lower part of the car. When these two coils are aligned, power can be transferred from the primary to the secondary coil.

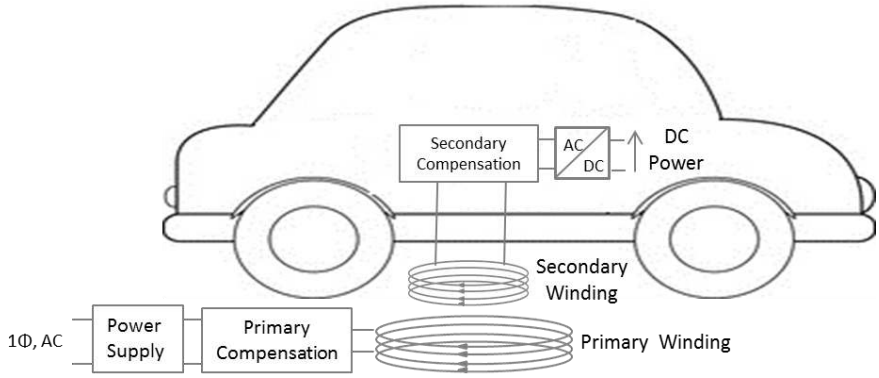

Figure 1.3 - CPT system for charging while EV is on idle

The main concept remains the same also for charging the car while-driving. However, in this case the primary coils that will be installed over the road should be longer and much more in number, as the car will be charging only as long as it is on top of one of the primary coils.

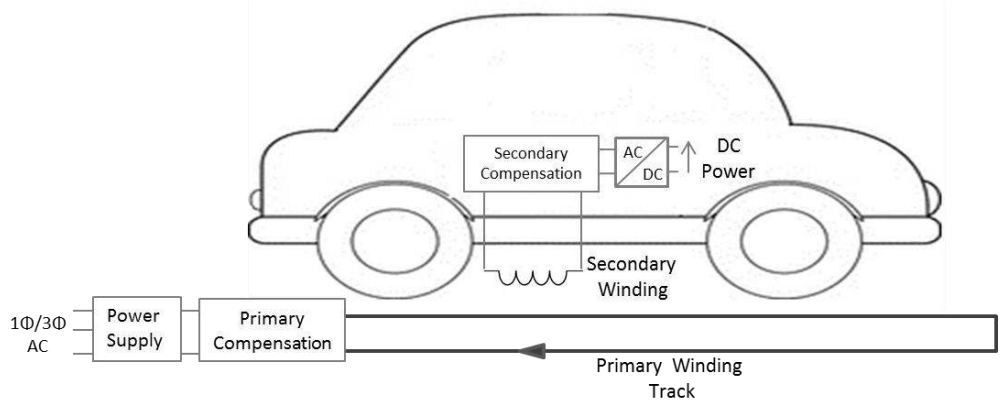

Figure 1.4 - CPT system for charging-while-driving

In case of an extensive implementation of CPT systems, for example at traffic lights in the city centers or at major roadway interconnections, a range extension and/or a decrease of the battery size may be possible [5]. This means that the most significant drawbacks of electric mobility, the limited driving range, the long charging time and the high cost, can be overcome.

1.3 Structure of electric vehicle with CPT system

Today's electric vehicles consist mainly of an energy source system to provide the input power, an electric motor which converts the electric power to mechanical power sent to the wheels and the motor controller which controls the power supplied to the motor and hence the speed [6]. The accelerator and the brakes provide the basic input signals to the controller, which gives the correct control signals to the power converters in order to properly regulate the power between the energy source and the motor. The energy source system consists mainly of the battery, an energy management unit and a charging unit. The energy management unit controls the power converters in order to regulate the power flow e.g. during regenerative braking process. The charging unit is used in order to safely charge the battery. A simplified block diagram of the internal structure of an electric vehicle can be seen below.

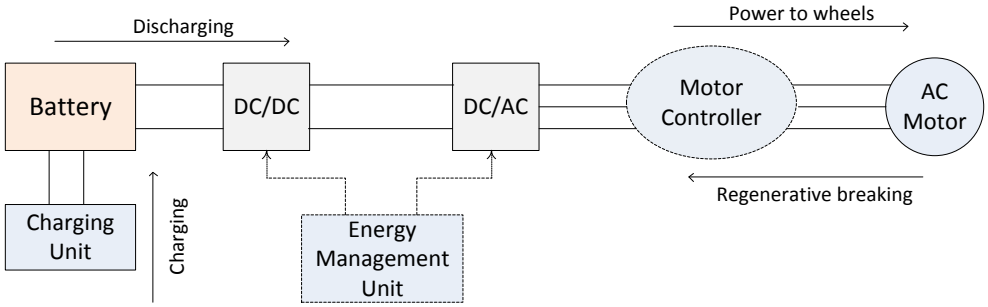

Figure 1.5 - Internal structure of Electric Vehicle

When Contactless Power Transfer system is installed in the electric vehicle, additional power is induced to the system that can supply the motor or/and to charge the battery. As a result, additional control is required in order to control the power flow from the CPT system as well. The block diagram is now changed, as depicted in Figure 1.6. The different power flows within the electric vehicle can be seen in the figure.

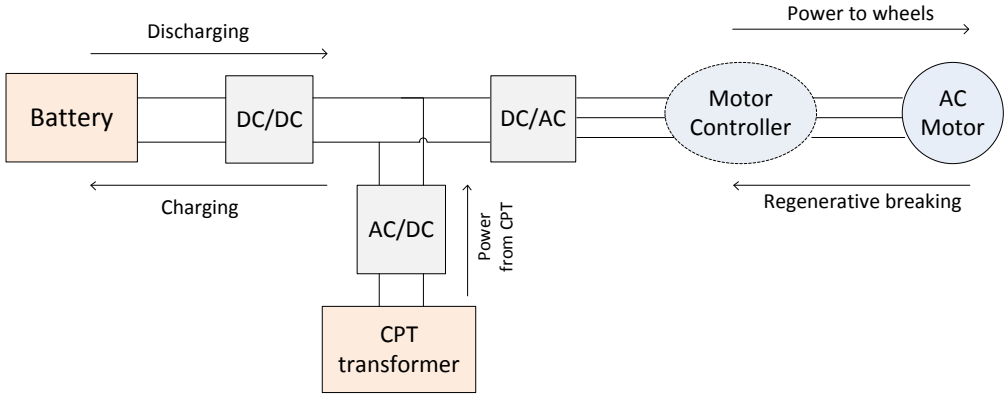

Figure 1.6 - Internal structure of Electric Vehicle with CPT system

When the power of the CPT system is consumed directly by the motor and not stored in the battery, the charge/discharge process is omitted. In this way performance of the battery can increase. Deep charging and discharging of the battery, which decreases its life time, occur less often. In order to deliver the required power at all times with an acceptable delay by the consumers, the response of the system should be fast enough.

1.4 Contactless Power Transfer system for charging while driving

The CPT system for charging while driving consists of long primary windings installed under the road and secondary pick-up windings, which are installed on the chassis of each electric vehicle. The primary windings are installed in segments, meaning that some parts of the road are covered with windings and some not.

The length of the CPT system can be expressed as the percentage (%) of the road covered with primary windings. All these primary coils can be distributed over the road in many ways. The primary coils, installed one next to each other, create a CPT segment. The length of the CPT segment can be varied and the distance in between the segments can vary as well [5]. As, can be seen there is a great flexibility of how a CPT system can be designed.

For example, one case could be that a road of 30km is covered by 20% by CPT system. These 6 km of primary coils can be distributed in many ways. In the figure below, we can see some alternatives of the way the CPT segments are distributed over the road.

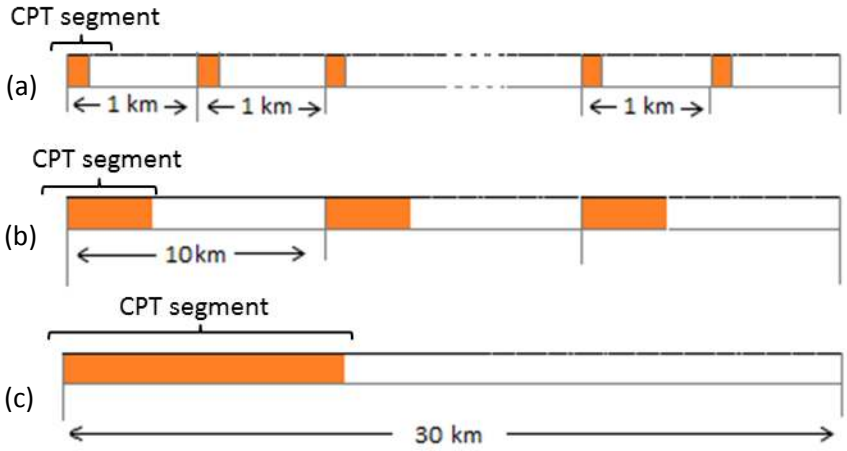

Figure 1.7 - Example of distribution of CPT segments over the road

1.4.1 CPT Segment

To go more in depth, every CPT segment consists of one, two or multiple primary coils placed adjacent to each other. The several structures of the CPT segments are to be presented now. The structure of the CPT segment actually refers to length and the number of the primary coils each segment consists of.

One possible structure is a CPT system consisting of small coils placed one next to another (see

Figure **1.8** - a). The coils are small enough so that only one car would be driving on top of this segment at every moment of time.

The other structure consists of longer primary coils, so there are multiple cars above this segment at every moment of time, like in

Figure **1.8** – b, c, d. All the cars driving on top of a primary winding, share equally the total power provided from this winding [7].

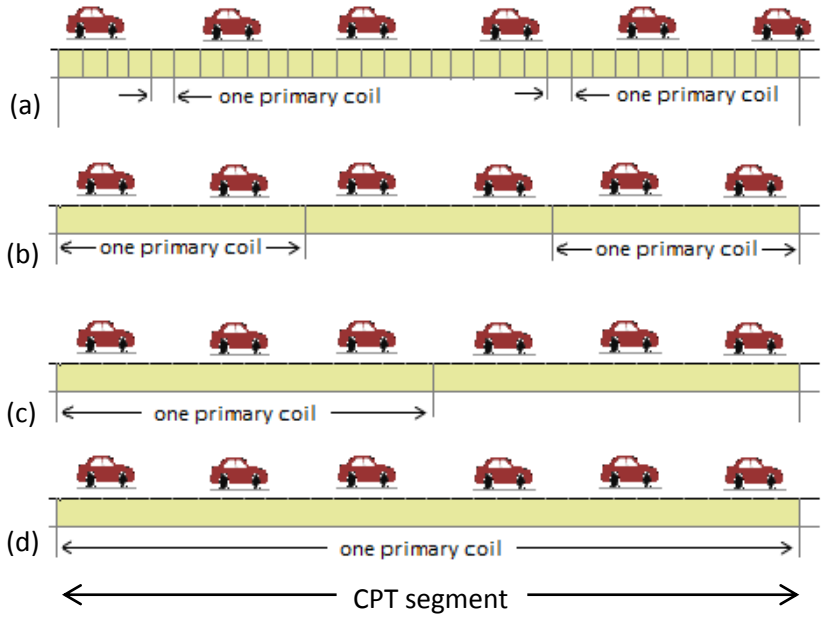

Figure 1.8 - CPT segments with varying number of primary coils

1.4.2 Energy transferred by CPT system

The energy that is transferred to the vehicle from the CPT system is proportional to the time the vehicle is on top of it. This time integral is the speed of the car divided by the length of the CPT system. Therefore, the energy transferred depends greatly on the speed of the car and on the length of the road that is covered with CPT system. In order to have more energy transferred, longer parts of the road could be covered with CPT or driving on smaller speed may be an option.

$$Speed = \frac{length}{time} \Rightarrow time = \frac{length}{speed}$$

Another parameter of the CPT system is the power transfer capability. In literature it is stated that a CPT system can transfer from few watts to some hundred kilowatts. The power transferred per EV can be considered smaller up to 50 kW, as this is also the maximum charging power of DC fast chargers.

Knowing that energy is the product of power and time, keeping in mind that the charging time is proportional to the length of the CPT system, we conclude that the two parameters that affect the total energy transferred are the power of the CPT system and the length of the CPT system. Here, we assume

than the driver is not willing to change its driving behavior and therefore the speed of the car cannot be affected.

$$Energy_{CPT} = Power_{CPT} \cdot \Delta t = Power_{CPT}\,[kW] \cdot \frac{length\ of\ CPT\ system\ [km]}{speed\ of\ car\ \left[\frac{km}{h}\right]}$$

1.5 Considerations on the parameters of the CPT system

In order to design the CPT system 3 parameters have to be considered, the operating frequency, the power transfer capability of the primary windings and the length of the primary windings. Increasing or decreasing the values of each parameter has some advantages as well as disadvantages. In this chapter all these considerations are discussed and in the end a summary is presented.

1.5.1 Frequency, Power and Length of the primary windings

The operating frequency of the CPT system affects

- The power transfer efficiency of the CPT transformer
- The efficiency of the inverter supply
- The maximum length of the winding due to electromagnetic reflection (to be analyzed further)

The length of the primary windings affects

- The number of inverters required by the total system
- The maximum power capability of each winding, as every winding should provide the required power to all the cars driving on top of it
- The inductance of the winding and as a result the capacitance needed for resonant mode coupling

The power capability of the primary windings affects

- The resistive losses of the system
- The length of the winding, as every winding should provide the required power to all the cars driving on top of it

Every CPT transformer requires an inverter to create the appropriate high frequency AC current which is fed to the primary winding. As a result, the more primary windings are installed, the more inverters are required. These inverters add a significant cost to the overall system, so this is one main reason why installing longer primaries is a preferable structure than installing many small ones.

As far as the power transfer capability of the system is concerned, there is an upper limit to some hundred kilowatts. Most of the tested systems are just a few kilowatts, although it is stated in literature that transferring hundred kilowatts systems are possible. Therefore, there is a limit on the number of vehicles that one primary winding can power and as a result a limit for the length of the primary winding exists, due to the limit of the total power capability.

An example of total power capacity of the primary for different lengths of primary windings will be shown next, in order to understand this dependence.

Taken that cars are driving with a speed of 80km/h and the distance between each car can be taken as 2-3 seconds (44-66m), overall about 60 meters correspond to each car. Knowing the length of the primary, the number of cars per segment can be estimated. Then, the total power of the segment can be calculated for the various possible values of the power transferred to every car.

$$Power\ of\ primary = (\#\ cars\ on\ primary) \cdot (power\ to\ each\ car)$$

Table 1.1 - Total power capacity of CPT primary winding [kW] depending on length [m]

Power transferred to each car	Length of primary winding			
	100m	**200m**	**500m**	**1000m**
10 kW	17 kW	33 kW	83 kW	165 kW
20 kW	33 kW	66 kW	165 kW	330 kW
30 kW	50 kW	99 kW	248 kW	495 kW
40 kW	66 kW	132 kW	330 kW	661 kW
50 kW	83 kW	165 kW	413 kW	826 kW

We can see that taken into account the threshold of transferring until few hundreds of kW per primary winding, then primaries of 1km long are possible only for transferring few kW to every car. For transferring 20-30kW, primary windings up to 500 meters long are realistic.

There is also a maximum upper limit as far as the length of the primary winding is concerned that comes from the theory of the 'lumped element model', according which the length of an electric circuit should be of a lower order of magnitude compared to the circuit's operating wavelength.

$$\lambda = \frac{c}{f}$$

Where,

λ, is the wavelength
$c = 3 \cdot 10^8 m/s$, the speed of light
f, the operating frequency of the CPT system

The reason for this is that in case the length is comparable to the wavelength, the electromagnetic wave reflection will become significant, affecting greatly the power waveform of the CPT system. In most studies electromagnetic reflection has been ignored and the functionality of the system has been proven only under these conditions. As a result, in this thesis the same assumptions were taken and so this condition has to be met.

If L is the length of the CPT primary winding, then

$$\mathrm{L} \ll \lambda\ .$$

Table 1.2 - Maximum length of CPT primary winding for different operating frequencies

frequency (kHz)	wavelength (km)	Max length of primary (m)
10	30	3000
50	6	600
100	3	300
200	1.5	150
300	1	100

Before, we saw that 500m length of the primary is realistic for transferring 20kW per EV, however now we see that the CPT system in such case can only be operating on frequencies lower than 50 kHz.

Moreover, the frequency of the system does not affect only the maximum limit on the length of the primary, but also the system efficiency. The efficiency depends greatly on the load for lower frequencies, although for frequencies greater than a threshold, the efficiency can be considered constant as the copper losses begin to be the most prominent loss factor [4]. The optimum frequency depends on the resonant frequency of the system. For high frequencies, there is a greater limitation on the length of the primary, as can be seen in Table 1.2.

However, the length of the primary is not the only important limitation as far as the operating frequency of the system is concerned. There are also significant switching losses at the inverter when operation takes place at high frequencies. However, as mentioned, the efficiency of the CPT transformer increases when operating in high frequencies.

All the above considerations show that there is great flexibility on the design of a CPT system and there are many limitations at the same time. As a result, a final general conclusion on the design is difficult to be drawn. Many factors, like the increasing frequency, have positive as well as negative results to the overall performance of the system.

Combining the above overall analysis and taking into account that a realistic operating frequency would be about 100 kHz, the maximum length of primary is about 300m.

However, depending on the case, an extended length assessment study could take into account all the aforementioned factors, in order to find the optimum configuration.

To sum up, all the considerations mentioned before are summarized in Table 1.3.

Table 1.3 - Parameters of CPT system and their advantages/disadvantages

Parameter	Increase ↑	Decrease ↓
Frequency (*f*)	- increased efficiency - efficiency becomes constant, independent of load	- lower switching losses - greater limit on maximum primary winding length

	- more switching losses - higher cost of inverter	- decrease efficiency Efficiency dependent on load
Power (*P*)	- Larger segment possible/ as more cars can be powered - less inverters	- lower losses (inverter & ohmic) - systems already tested
	- Higher power capability of inverter - higher losses - real systems have not been built	- only one car can be powered per winding - many inverters are needed
Length of primary (*L*)	- Less inverters (considerably lower cost) - possible advantages concerning construction issues	- transferred power constant, independent of number of cars passing -increased efficiency
	- real systems have not been built - increase of power also needed to 'serve' all cars driving on top	- only one car is powered per primary -many primaries are needed, so many inverters as well

1.6 CPT charging and EV battery lifetime

One major issue on batteries, and especially Li-ion batteries that are commonly used for automotive applications, is the limited battery lifetime. In this section the battery degradation mechanisms of Li-ion batteries will be presented briefly and how the CPT system is connecting with these degradation mechanisms will be discussed [8].

1.6.1 Battery degradation mechanisms

- Temperature

Operating temperature is a major parameter for a battery. Operating at very high temperatures or at very low temperatures highly degrades the battery. In a short term increasing the temperature will lead to increase of the power and the capacity of the battery. The voltage and the current of the cell will increase, as the activation energy for the chemical reactions will be lowered and the lithium ions can diffuse faster. However, also the side reactions of the battery will become faster. In that case the capacity mechanisms will occur sooner reducing the battery's performance and lifetime [9]. The increase of the reaction rate will increase the current, which concludes in higher heat dissipation (I^2R) and increases the cell temperature further. When the temperature of the cell rises, the layer between the anode and the electrolyte will deteriorate and might break down.

During charging at low temperatures, the lithium ions may not intercalate fast enough to the anode and may diffuse. In this way, metal lithium may be created and when it grows up to the cathode, the battery cell is short-circuited. This phenomenon is called lithium plating.

We can see that there is a lower as well as an upper limit for the operating temperature.

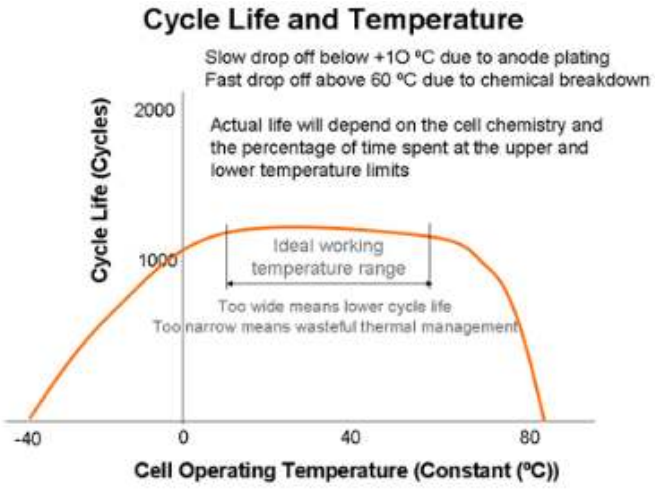

Figure 1.9 - Battery life vs. operating temperature [9]

In order to maintain the temperature in the safe operation margin and protect from degradation, good thermal management of the battery is required.

- Charging C-rates

When charging with high C-rates, it means that high currents go through the battery cell. As current dissipates heat (I^2R), the temperature rises with negative effects for the battery as described above. High currents cause also other ways of degrading the battery and lead to inefficient charging as the maximum cell voltage may be reached without reaching the maximum state of charge.

- Overcharge

During overcharge, the battery is charged beyond the maximum voltage and electrical energy keeps entering the battery, but no intercalation can take place anymore. Then, there is a severe increase in the cell internal resistance and as a result the battery temperature rises dramatically which is one of the major capacity fading factors.

When a battery cell is overcharged the electrolyte may decompose resulting in gas generation. This causes rise in the pressure of the cell which can be dangerous. Furthermore, during overcharge there is a reduction of the active material at the cathode as well as the anode (lithium plating).

- Overdischarge

If a battery is overdischarged, then the copper current collectors at the anode side may corrode, dissolute into the electrolyte and migrate to the cathode. Through this conductive path, when recharged the cell may short-circuit and rapidly increase its temperature when recharged or localized overpotential can occur. Due to the corrosion, the electronic conductivity may deteriorate which results in power fading. Furthermore, overdischarge causes the decomposition of the SEI layer on the anode resulting in capacity fading.

- Depth of discharge (DoD)

The depth of discharge (DoD) is the percentage of the cell capacity after it is discharged during one cycle. If a battery is cycled with larger DoD, then more capacity fading per cycle occurs. During high DoD there is greater loss of Li-ions and active material. Also higher DoD means lower SoC or in other words more lithium at the cathode. In that case the cathode material can be distorted or decomposed and dissolute into the electrolyte. This results in reduction of cathode material and capacity fading. However, the severity of capacity fading in this case depends on the cathode material.

To sum up, in order to minimize the capacity fading mechanism a Li-ion battery should operate within a specific range of temperature and voltage. Charging with low C-rates is more beneficial and proper control should take place in order to prevent overcharging or overdischarging. Operating at high state of charge and having small discharge cycles help increase the battery life.

1.6.2 Effect of CPT charging on EV battery life

When on-road CPT systems are installed, the EV battery is charging while the car is driving on top of the CPT and discharging when the car is driving on parts of the road not covered with CPT.

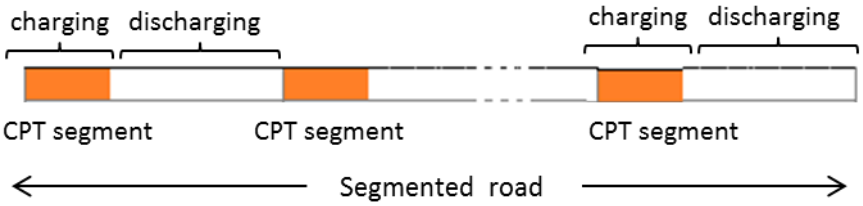

Figure 1.10 - Segmented road with CPT system

In this way a pulsating charging-discharging mode is created. In [8], it was found that when the battery is charged in short pulses even with high currents, the life degradation may not be severe. During the pulses the lithium ions of the surface of the electrode will react. However, local overpotential may be prevented, in case the time between these pulses is long enough so that the Li-ions can diffuse to the electrode-electrolyte interface. Also, severe temperature rise may be prevented if the recovery periods are long enough and the cell has a sufficiently large thermal capacity.

Using the simulation model proposed in [8], the temperature rise for a CPT system was estimated. The initial temperature was 298K and the length of segment as well as the distance between segments was varied from 300m to 4.5km. The figure for a CPT system of 30kW is shown below.

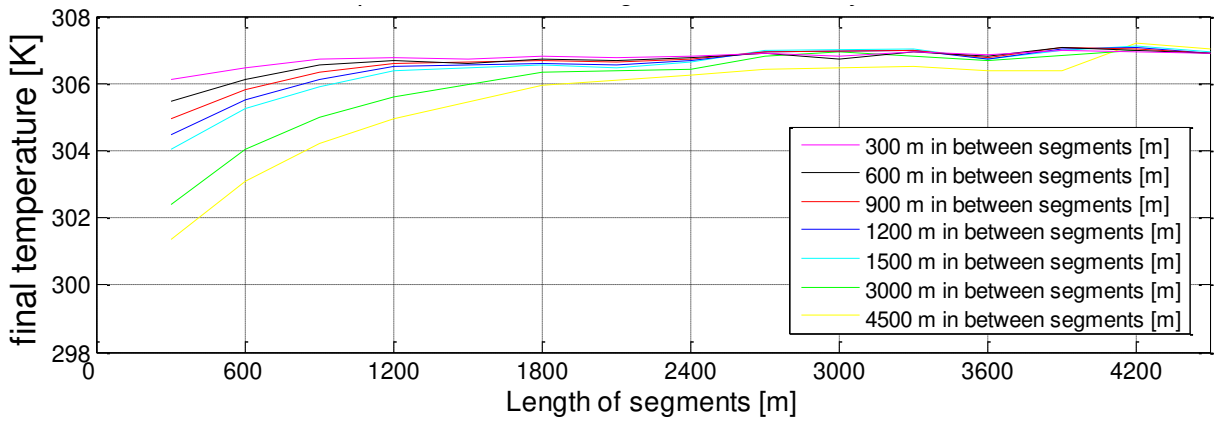

Figure 1.11 - Temperature rise for different configurations of CPT system (30kW)

From the simulation results, we can see as expected that having longer distance between the segments results in lower temperature rise. For segments longer than 1.5 km the difference in temperature rise becomes negligible.

It is important to mention that in the above simulation model the heat production only by the reactions inside the cell during charging was measured. However, large battery packs usually have a thermal management system which cools down the cell if required. This thermal management systems extract the heat produced using air or liquid via fans or pipes. These thermal management systems provide heat during low temperature operation to enhance the battery performance. Moreover, the dissipated heat to the environment has not been calculated, which can be a more or less significant especially when the car is driving at a high speed, there is air at the environment temperature blowing.

A great advantage of CPT charging while driving was shown, as having some space between the segments where the battery is discharging seems to prevent the degradation of the battery [10]. In case the CPT power is quite high (40-50kW) then the charging pulses are shorter and the resting time between is greater. In this way the negative effect of the high currents can be eliminated.

Larger gap between the charging points of the battery means smaller possibility of overcharging the battery. If the EV battery is discharging for some time and then it is charging again and so on, the SoC never reaches the maximum. In this case, the power of the CPT system can always be absorbed and there is less possibility of power lost or overcharging. As it was explained before, overcharging a Li-ion battery is extremely harmful and deteriorates the battery. A matter of safety arises when a battery is overcharged.

CPT systems provide charging in 'microcycles', meaning that the battery experiences very shallow cycles. Operating at small depth of discharge has advantages as far as the battery life is concerned. The depth of discharge depends greatly on the distance between the segments and on the battery size. If decreasing significantly the battery size then of course the battery would experience greater cycles.

1.6.3 Hybrid energy source system of EV with battery and supercapacitor

When charging an EV battery by using on-road CPT systems, it is charged suddenly with a high power for short time integrals. In this way the efficiency of the charging process decreases as the battery can absorb limited amount of current at any time. A solution could be to include a supercapacitor to the system which will get charged from the CPT and then it will charge the battery at lower currents for longer period of time.

Supercapacitors are already used to improve the performance of electric vehicles [11]. A supercapacitor is a component which has relatively high specific power capacity in comparison to batteries much like a capacitor, while it has much higher specific energy than a conventional capacitor, more like a battery. A supercapacitor has 10 times higher specific power but only half specific energy compared to a Li-ion battery. Supercapacitors can be charged and discharged many times (about one million cycles) without performance deterioration, in other words their lifetime is much larger than batteries. An electric car with a hybrid supply system consisting of batteries and supercapacitors may increase the time response for accelerating, for charging during regenerative braking as well as increase the useful life of the batteries [12]. Fast charging from contactless power transfer while-driving can become more efficient with the assistance of supercapacitors. Besides, supercapacitors allow charging even when the battery is fully charged.

However, parameters that have a negative impact on the lifetime of a supercapacitor are high voltage and high temperature. A supercapacitor should operate in a specific range of voltage and temperature; otherwise its life length is significantly shortened. Furthermore, when a supercapacitor is used to supply power to an electric vehicle, then the total cost of the system dramatically increases. Because of the high current cost of the supercapacitors, the electric system of an EV should be carefully sized.

Overall, it could be said that an energy source system of battery and supercapacitor along with CPT charging should be further investigated and might provide additional advantages for electric vehicles. Moreover, an EV only with supercapacitor and CPT system could be another option which can also be studied.

1.7 Discussion on CPT for charging while driving

To conclude, on-road CPT systems consist of long primary windings installed on the road and secondary windings installed at the chassis of every EV. High frequencies and resonant mode coupling are required in order to transfer power efficiently. The primary windings are installed on the road in segments so that the road is not fully covered with CPT tracks.

As far as the specifications of every primary winding is concerned, the operating frequency, the power transferred and the length should be specified. There are many advantages and disadvantages and in many cases the benefits come in opposition to each other. An operating frequency of 100 kHz is a realistic value which provides quite high transfer efficiency. The maximum length of the primary winding in such case can be up to 300m.

The primary windings can be placed one next to the other and create a CPT segment. The segments can be distributed in many ways, with longer or shorter distances in between. The concept of segmented road has many advantages. In this chapter the effect of pulsating charging on the battery life was investigated. It can be seen that short segments with a considerable distance in between helps saving the battery life. Other aspects of the distribution of segments are provided in next chapter.

2 Overview of the road system in the Netherlands

The implementation of CPT systems for charging-while-driving can be more effective if they are installed on roads with high usage and as a result high traffic. Therefore, in this chapter an overview of the road system infrastructure and the Dutch driving pattern will be presented in order to become able to investigate the extensive implementation of CPT systems in the Netherlands.

2.1 Road system infrastructure

Two main characteristics of the Dutch road network are that it is very dense and it is considered to be in a great condition. The Netherlands has 5.121 km national highways. Provincial roads have a length of 7.863 km and other municipal roads 117.637 km [13]. We can see that although the Netherlands has the highest highway density in Europe, highways are a just small percentage of the total road system length. Therefore, the Netherlands has a large highway system, which covers only 4% of the total road system.

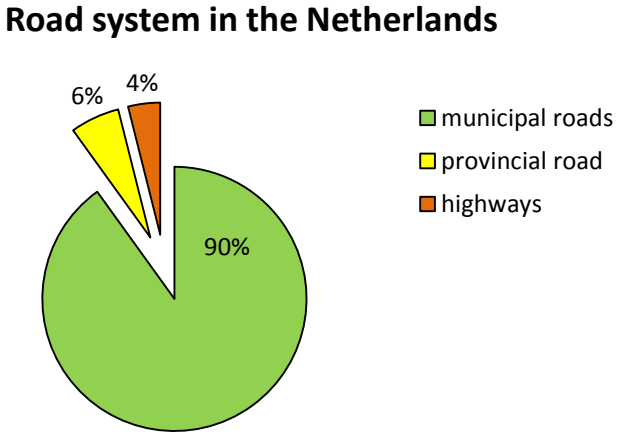

Figure 2.1 - The Dutch road system

It is important to mention the fact that Netherlands has a density of about 57.5 km highways per 1,000km², which is the largest motorway density of the European Union. This may come from the fact that there are no very big cities; all cities have less than a million citizens. As a result, there is a great interconnection system between the cities. Also, Dutch highways are one of the busiest and it is common for Dutch people to commute to another city in order to work.

Rank	Country	NUTS	Length of motorways (km)	Land area (km²)	Motorway density (km/1000 km²)
1	DE	Bremen	75	404	186
2	UK	Greater Manchester	177	1 276	139
3	NL	Utrecht	177	1 386	128
4	NL	Zuid-Holland	353	2 818	125
5	DE	Düsseldorf	649	5 290	123
6	AT	Wien	43	396	109
7	DE	Hamburg	81	755	107
8	NL	Noord-Holland	283	2 670	106
9	NL	Limburg	219	2 153	102
10	UK	Merseyside	64	644	100
11	NL	Noord-Brabant	483	4 919	98
12	ES	Comunidad de Madrid	760	8 028	95
13	UK	West Midlands	81	901	90
14	DE	Berlin	77	891	86
15	BE	Prov. Vlaams-Brabant	175	2 100	83
16	NL	Gelderland	393	4 975	79
17	BE	Prov. Antwerpen	220	2 792	79
18	DE	Köln	558	7 364	76
19	BE	Prov. Hainaut	284	3 773	75
20	UK	South Yorkshire	115	1 551	74

* Non full EU-27 coverage, see methodological notes

Figure 2.2 - Areas with greatest motorway density in EU [14]

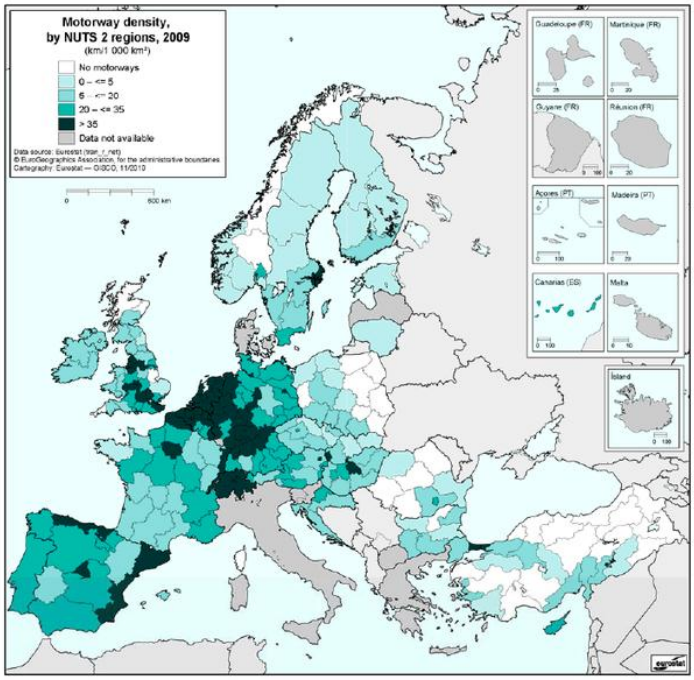

Figure 2.3 - Map of EU with motorway density [15]

As far as some regional data concerning the road infrastructure is the Netherlands, we can see that the length of highways and the length of all the roads follow the same distribution regionally. Moreover, we see that the provinces with the biggest cities have the most dense road infrastructure.

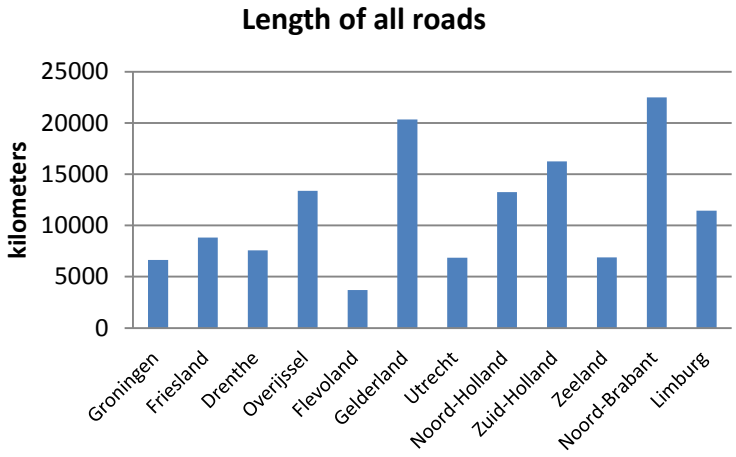

Figure 2.4 - Length of roads in Dutch provinces [16]

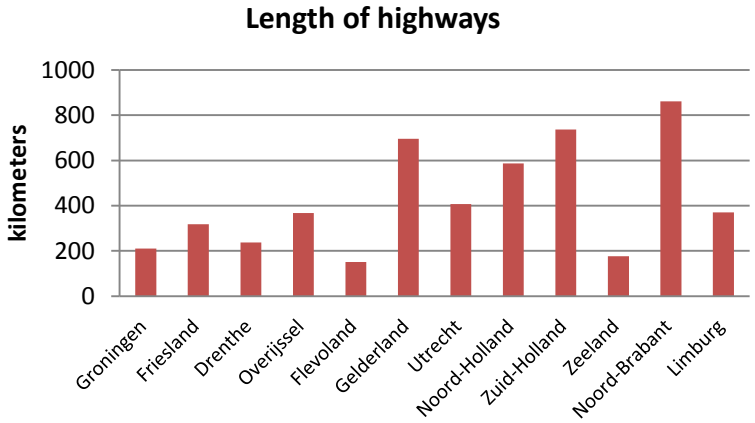

Figure 2.5 - Length of highways in Dutch provinces [16]

Apart from a very high density (length of roads per country surface area), the Dutch motorways are considered to have of very high traffic intensity. The average traffic intensity is 50,000 to 100,000 vehicles per day in rural areas and 100,000 to 200,000 vehicles on inter-urban routes in the Randstad (provinces of Utrecht, Noord-Holland, Zuid-Holland and Flevoland) and urban ring or perimeter roads. The busiest is the A16 motorway in the Netherlands in Rotterdam with 230,000 vehicles daily [17].

2.2 Dutch Mobility analysis

In order to design a Contactless Power Transfer system, it is really useful to see as well what kind of roads people use mostly. From the data of the research for mobility in the Netherlands, there is information about the percentage of the total number of car trips as well as the total distance covered depending on the length of each trip [18].

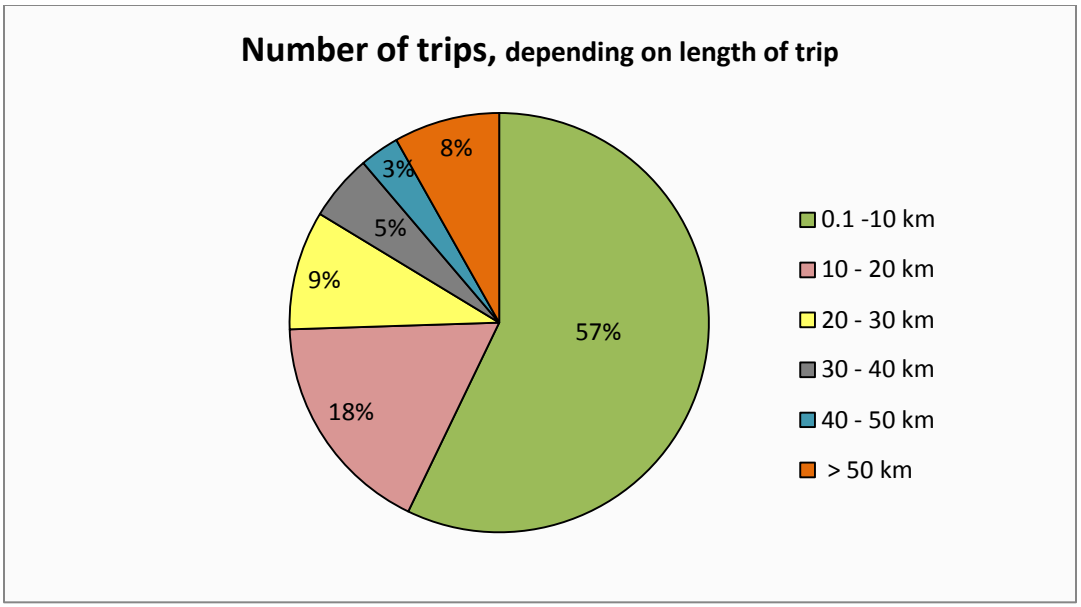

Figure 2.6 - Number of trips depending on length of trip

From Figure 2.6, we can observe that the majority of the trips are short (0.1-10km). However, in short trips the distance covered is also small. What it is important to investigate is on what kind of roads most of the driving distance is covered. For that reason, in Figure 2.7, the distribution of the driving range is presented, depending on the length of the trip. We can see now that only 13% of the driving distanced is covered in short trips (0-10km). On the other hand, half of the driving distance is covered in long trips, longer that 40km. It means that a great percentage of the distance driven is covered on highways considering the Dutch road system.

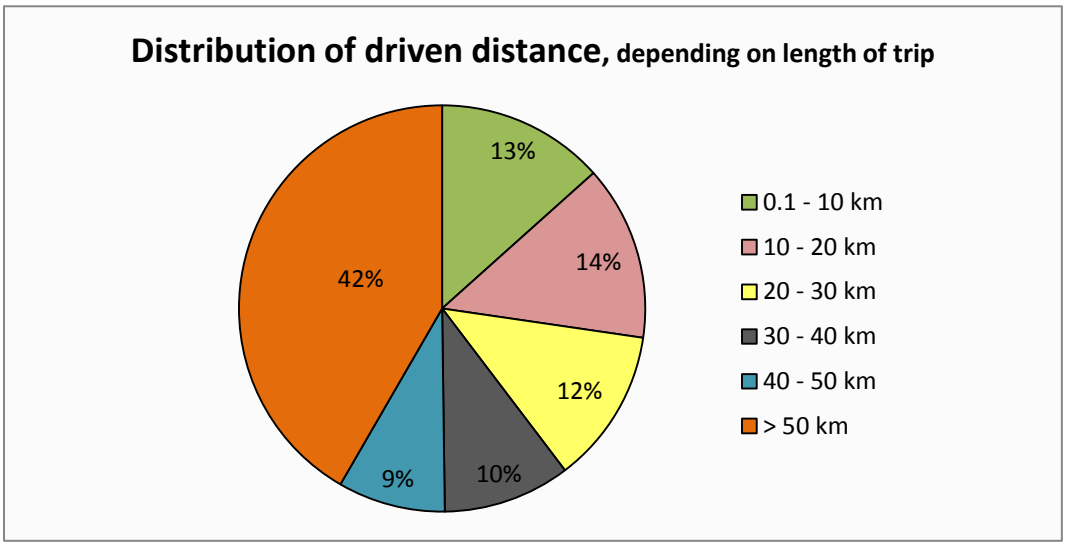

Figure 2.7 - Distance covered, depending on length of trip [18]

To sum up, highways amount to be 4% of the total road system and the greatest part of the total driving distance is covered on long trips, during which drivers would use the highways for a part of their trip.

A next step, in order to investigate on what kind of roads people choose to drive and to what extent, is to estimate the percentage driven on streets and on highways. In the Netherlands as there are no very big cities, the total distance driven by car within every city can be considered limited. In the next table the largest cities of the Netherlands are listed and the average distance from the city center to the closest highway is shown.

Table 2.1 - Distance from the city-center to highway for the biggest cities in NL

City	Distance from center to highway
Amsterdam	7km
Rotterdam	5km
The Hague	5km
Utrecht	5km
Eindhoven	7km
Tilburg	6km
Almere	4km
Groningen	5km
Breda	4km
Nijmegen	6km
Apeldoorn	5km
Enschede	7km
Haarlem	4km
Arnhem	6km
Zaanstad	4km

We can see that there is an average of about 5km distance to drive on city streets before reaching a highway. So, for every trip it can be assumed that 10km are driven on city streets and the rest on highways. Combining this assumption with the distance covered per trip length of Figure 2.7, the percentage of distance covered on highways for trips longer that 15km is 80%, where the distance covered on smaller roads is 20%. For trips shorter that 15km, we can assume that there is enough time in between the trips to charge the EV battery by conductive charging. The level of conductive charging (standard, semi-fast or fast) depends on the time duration in between these trips.

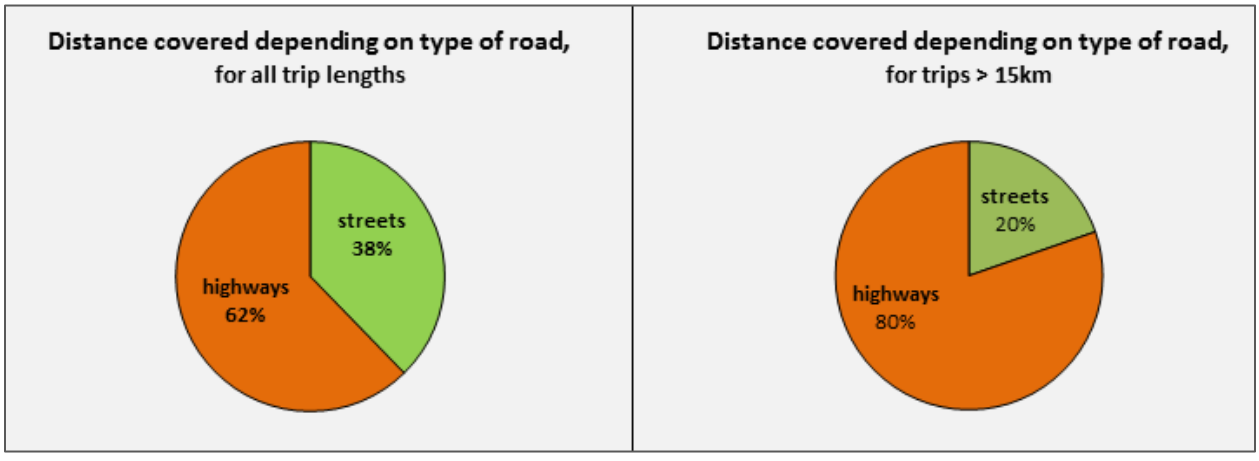

Figure 2.8 - Distance covered depending on type of road

From the above figures, we can see that a large percentage of the distance driven by every vehicle in the Netherlands is covered on highways. Taking into account the length of each type of road (Figure 2.5),

we observe that cars are driving mostly on just 4% of roads (which is about 5.000 km of road length or 15.000 km considering that most highways have 3 lanes).

The fact that highways are the mostly used roads is not only a Dutch phenomenon. Also in the U.S. it is state that interstate highways are just 1% of the total road infrastructure, but they carry 22% of the distance travelled. [19]

As a result, the implementation of Contactless Power Transfer System on highways can have a great impact on the driving range of electric vehicles and the time required for conductive charging. Overall, CPT systems may be the pathway for the transition from the fueled-cars to electric mobility.

2.3 Traffic data for highways

In this section, specific data concerning the traffic on an hourly basis for Dutch highways will be shown. First, some general data for various highways will be presented and then the data for the simulated highway will be analyzed. The data concerns the flow rate of vehicles in number of vehicles per hour. Estimation on the driving speed will also take place in order to obtain the traffic density in number of vehicles per unit area. In this way, data on the number of vehicles that are charged by the CPT system throughout the year can estimated.

2.3.1 Vehicle Flow Rate

In this section the traffic flow for highways will be presented. The general pattern of the vehicle flow will be shown. More specifically, the changes in traffic depending on the hour of the day, the day of the week and the month of the year will be presented.

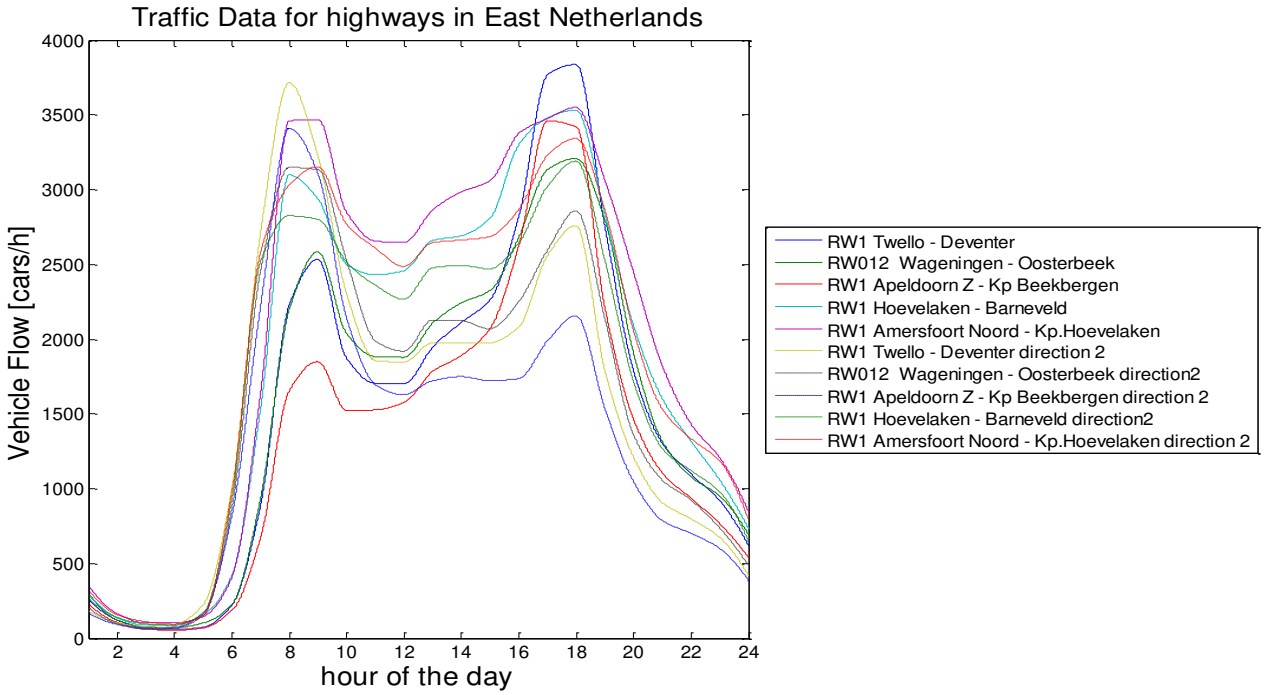

Figure 2.9 - Traffic data for highways in the East Netherlands [20]

After collecting data concerning the amount of cars during an average day in various highways [20], it can be observed that the daily road traffic follows more or less the same pattern. There is a peak in the morning at around 9am and another peak in the afternoon at around 6pm. At this second peak, the largest road traffic of the day occurs in most cases.

As already mentioned, the traffic intensity in Dutch highways varies from 50.000 to 100.000 cars per day. Data for a highway with an average traffic will be presented and will be further used within this study. The vehicle flow of this highway follows the average daily traffic pattern shown in the Dutch mobility analysis [18], [21].

The number of vehicles (all categories) passing during an average working day are 50.000 per direction or 100.000 taking into account both directions. As far as the number of cars (light vehicles) is concerned, it is 37.000 cars per direction per day or 74.000 for both directions. The data are for highway A1 at the east the part of the Netherlands between Deventer and Twello (kilometer 97.4) for the year 2010. At this section the highway has two lanes per direction.

All the main characteristics of the road are put together at the following table.

Table 2.2 - Characteristics of simulated highway

Highway	A1
Begin - End	Amsterdam - De Lutte
Total length	157 km
Measurement point	Twello - Deventer (97.4km)
Number of lanes at measurement point	2 lanes
Average daily traffic intensity	100.000 vehicles (74.000 cars)

Figure 2.10 - Highway A1 [17]

The vehicle flow for all categories per each hour of the day is given below. The peak traffic can be easily seen in the figure.

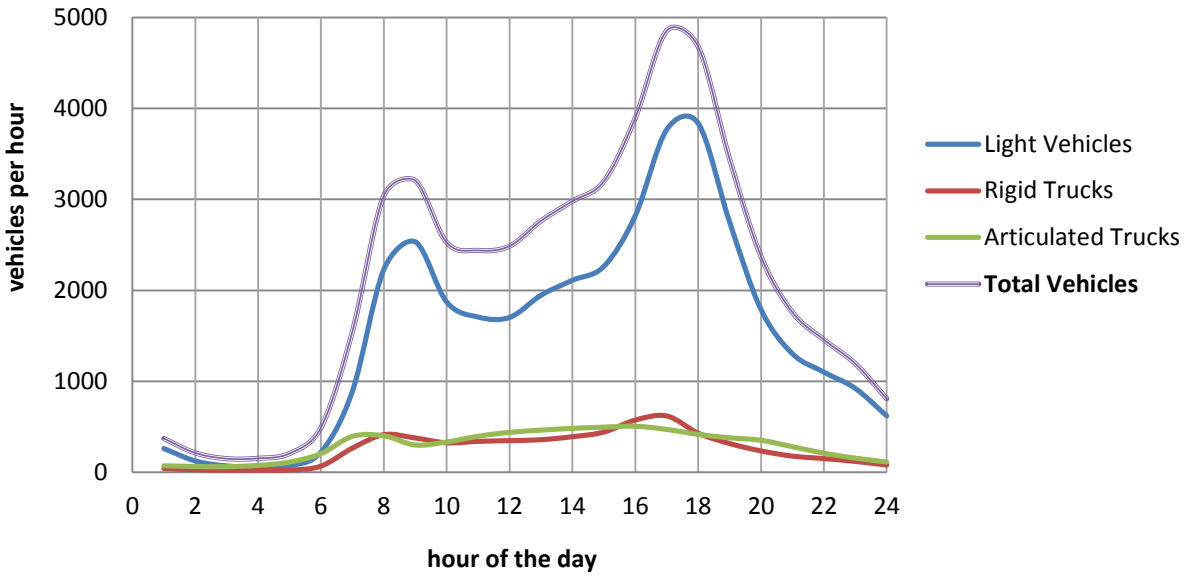

Figure 2.11 - Flow of vehicles on an average day [20]

In order to derive the traffic in highways for one whole year, statistics for each month of the year and each day of the week were used.

Table 2.3 - Number of cars in % compared with the average week day [20]

	Mon	Tue	Wed	Thu	Fri	Sat	Sun
Jan	86.0	91.6	90.8	92.8	83.7	54.9	50.0
Feb	89.4	94.3	93.4	97.1	98.1	64.3	58.8
Mar	97.5	103.5	103.6	105.8	105.8	71.8	66.0
Apr	97.4	106.6	107.0	112.1	97.0	74.2	70.4
May	101.3	105.6	99.8	109.3	103.7	73.7	69.5
Jun	98.5	104.9	105.8	109.5	110.7	73.9	72.9
Jul	91.3	92.1	92.3	98.4	97.5	69.8	64.3
Aug	89.3	92.5	92.2	94.8	100.7	73.8	67.9
Sep	99.5	102.7	102.3	105.4	108.5	75.5	70.9
Oct	100.5	104.0	103.9	107.6	108.7	74.6	70.0
Nov	98.4	101.8	103.0	105.9	105.5	72.1	66.5
Dec	82.8	88.8	91.7	84.8	85.2	58.3	53.7

Statistical data show that there is less traffic during the weekends and during months like December, January and July, August as at that period less people need to commute.

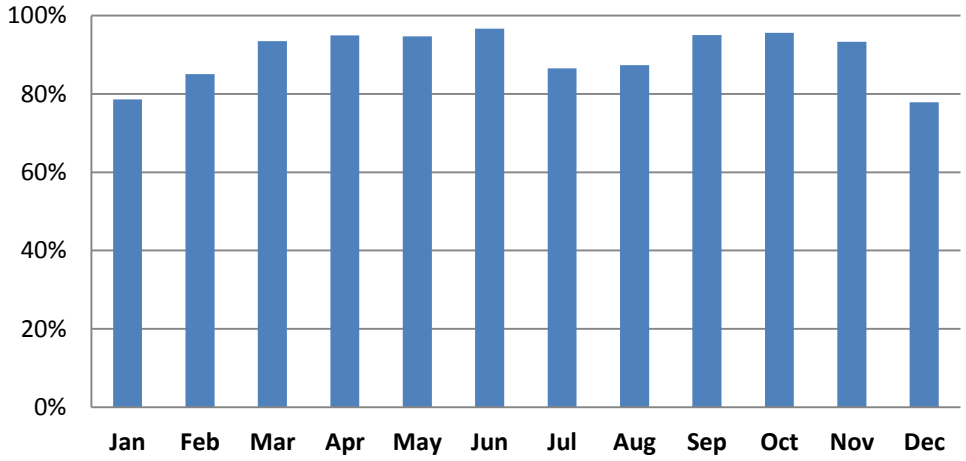

Figure 2.12 - Monthly Distribution of vehicles' flow

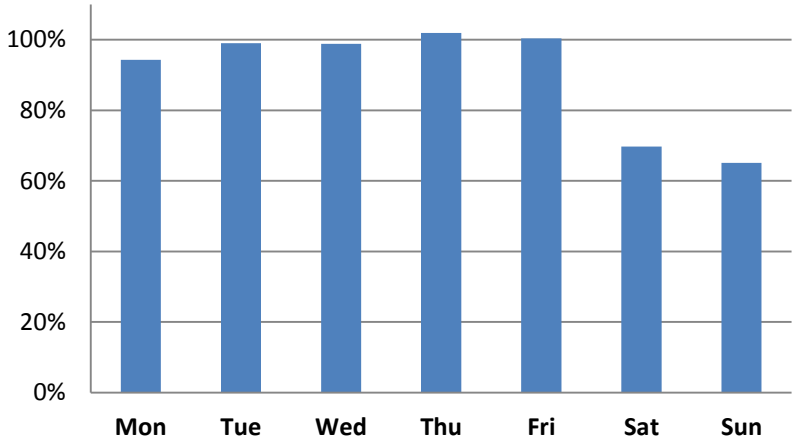

Figure 2.13 - Weekly Distribution of vehicles' flow

All the data presented in this chapter will be later used for the calculation of power demand of electric vehicles which are driving on highways.

2.3.2 Driving Speed Estimation

Depending on the vehicle flow, the average speed of cars can be estimated. In transportation systems, 'free-flow speed' is the speed that the driver would choose to travel at zero vehicle flow, if there were no other cars or no adverse conditions (e.g. special weather conditions). Taking into account the free-flow speed for a specific road and the vehicle flow during the day, there are flow-speed curves in order to estimate the speed. According to the Highway Capacity Manual 2010 [22], the speed-flow curves are as depicted below, where 'LOS' is the Level of Service, 'pc' is the passenger car and 'ln' is the lane.

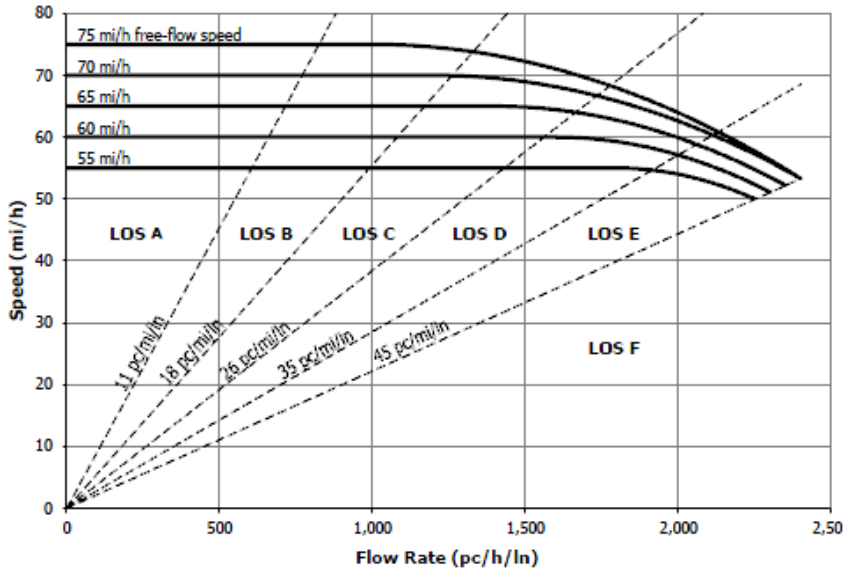

Figure 2.14 - Highway speed-flow curves [22]

Table 2.4 - 'Level of Service' of Highways

LOS	Description
A	Traffic flows at or above posted speed limit. Motorists have complete mobility between lanes.
B	Slightly congested, with some impingement of maneuverability.
C	Ability to pass or change lanes constrained. Posted speeds maintained but roads are close to capacity. This is the target LOS for most urban highways
D	Speeds somewhat reduced, vehicle maneuverability limited. Typical urban peak-period highway conditions
E	Flow becomes irregular, speed vary and rarely reach the posted limit. This is considered a system failure.
F	Flow is forced, with frequent drops in speed to nearly zero mph. Travel time is unpredictable.

The free-flow speed certainly depends on the speed limit. The ideal free-flow speed is generally taken some km/h greater than the speed limit. The real free-flow speed is the ideal decreased by some factors which depend on the lane width, the right shoulder lateral clearance, the number of lanes, the interchange density and whether the highway is divided or not.

For the Netherlands, the speed limit for highways is normally from 100km/h to 120km/h, in some urban areas can be 80km/h and in some experimental projects has lately become 130km/h. In the vast majority of highways, the two directions are divided and have at least two lanes per direction. Taking all the above into account and as the scope of this project is to investigate a typical Dutch highway, the free-flow speed will be assumed to be about 110km/h (or about 70mh, as the previous diagram is scaled for miles per hour).

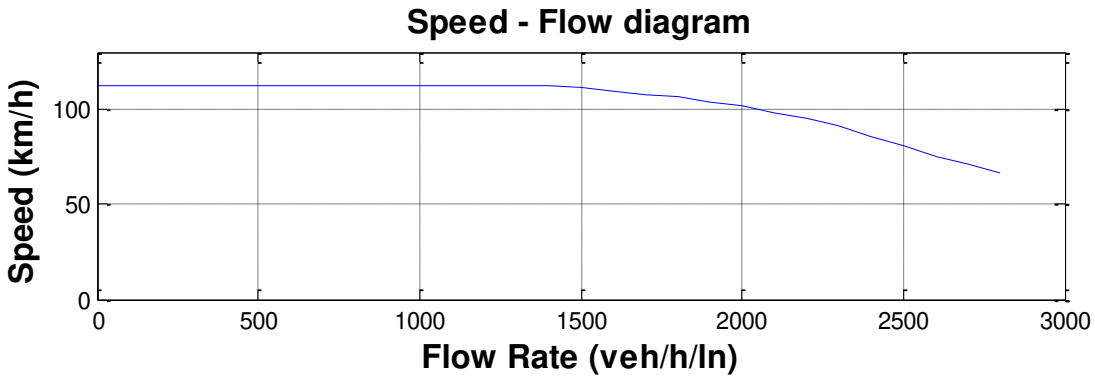

Figure 2.15 - Speed-Flow diagram used in the simulations

2.3.3 Traffic Density

Combining the speed-flow diagram (Figure 2.15) with the daily flow rate (Figure 2.11) the speed of the vehicles can be estimated. The results are depicted below in Figure 2.16 which shows the speed of the vehicles and also the flow rate per lane of all vehicles (light vehicles, rigid & articulated trucks).

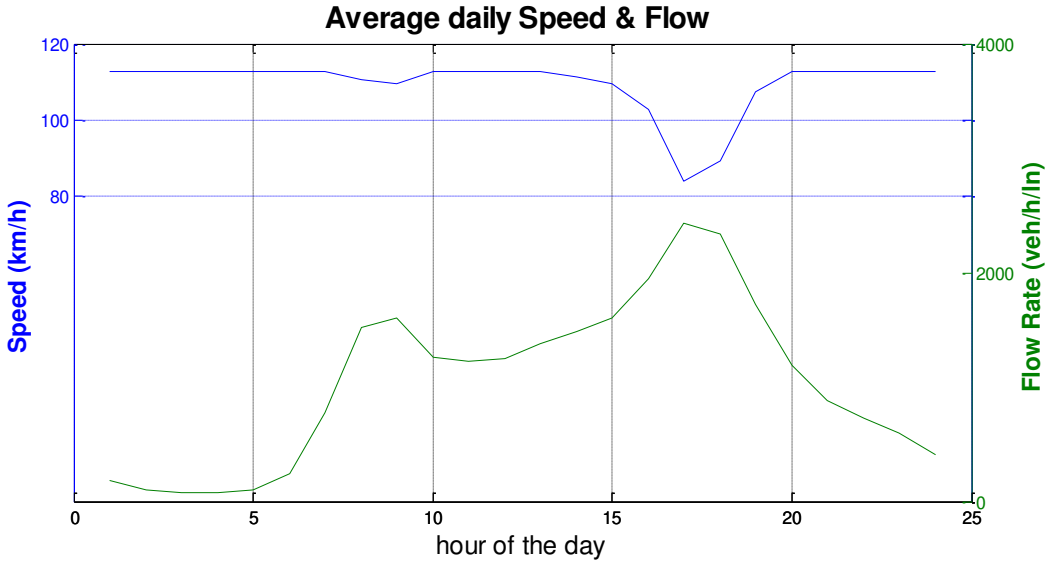

Figure 2.16 - Average vehicle speed and average vehicle flow

Finally, the absolute number of cars (light vehicles) for a particular length of highway can be also estimated. The following graph shows the average traffic density in number of cars per kilometer per lane.

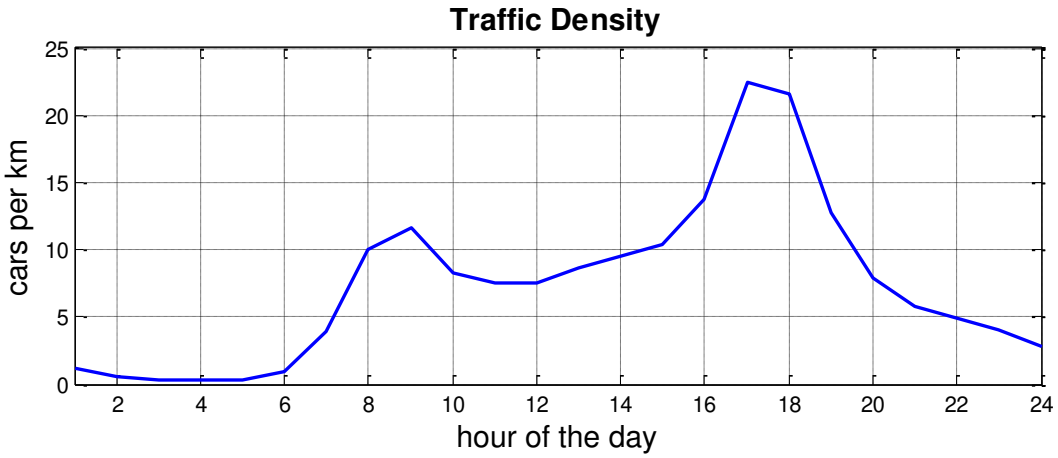

Figure 2.17 - Average Traffic density [cars/km]

2.4 Discussion on the implementation of CPT to the Dutch road system

In this chapter, an overview of the road infrastructure and the Dutch driving habits was presented. In this study, highways are chosen to be the type of roads at which CPT systems would be implemented. The main reason is that highways are 4% of the roads in the Netherlands and they are the roads mostly used. These on-road charging systems would be directly powered from green energy sources. Therefore, implementing wind turbines and solar panels on the highway roadside is more feasible than implementing them in urban areas e.g. city centers.

Data for the daily vehicle flow on a typical highway were presented and the number of cars using the highway at each point of time was estimated. Next, an analysis for the coverage and power requirements of the CPT systems will take place. Therefore, after combining the traffic data with the CPT system specifications, an estimation of the power demand curve of the electric vehicles is possible.

3 Implementation of CPT system on Highways

If CPT systems for powering EVs while driving are to be implemented, then it is more feasible to choose roads with the highest traffic. As a result from the analysis of the previous chapter, the implementation of CPT systems on highways will be further investigated. First, the model used to simulate an electric vehicle driving on a road with a CPT system will be presented. This simulation model was created in Matlab-Simulink©. Then, from the simulation results, conclusions can be drawn on the specifications of the on-road charging system depending on the EV driving range achieved and the EV battery size.

3.1 Driving cycle for highway driving

A typical driving cycle for highway driving can be simulated as the standard Highway Fuel Economy Driving Schedule (HWFET). This driving cycle consists of 765 sec, in which a distance of 16.5 km is covered. The average speed is 78km/h, the maximum acceleration is 1.43m/s^2 and the maximum deceleration is 1.48m/s^2.

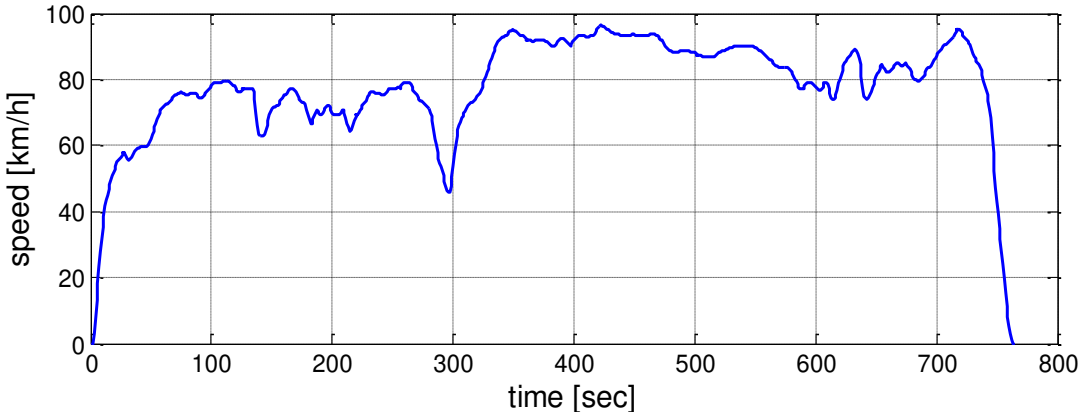

Figure 3.1 - Highway Fuel Economy Driving Schedule (HWFET)

However, during the simulation the range of 16.5km is not sufficient, so an extended driving cycle based on the HWFET was used. The used driving cycle consists of a repetition of the part of the HWFET where the speed of the car is greater than 50km/h. The times the HWFET is repeated depends on the driving range that has to be simulated.

3.2 Power consumption of electric vehicle

The power that the car needs in order to drive should be determined as well. Every car motor has to create a force to overcome the aerodynamic (F_d), the rolling resistance (F_r) and gravity (F_g) force. It also needs additional force (F_a) in order to accelerate. As a result, the total force created by the car is the sum of the aforementioned forces [6].

$$F_v = F_d + F_r + F_g + F_a$$

- aerodynamic force: $F_d = \frac{1}{2}\rho C_d\, A_v\, v^2$
- rolling resistance force: $F_r = f_{rr}\, M_v\, g\, \cos a$

- gravity force: $F_g = M_v \frac{dv}{dt}$
- force to accelerate: $F_a = M_v\ g \sin a$

Where,

ρ Air density = 1.204 kg/m3 at 20oC, 1 atm
C_d aerodynamic drag coefficient
A_v vehicle frontal surface area (in m2)
v Vehicle speed (in m/s)
f_{rr} rolling resistance coefficient, or coefficient of rolling friction, typically 0.01 for car tires on concrete or asphalt
M_v vehicle mass (in kg)
g Gravity = 9.81 m/s2
$\sin a \approx \tan a = H/L =$ road grade Z (for small a)
$\cos a \approx 1$ (for small a)

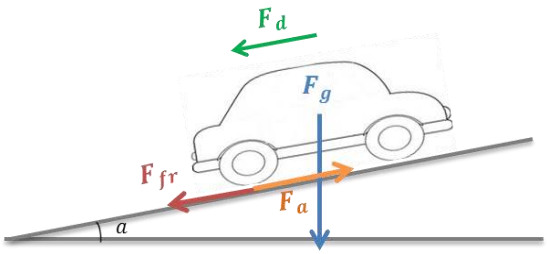

Figure 3.2 - Forces acted to a vehicle while driving

The power required by the motor can be now calculated as the total force multiplied by the velocity of the vehicle.

$$P_v = F_v \cdot v = \frac{1}{2}\rho C_d\ A_v\ v^3 + f_{rr}\ M_v\ g\ \cos a\ v + M_v \frac{dv}{dt} v + M_v\ g \sin a\ v$$

The total power consumption should also take into account the motor efficiency (η) and the power for heating, air-conditioning and other accessories (P_{other}).

$$Total\ Power = \frac{P_v}{\eta} + P_{other}$$

Typical values for the parameters of light vehicles as well as trucks are shown in the table below.

Table 3.1 - Vehicle parameters

	Cat. 1 - Light Vehicles	Cat. 2 - Rigid Trucks	Cat. 3 - Articulated Trucks
C_d [kg/m]	0.29	0.70	0.85
A_v [m^2]	2.8	8.75	9.5
M_v [kg]	1521	20000	30000
f_{rr}	0.0100	0.0080	0.0045
η	0.80	0.80	0.80
P_{other} [W]	800	1200	1200

When the electric machine is in 'motor' mode, the energy from the battery is turned into mechanical energy in order to propel the vehicle. However, the power can flow backwards when the vehicle is going downhill or braking. In this case, the kinetic energy from the car can be used to drive the motor, which works then as a generator and produces electric power which is stored in the battery. This process is called regenerative braking. The efficiency of using the energy from regenerative braking can be estimated by taking into account the efficiency of the electric machine twice (for the energy produced during the generator mode and for the energy is actually used at the motor mode), the efficiency of the power conversion steps and the charging/discharging battery efficiencies. Overall, it is found in literature that about 40% of the energy from the regenerative braking is actually used to drive the car (this includes also every kind of losses that occur during this process, e.g. energy lost in heat during braking). Regenerative braking is included in the simulations, wherever the vehicle is decelerating. The road was assumed to have to inclination (z=0). The excess of power in such case will be used to charge the battery.

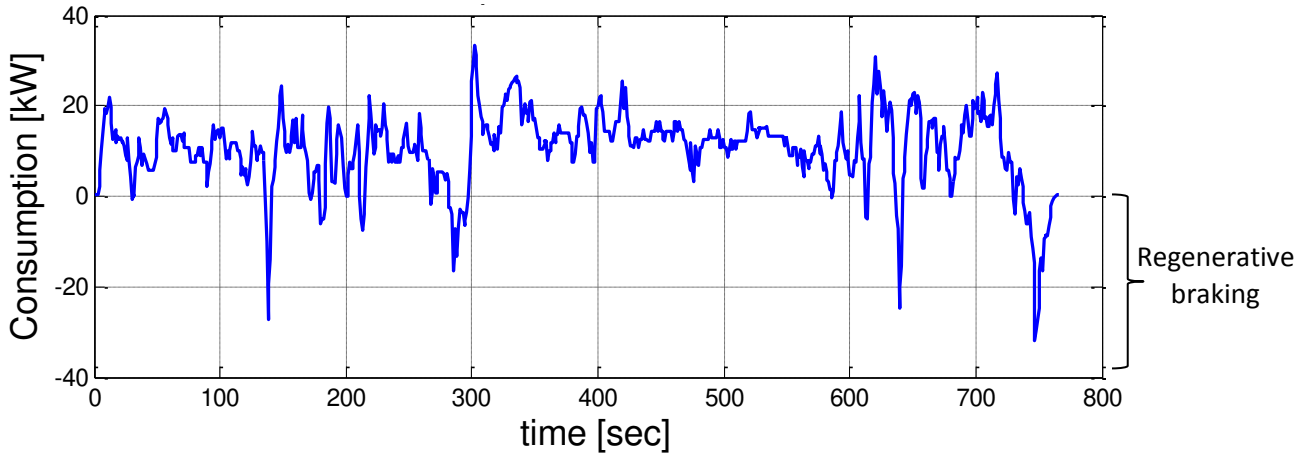

Figure 3.3 - Power consumption during the HWFET

3.3 Battery of the electric vehicle

The parameters of the battery used in the model, which are parameters of Nissan Leaf, are shown in the table below.

Table 3.2 - Parameters of the simulated EV battery

Type	Laminated Li-ion
Total Capacity	24 kWh
Maximum power output	90 kW
Voltage nominal	360 V
Rated Capacity	66.7 Ah
Mass	294 kg

The battery model which was used during the simulation was the standard Simulink model. This model has some simplifications; however, it is considered accurate enough as far as this research is concerned.

The electric vehicle was simulated with the extended HWFET cycle for time duration of 6636 sec or 1.8 hours. As the battery should not be overcharged or overdischarge, the effective range of the state of charge was considered to be 20-95%. Running the simulation with an initial SoC of 95%, the driving range can be found when the SoC reaches 20%.

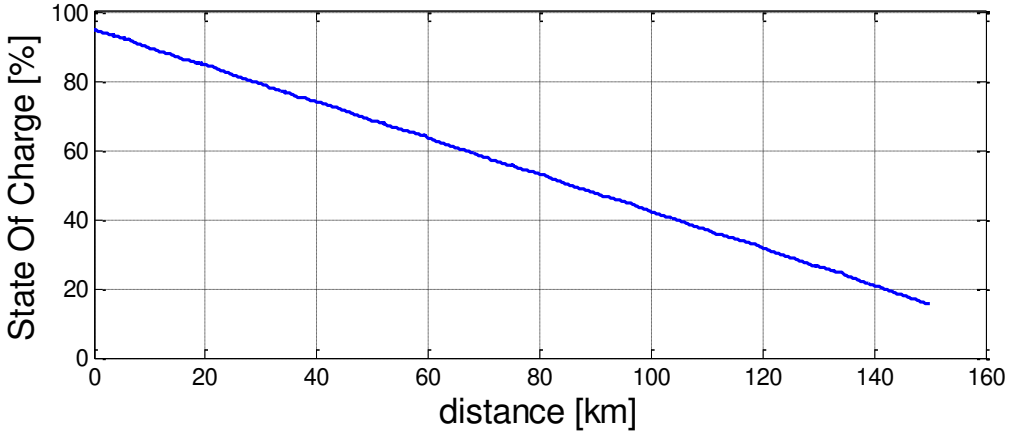

Figure 3.4 - State of charge of EV battery during HWFET

From the simulation results, we can conclude that the total range for highway driving of the electric vehicle is about 140km.

3.4 Power curve of the CPT system

The CPT system can operate for various peak power values. A reasonable range of the power transferred is from a few kilowatts to hundreds of kilowatts per primary winding. However, the main question is how much power is transferred in a real scenario, when a car is passing on top of a segment. For this research, an efficiency of 75% for the CPT system is considered. This takes into account the losses of the inverter, the CPT transformer and the rectifier which provides the DC current to the EV battery or motor. The efficiency of 75% is the lowest value found in literature; however it is a realistic value when charging-while-driving at high power is considered. This value of the efficiency is valid when there is no significant misalignment between the car and the primary winding. The effect of misalignment is of great importance and may cause a great drop of the efficiency of the system. [23]

Generally, the amount of power that can be provided depends on the mutual inductance between the primary and the secondary winding. The mutual inductance has its peak value in the middle of the winding and is decreased in the beginning and at the end of each winding. So, this also holds for the power of each segment.

The time needed for the power to reach its maximum is proportional to the gap between the secondary and the primary. As this distance is about 15cm, this ‘rise-up’ time of the power from 0 to maximum, becomes less significant as the length of the primary coil increases and also as the speed of the car increases. As a result, in this research project, where charging-while-driving on highways is investigated, power loss at the two edges of the primary coil is not considered important.

To sum up, the power of the CPT system has the format of pulses, where its ‘period’ depends on the distribution of the primary windings over the road (see Figure 1.7) and the ‘pulse width’ depends on the percentage of road that is covered by CPT.

3.5 Model of electric vehicle with CPT system

By combining all the above, a simulating model was created in Matlab-Simulink©, having as inputs the driving cycle and the specifications of the CPT system. The power consumed by the EV and the power produced by the CPT would be calculated and in the end the state of charge of the battery can be recorded in order to estimate the driving range under the given conditions.

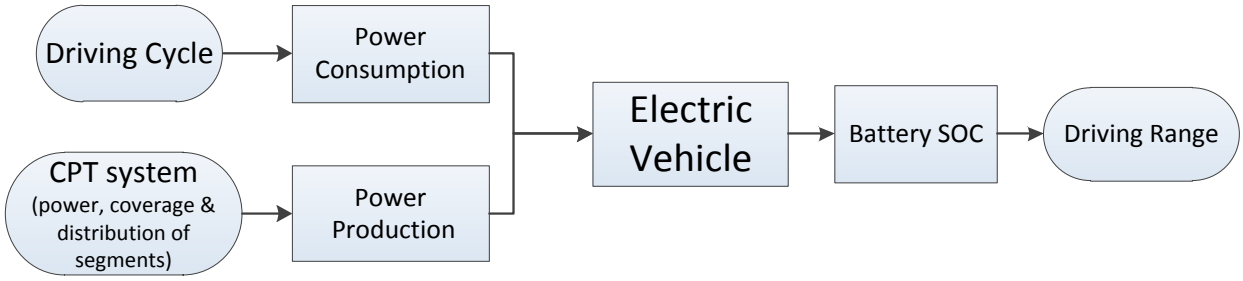

Figure 3.5 - Model overview of Electric vehicle with CPT system

An example of the simulation results is shown below. The CPT system for this example has a power of 30kW and coverage of 30%. The CPT power has the form of pulses, where the width depends on the coverage and the distribution of the CPT segments as well as the vehicle's speed. As the vehicle speed is varying during the simulation, the width of the CPT power pulses is also not constant.

We can see that for the 500sec of the simulation, the state of charge of the battery would normally fall from 95% to 84%, where if there is CPT system the final SoC has decreased by only 3% to 92%.

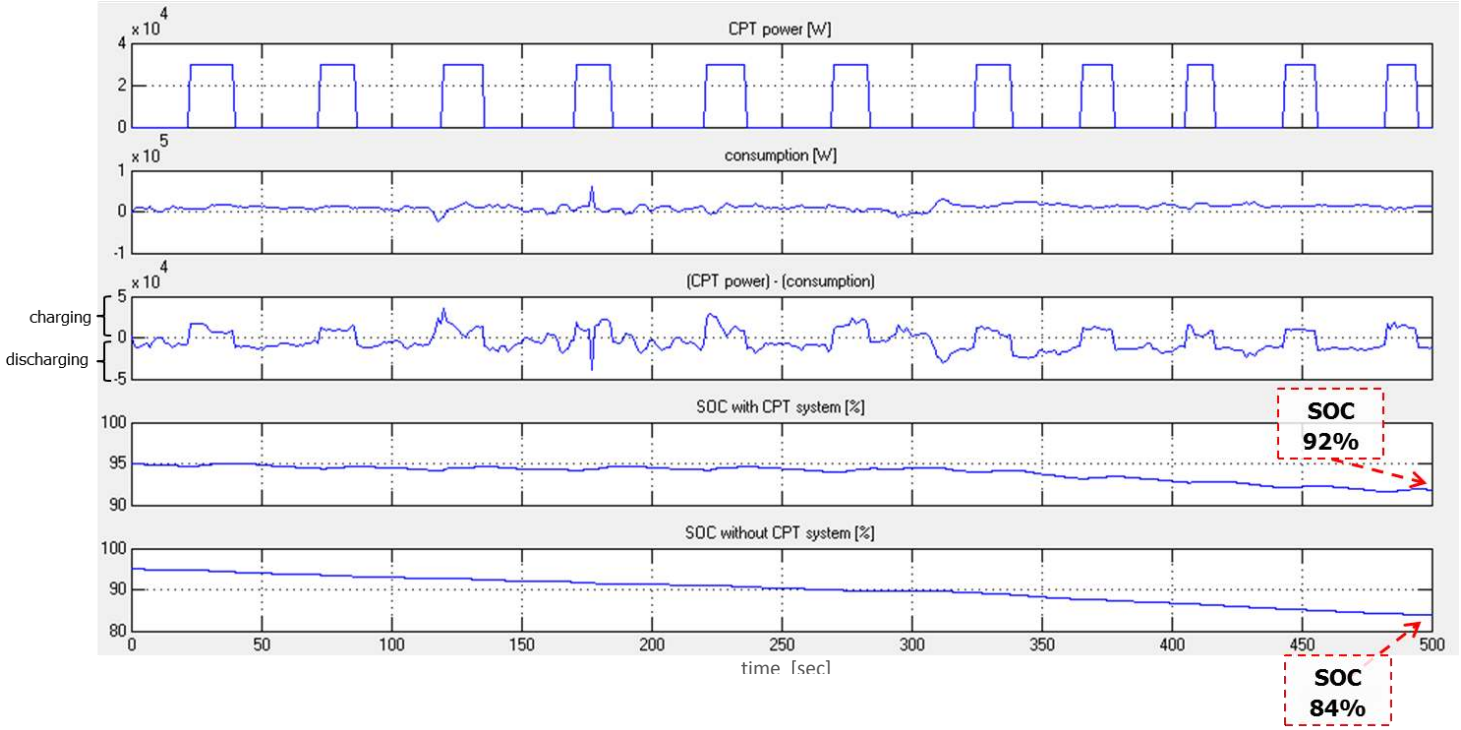

Figure 3.6 - Example of simulation results of EV model with CPT

3.6 State of charge of EV Battery while driving on road with CPT

In this chapter, the simulation results of implementing CPT on highways will be presented. The assumptions for the vehicle and battery parameters made during the simulation were the ones presented previously. Concerning the distribution of the primary windings, for these first simulations, the road was considered to be divided into sections of 1km, out of which the corresponding percentage (10-100%) was covered with primary windings.

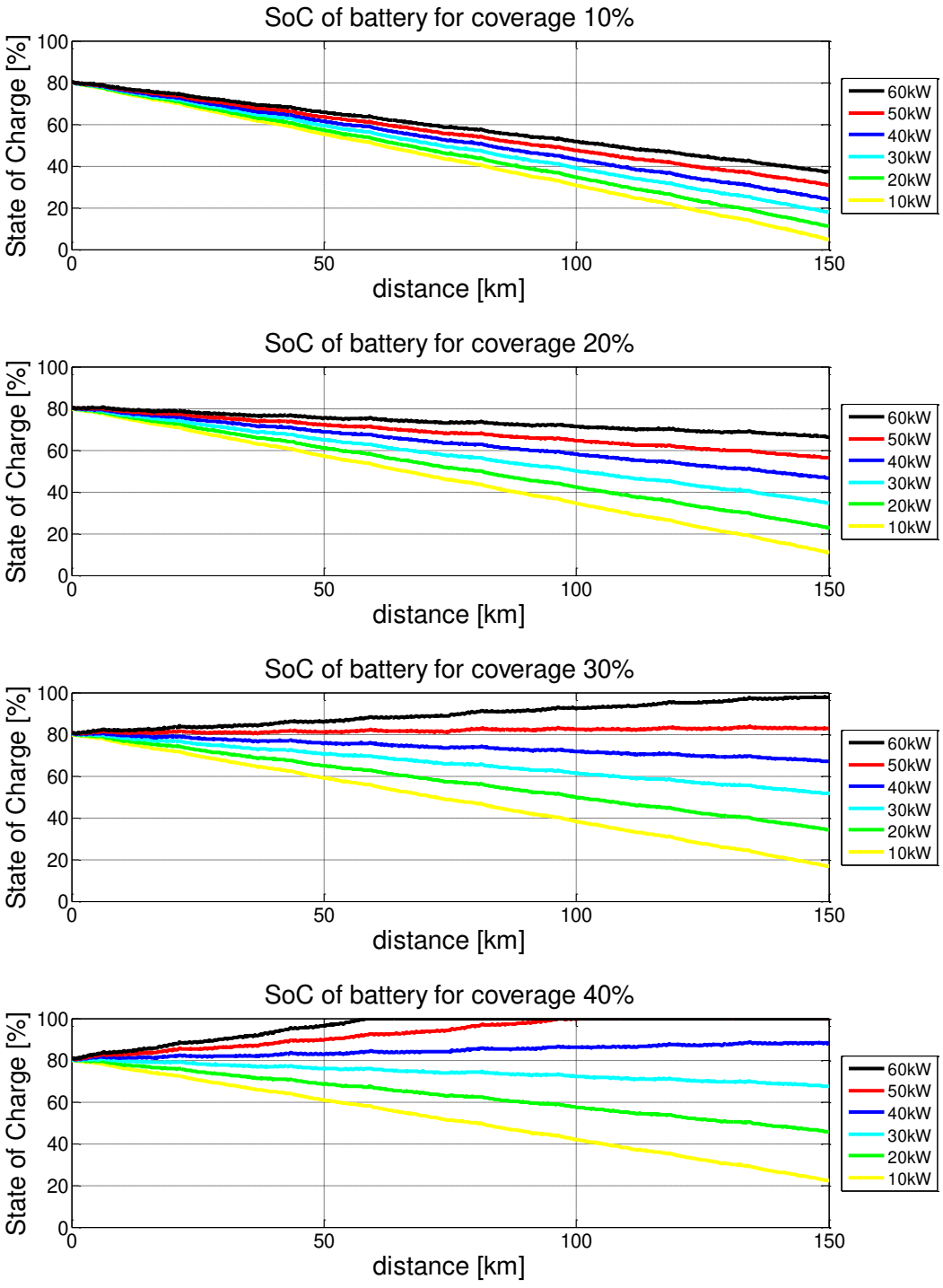

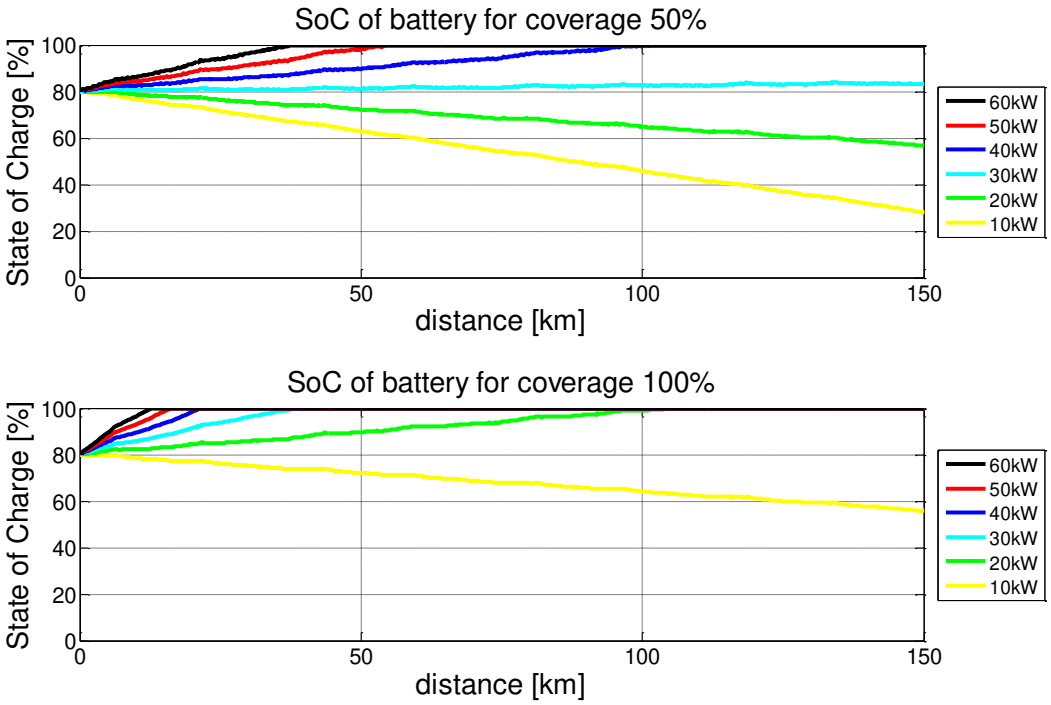

Figure 3.7 - State of Charge of EV battery for different CPT systems

From the previous graphs we can see that for coverage of 10% and 20%, the CPT system provides some range extension. However, as the coverage increases, it is remarkable that for same combinations the state of charge of the battery remains the same or it can also increase. For example, when implementing a CPT system of 30kW with 50% coverage of the road, the state of charge of the battery remains more or less constant. This basically means that the electric vehicle does not require other ways of charging, if it is driving on a road with CPT installed. All the energy required in order to drive is provided from the CPT. Also in some combinations more energy is provided than needed, so the battery is charged further and the vehicle may drive more on roads not covered with CPT.

3.7 Driving Range Extension

From the previous section, we can see that CPT systems can definitely provide an extension of the driving range of the electric vehicles. Now, a calculation of the total driving range for all the possible combinations of the CPT system will be presented. The driving range of the car is taken as the total distance the car can drive as the SOC of the battery drops from 95% to 20%. As already mentioned the driving range for the simulated conditions and battery parameters was 140km. The calculated values presented below can be compared to the driving range of a gasoline fueled cars which is about 500km.

The resulting driving ranges for possible CPT systems (power & coverage) are tabulated below. In some combinations, the state of charge of the battery keeps rising while the car is driving, so we could say that the driving range is ‘infinite’.

Table 3.3 - Driving Range of EV for different CPT systems

Coverage Power	10 %	20 %	30 %	40 %	50 %	60 %	70 %	80 %	90 %	100 %
10 kW	153	165	179	196	218	244	277	320	379	468
20 kW	165	198	248	331	493	934	7254	∞	∞	∞
30 kW	183	250	400	931	∞	∞	∞	∞	∞	∞
40 kW	203	342	898	∞	∞	∞	∞	∞	∞	∞
50 kW	232	488	∞	∞	∞	∞	∞	∞	∞	∞
60 kW	264	857	∞	∞	∞	∞	∞	∞	∞	∞

The results are also represented in the form of a bar diagram, as shown in Figure 3.8. For power range of 10 to 60kW (which is the maximum power used for charging vehicles via fast charging), the driving range for CPT road coverage of 10% to 100% is shown in the diagram. The 100% coverage means that all the road is covered with primary coils. As mentioned before, it is interesting to compare the 140km range of today's electric vehicles to the 500km range of today's petrol-fueled vehicles (values also shown at the diagram).

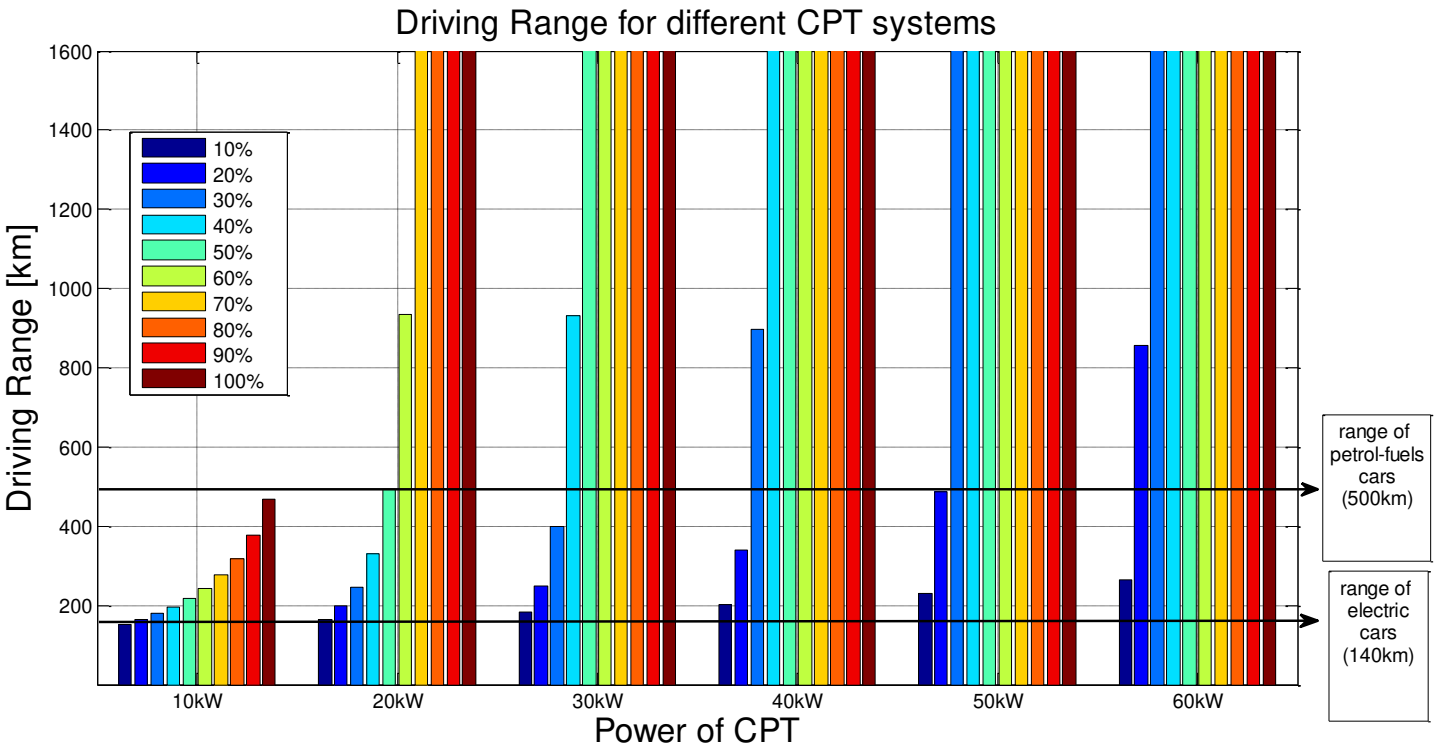

Figure 3.8 - Driving Range for different CPT systems

We can observe that in case of CPT power of 10kW, there is an increase in the driving range, however only with 100% coverage, the range becomes comparable with conventional cars. For coverage of more than 50%, a very high driving range can be achieved for power greater than 20kW.

Combinations, such as 60% & 20kW, 40% & 30kW and 30% & 40kW provide a range double than what is today's conventional driving range.

The combinations for low power and smaller coverage are also presented in a separate diagram.

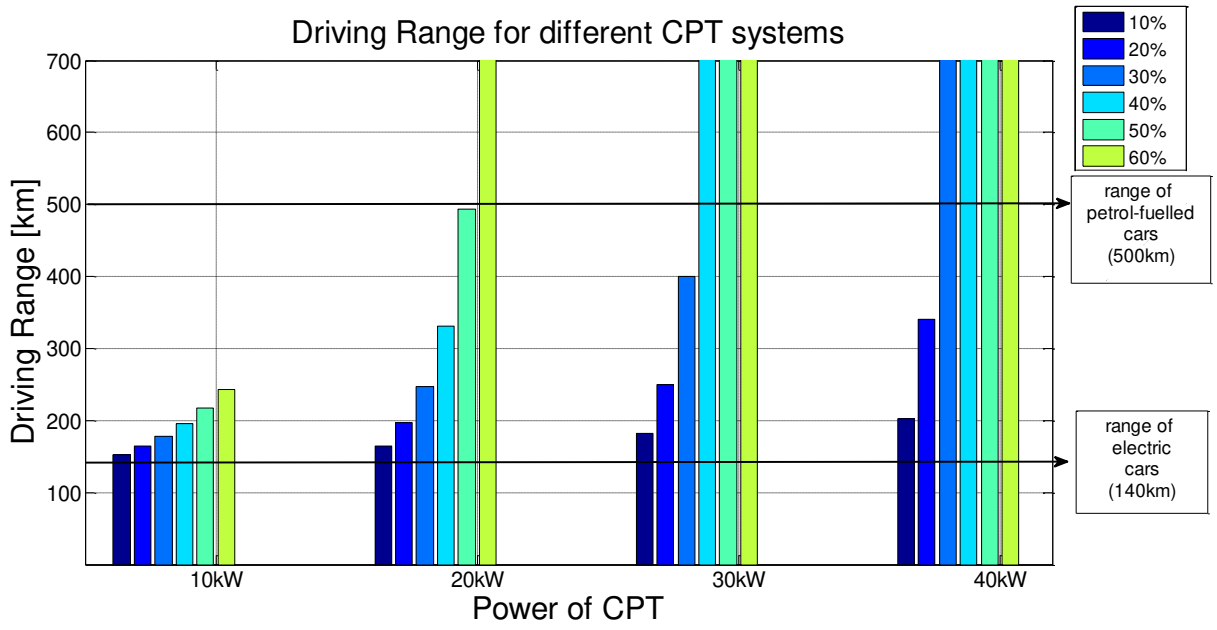

Figure 3.9 - Driving Range for different CPT systems (zoom)

The combinations where the electric vehicle achieves a range of 300km or 500km or an 'infinite' range are shown in Figure 3.10. It is important to mention again that by 'infinite' driving range, it means that the battery is being charged during driving on this road ($SoC_{final} > SoC_{initial}$). As a result, in case the car would be driving only on road with CPT, then the range would actually be infinite. However, in this study it is assumed that the highways are covered with CPT as they are mostly used, but the other urban or rural roads are not.

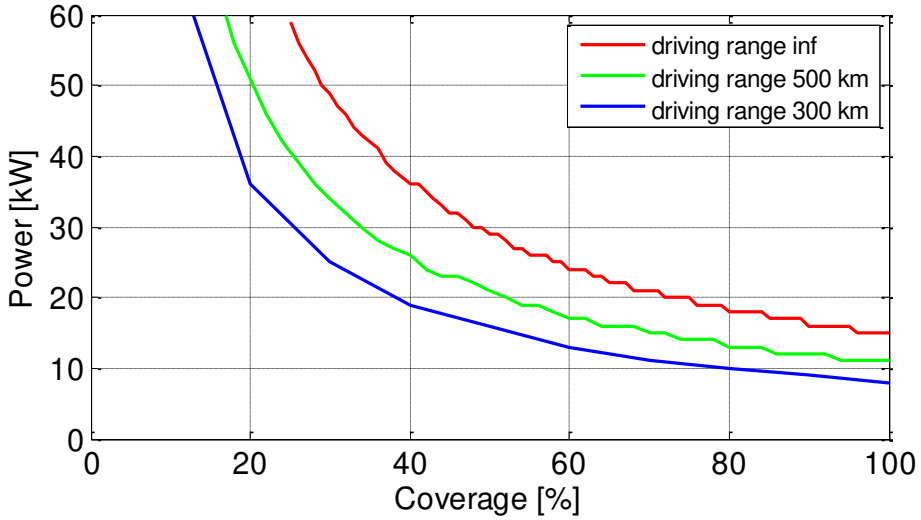

Figure 3.10 - CPT system specifications depending on driving range

The results for many battery sizes and driving ranges can be found in the Appendix A.

3.8 Length & Distribution of CPT segments

In the simulations presented before, the road was considered to be divided into sections of 1 km, so the segments of primary windings cover a length of 100m, 200m, 300m etc. for coverage of 10%, 20%, 30% etc. leaving in between 900m, 800m, 700m etc. of free road respectively. At this point, it will be investigated how the distribution of the CPT segments over the road affects the charging of the battery and the driving range. The 'period' of the road segments are taken as 1, 2, 3, 5, 10, 50 and 150 km. The concept of a varying distribution of the primary windings was previously explained in Chapter 1.4, page 21. To explain it further, for a 'period' of 10 km, it means that for every 10 km the corresponding coverage is covered with CPT (1 km for 10%, 2 km for 20%, 7 km for 70% etc.) or for 30 km, it is 3 km for 10%, 6 km for 20%, 9 km for 30% etc. This road configuration continues for several kilometers. This means that the length of each segment varies, but also the space in between the segments varies. However, in the simulations, the total energy provided was the same no matter the distribution of the primary CPT windings. In that way we are to able to compare the configurations and safely draw conclusions.

In the bar charts below, the driving range for a specific power (10-40kW), for various coverage and 'period' of CPT (1-150km) is plotted.

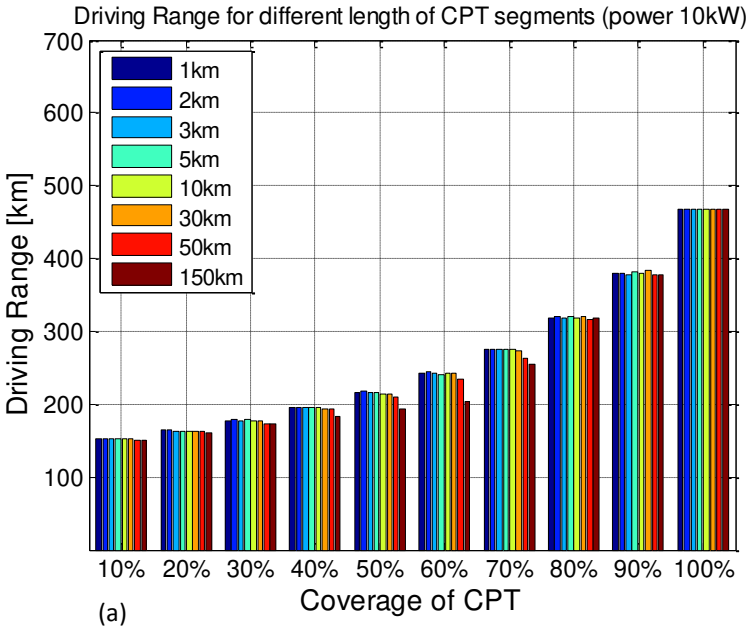

(a)

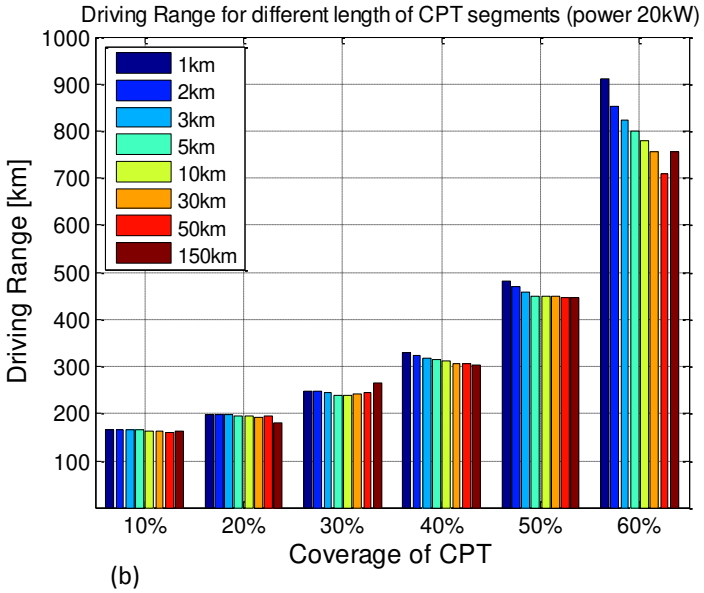

(b)

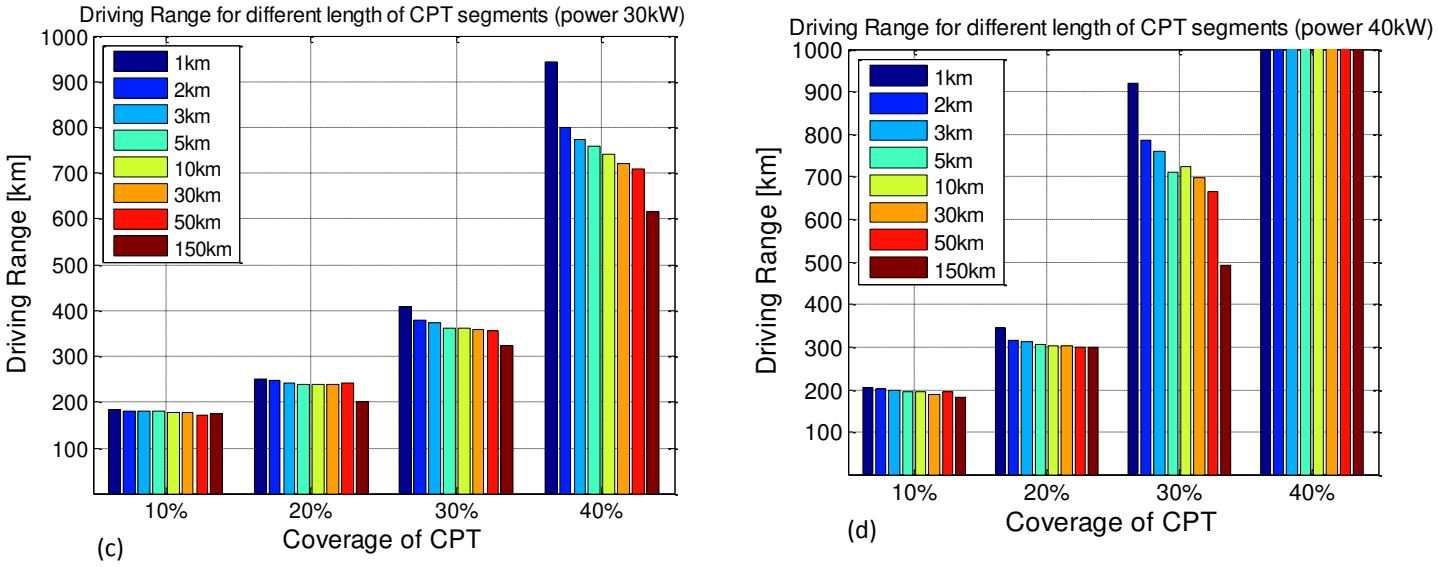

Figure 3.11 - Driving Range for different distribution of CPT segments

Overall, we can see that the distribution of the CPT segments affects the total range only at high power or at high coverage. This happens if the road covered with CPT is long, so at some point the battery reaches its maximum state of charge and the energy provided by the CPT cannot be stored. On the other hand, if the distance between the CPT segments is also quite large, then the battery of the EV might reach the minimum state of charge before the vehicle reaches the next CPT segment. Of course the initial state of charge of the battery plays an important role for these simulations. However, as the total driving range of the vehicle is to be calculated, a full battery should be taken into account, so the initial state of charge was considered as 95%.

In the next figure, we can see the changes in the state of charge of the battery for CPT of 30kW and 40%, as in the fourth column of Figure 3.11 (c). We can clearly see why some energy provided by the CPT cannot be absorbed from the battery for very long segments, as it reaches the maximum state of charge.

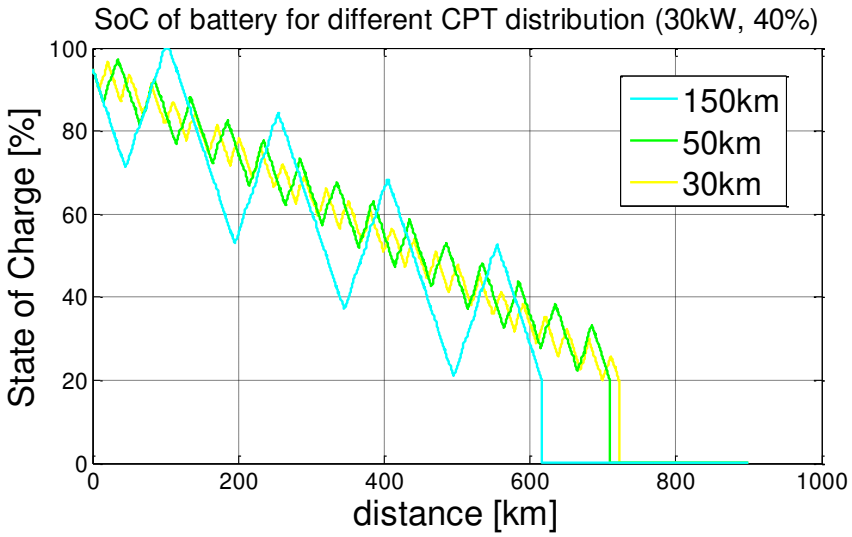

Figure 3.12 - State of Charge of EV battery for different distribution of CPT segments

As a result, there should be a balance between the energy consumed from the vehicle at the distance in between the segments and the energy provided from the CPT at each segment.

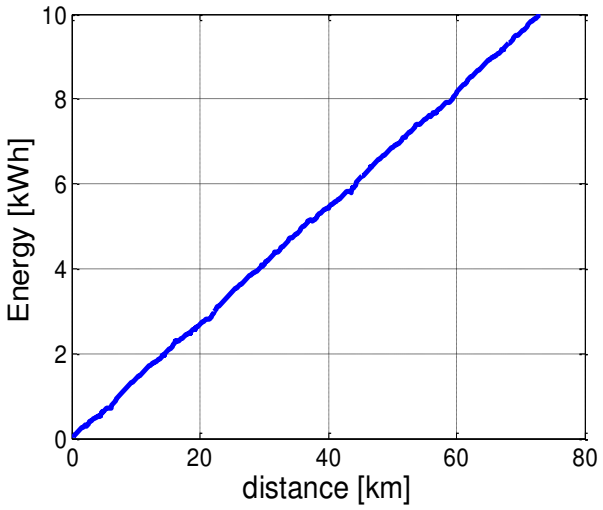

Figure 3.13 - Energy Consumption of EV

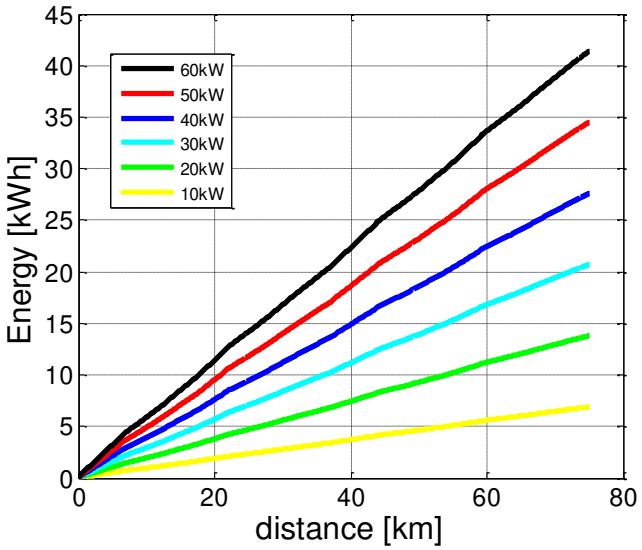

Figure 3.14 - Energy Production of CPT system (100% coverage)

The average energy consumption is 130Wh/km for driving on highway. Also, the average energy production from the CPT system varies between about 100Wh/km for the 10kW CPT to the 555Wh/km for the 60kW CPT. We see again that depending on the desired result, a different configuration of a CPT system can be designed. For example, we can see from Figure 3.13 that an EV needs about 8kWh in order to drive 60 km. Then, we can go to Figure 3.14 and see the length and the power of the CPT which can provide this 8kWh.

To conclude, for reasonably long CPT segments (up to some kilometers) the driving range remains more or less the same. As a result, the distribution of the CPT segments is not an important parameter as far as the driving range is concerned. In any case, having short segments provides that the energy from the CPT system would be stored to the EV battery.

3.9 Decrease of electric vehicle's battery

3.9.1 Driving range for highway driving with CPT system

Driving on a CPT system provides range extension, with many combinations of CPT coverage and power range greater than one of today's conventional vehicles can be achieved (see Figure 3.8). A consumer may not require such a high driving range, considering the high cost in order to provide it. So, one main idea is to decrease the battery size of the vehicle, so as to diminish a great part of the cost of electric vehicles.

Next, simulation in which there is a decrease of the size of the EV battery will be presented.

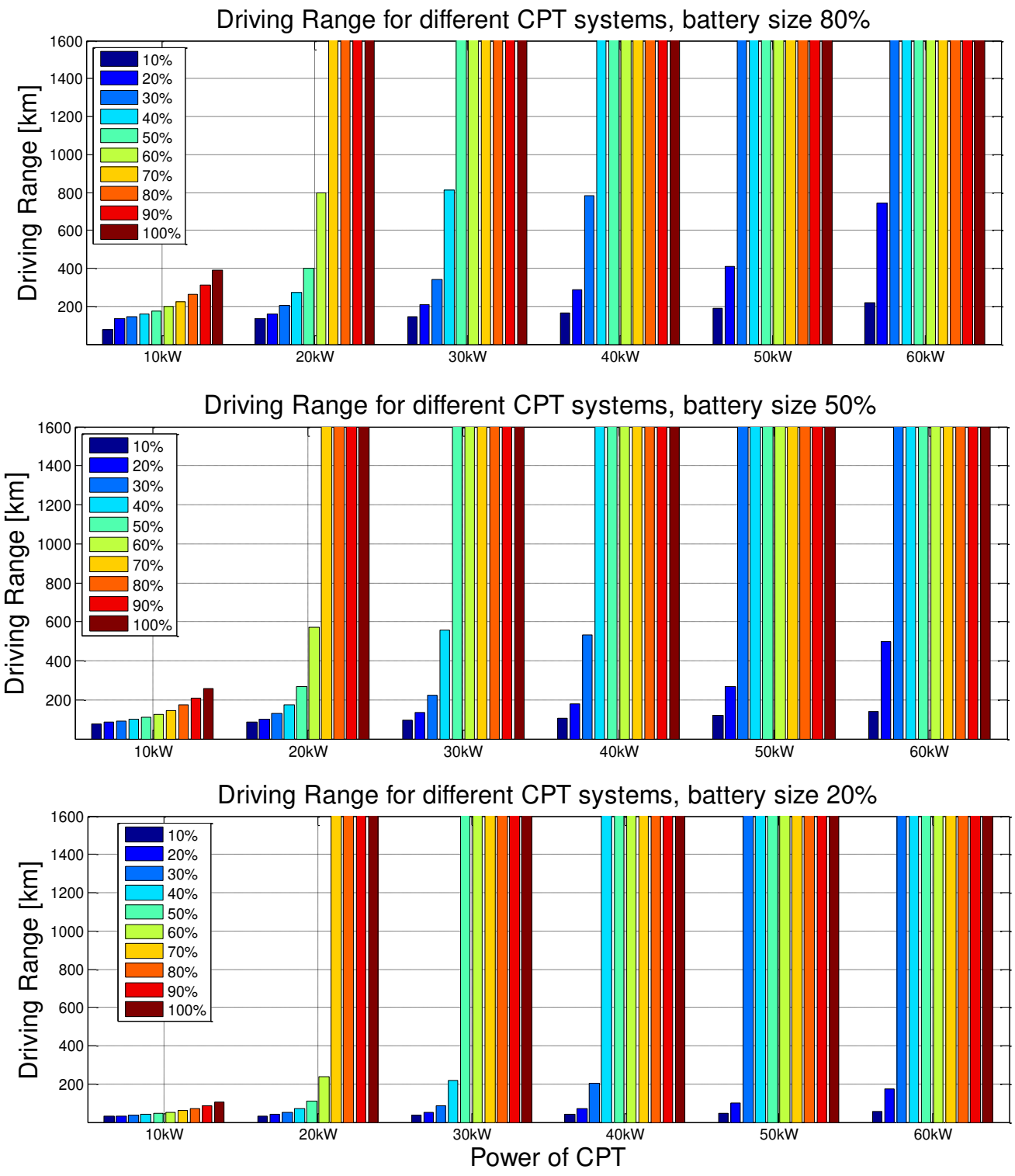

Figure 3.15 - Driving Range for different EV battery sizes

We can see from the figures above that in case of a great implementation of CPT, the battery of the electric vehicle can be decreased to sizes as low as 20% of the size of an electric vehicle today. In this way, the total cost of the electric vehicle will decrease dramatically and the driving range can also be

increased to even more than the driving range of conventional cars. Also, the total mass of the vehicle will be reduced which may decrease the consumption.

Depending on the driving range that is to be achieved, the alternative combinations of CPT systems can be defined. The case of a driving range of 500km for different battery sizes is presented in the next set of graphs. Here to mention again that battery size of 100% is 24kWh.

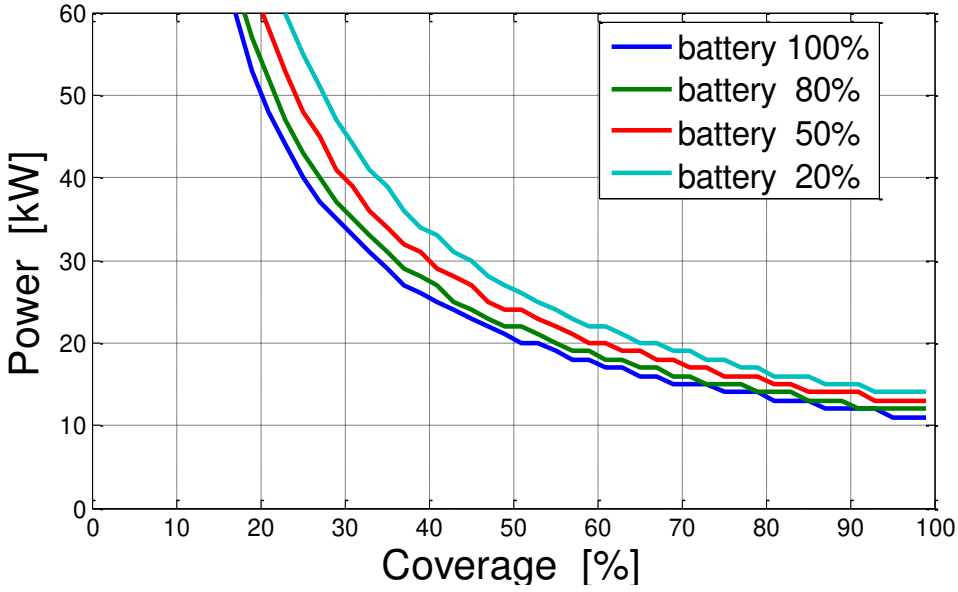

Figure 3.16 - CPT system specifications depending on battery size for 500km driving range

We can see that for smaller coverage the battery size has a great effect on the amount of power needed. This is logical, as the distance not covered is greater and there is need for larger reserve energy from the battery. As the coverage increases, most of the time there is some constant power supplied by the CPT system and the variations of the state of charge of the battery are smaller. For small coverage, the time where the car is supplied only from the battery is longer, so the battery should have enough energy stored to drive the motor.

As we can see, when the battery size is smaller, the charging/discharging process is faster. The charging rate should be considered in order to decide on the length of the CPT segment and the discharging rate should be considered in order to decide on the distance between the segments. However, the time one vehicle is on a CPT segment depends greatly on its speed, which can be different for each passing vehicle. For this research, the aforementioned highway driving cycle was taken as the driving cycle, although in reality this cannot represent the behavior of every driver.

As the battery becomes smaller, then the distribution of the CPT segment becomes more important. If the segments are quite long, then the battery will reach the maximum state of charge sooner and the battery will not absorb the remaining CPT power. Also, if there is a long distance between the segments, then the battery will become empty in a shorter period of time. In order to get an idea of the aforementioned issues, simulation results for different distribution of the system for 50% and 20% battery size are presented below. For small coverage percentages, the differences are not significant.

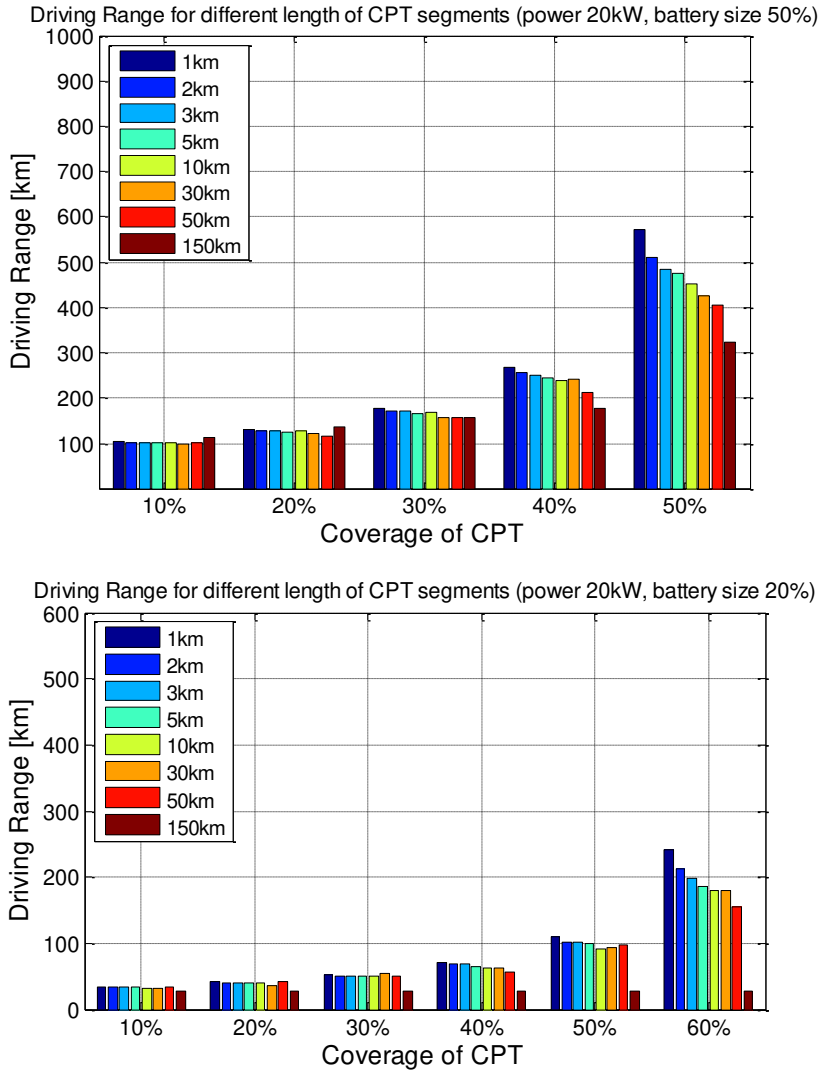

Figure 3.17 - Driving Range for different distribution of CPT & different battery sizes

Overall, we can see that only in case of very long CPT segments the total efficiency of the system drops. By choosing segments of few kilometers long, the energy is transferred and can be used by the electric cars to the fullest.

3.9.2 Driving range for urban driving without CPT system

When the battery size of the electric vehicle is decreased, the driving range of the EV on roads without CPT installed should be investigated. The CPT system was proposed to be installed on highways. However, the battery of the EV should still have the capacity to drive a realistic distance on roads within the city where there is not CPT installed.

By simulating the Urban Dynamometer Driving Schedule (UDDS), the driving range of the electric vehicle with decreased battery can be calculated.

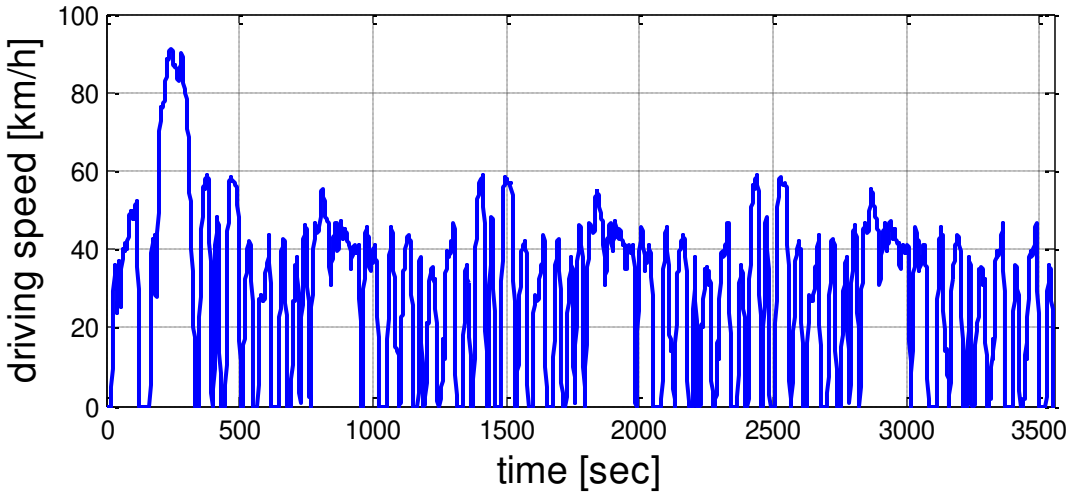

Figure 3.18 - Urban Dynamometer Driving Schedule

Table 3.4 - Driving range for UDDS for various EV battery sizes

Battery size	Driving range
100%	176 km
80%	143 km
60%	110 km
50%	92 km
40%	74 km
20%	36 km
10%	17 km

Keeping in mind that ¾ of the trips have length less than 20km (see Figure 2.6). A battery with a small capacity is able to cover this distance.

Moreover, CPT systems can be also installed in parking spaces are under the road at traffic lights in order to support the electric vehicle inside the city.

3.10 Conclusions on CPT segment power, length and distribution

There are some physical limitations on the size of the primary coils concerning the length and the power capability, as presented in Chapter 1. However, by placing the primary windings one next to the other a CPT segment is created. In this chapter, the coverage and the power of the CPT segments were estimated for achieving driving range extension and/or battery size decrease. The results for various driving ranges and battery sizes can be found in the Appendix A.

As far as the segment length is concerned, there are many general considerations to be taken into account. Firstly, the total length of the CPT system depends on the required coverage. For the given combination of driving range and battery size, the coverage percentage should be chosen such that the power transfer remains in realistic values. For example, in order to achieve 500km range and 50%

battery decrease, coverage at least 50% is proposed to keep the power to realistic values of 24kW per vehicle or lower.

The length of each CPT segment should be small and the segments should be well distributed over the road in order to optimize the efficiency of the system. For the battery of the vehicle, small shallow cycles are better than deep cycles, so smaller segments are more beneficial for the health and life of the battery (Chapter 1.6). Also, the simulations showed that in order to maximize the range, there should be a balance between the energy consumed by the car at the space without CPT installed and at the power produced by the CPT and absorbed by the EV battery.

From a general point of view, if the CPT segments are distributed on the highway (e.g. 1km of CPT and then 1km without CPT etc.) and are not very densely placed (e.g. 10km of CPT and then 10km without CPT etc.) then the usability from the consumers/drivers would be maximized. This is stated in respect to the fact that one driver might use the highway just for some kilometers. It is not reasonable if by chance this part of the road is not covered by CPT and the battery's state of charge decreases rapidly.

However, a greater distribution of the segments requires longer cabling that adds cost and losses to the system. Moreover, from the installation and maintenance point of view, it might be more beneficial that the CPT segments are more densely placed over the highway.

Another option is that the power/coverage/distribution of the segments could not be the same along the highway, but in some areas they could vary. At points where vehicles are entering the highway and they need high power for accelerating, the power of segments could be higher. Also in case the road has an inclination and the power consumed by the car is higher, the CPT should provide more power. On the other hand, on parts of the highway with negative inclination or at highway exits where less power is needed or there is power production from regenerative breaking, there is no need of CPT charging (or CPT with less power can be installed).

Another issue could be the system expandability. In case of lower coverage, more CPT segments can be easily added on a later time, when for example the number of EVs increases.

To conclude, in this chapter the configuration of the CPT system was investigated, depending on how efficiently the transferred power is used by the electric vehicles. Further on, the production of the power which is transferred by the CPT system will be investigated. The renewable energy needed to supply the CPT system will be calculated and some further remarks on the sizing and the distribution of the CPT system will be made.

4 Microgrid components and Cost estimation analysis

In this chapter a microgrid consisting of solar, wind energy and storage which will supply power to the electric vehicles via the contactless power transfer system will be studied. A brief overview of the existing microgrid systems will be presented, as well as some information about different topologies. Data for solar irradiance and wind speed and the power demanded by the electric vehicle will be presented. A discussion on the operation, the power and the cost of each component will take place. The models for sizing and for finding the optimum sizing of the microgrid will be introduced.

4.1 The microgrid concept

A cluster of distributed generators, loads and energy storage devices create the so-called microgrid. The distributed generators may be renewable energy sources (solar panel, wind turbines, fuel cell units) or also small diesel generators and microturbines. The loads are usually domestic loads for example of a small neighborhood. As electric mobility is gradually growing, electric vehicles are also an important load of a microgrid. All these subsystems, which are connected to each other, are controlled by a central energy management system.

Microgrids can provide a way to implement more renewable energy sources in the energy mix. Lately this becomes more and more important as there is a great effort to cope with the environmental impacts of coal-fired generation which is highly related to CO_2 emissions.

Microgrids have the great advantage to have a control strategy depending on the specific load and the specific energy sources. In this way the energy use of the system can be optimized and we can cope with the uncontrollable nature of the renewable energy sources, such as wind and solar energy. This makes microgrids the first step to the future smart-grid concept.

A microgrid can operate in parallel with the main grid, as a grid-connected system, as an autonomous stand-alone system, or at a transition between the two operation modes. It can be single phase or three-phase, AC or DC. The configuration is decided according to the loads and sources that the microgrid consists of. The control strategy is then different for the different operating modes. The goal when designing a microgrid is to provide energy in a safe, reliable and cost efficient way and to integrate as many renewable energy sources as possible.

There is much research taking place on the distributed generation and the microgrids. Many pilot systems have been already built worldwide in an attempt to discover, analyze and overcome the technical challenges of such systems.

In the Netherlands a microgrid has been built at Bronsbergen Holiday Park near Zutphen, 100km to the west of Amsterdam. This park consists of 208 holiday homes and the peak load is 150kW. The 108 of these houses have a PV system installed on the roof with a peak generation capacity of 315 kW. As a storage facility, there are two battery banks in the system in order to supply the load when there is no

generation from the RES system. It is connected to the medium voltage and the controller of the system measures the active/reactive power exchange of the microgrid and the main grid. [24]

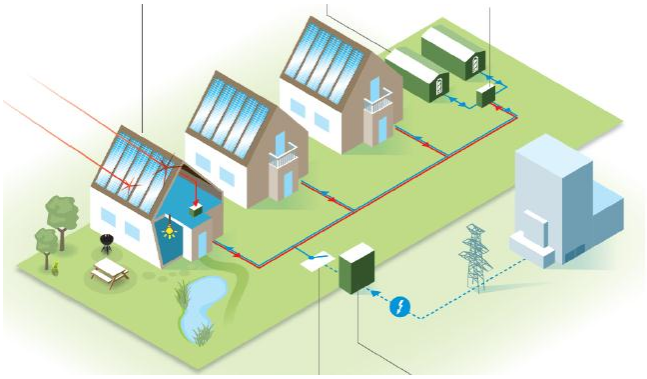

Figure 4.1 - Domestic Microgrid at Bronsbergen holiday park NL [24]

Another microgrid in the Netherlands is created at the Hoogkerk near Groningen by KEMA, the Dutch energy research center ECN, software company Humiq and utility Essent. This microgrid, called "PowerMatching City", consists of 25 houses with PV systems installed at the roof tops, equipped as well with micro cogeneration units, hybrid heat pumps and smart appliances. Some of the households have also electric vehicles, so the load consists mainly from the domestic use and the need for charging the electric vehicles. Power is also produced by a wind turbine and a gas turbine. Lately, there has been a plan to extend this microgrid by adding more electric vehicles. [25]

4.2 Microgrid for powering the electric vehicles driving on highways

In this study a microgrid for providing power to the Contactless Power Transfer Systems installed at highways will be investigated. The main concept is to install solar cells and wind turbines near the highway and have a storage facility in order to store the excess energy and provide it when the renewable energy sources do not produce enough power. In this way, a sustainable microgrid will be created which will power and charge the passing electric vehicles. As only green energy will be used, the environmental impacts and the CO_2 footprint of transportation are minimized.

The 'SolaRoad' or in other words a road that generates solar electricity is a new concept currently being developed by the TNO. This road will have integrated solar cells on its surface in order to produce power from sunlight. As this produced power is aimed to be used for powering electric vehicles, a combination with contactless power transfer would be ideal. The top layer of the road should be transparent in order to let certain wavelengths pass and reach the solar cells. By using high-grade materials and controlled production, TNO claims a road of consistent quality, durability and less long-term maintenance. A pilot project for implementing this concept on a cycle path is already planned. Also some tests have been done to prove that the top glass layer is strong enough to protect the solar cells below. [26]

Figure 4.2 - SolaRoad by TNO [26]

As the CPT system is installed in segments, the road is not needed be covered 100% with primary windings. This makes it possible to integrate the 'SolaRoad' concept at the parts of the road that are not covered by the CPT. There is also some available space in between the primary windings of the several lanes, which can also be used for installing these innovative solar cells. In the analysis that will be presented in the next chapters, the installation that is needed in order to power the electric vehicles will be investigated to get a further understanding of the required infrastructure.

Solar panels and wind turbines next to the highways have already been installed in the Netherlands as well as worldwide. This proves that from an infrastructure point of view it is technically possible and within the legal framework.

As far as solar energy is concerned, a photovoltaic energy system (220kW) has been integrated at the sound barriers at A9 highway in the Netherlands on 1998 by Nuon International/ Duurzame Energie. Similar projects have also been made at other countries like Switzerland, Germany and Denmark. Also, new technology of semi-transparent glazing PV modules is reported in literature that could be used as sound barriers for highways [27].

Another innovative project for sustainable highways is the 'Sustainable Energy Highway' at A15. The project plan mainly consists of installing 20 wind turbines with average power of 2.5 MW along the road. Moreover, solar panels at the rooftops of buildings nearby are also planned to be integrated with an estimated power of 5MWp. This project includes also a campaign for promoting electric vehicles. [28]

Figure 4.3 - Sustainable Energy Highway A15

We can see that there is extensive research on the transition to electric mobility and also in a transition to sustainable and green highways. If the power produced near the highways is to be directly used by the electric vehicles, then the way to achieve that is by installing Contact Power Transfer Systems through which the passing electric vehicles will be powered or charged.

4.3 Distributed Generators

As already mentioned the microgrid proposed in this thesis consists of energy generation from solar panels and wind turbines. In this chapter the key issues of these distributed generators are presented, as well as some statistics concerning the solar irradiance and the wind speed in the Netherlands.

4.3.1 Photovoltaic System

A photovoltaic system consists mainly of the PV panels which are connected in series or in parallel, in order to form PV arrays depending on the required power and voltage output of the system. Most PV systems have a maximum power point tracking system (MPPT), so the system can operate always at the maximum power point, increasing the overall efficiency.

The power produced from the photovoltaic system depends mostly on the solar irradiance at the geographic area where the panels are placed. However, other factors as the module temperature and the tilt angle affect the generated power as well. Different kinds of losses exist, like the maximum power point losses and the cable losses [27]. In this thesis data for the solar irradiance are used in order to determine the solar power produced at every point in time. A uniform efficiency of 12% is considered as far as the photovoltaic system is concerned (the efficiency of the inverter is not included in this value).

Solar irradiance has a great variation throughout the year, reaching its peak during the summertime. However, the sun reaches its peak daily at around 12.00; however the amplitude of this peak is different depending of the year season. Some statistical data withdrawn from the measurements of the irradiance for the years 2001 to 2010 will be shown next, in order to obtain a clear view of the seasonal variations of solar power (data from Cabauw, KNMI [29]).

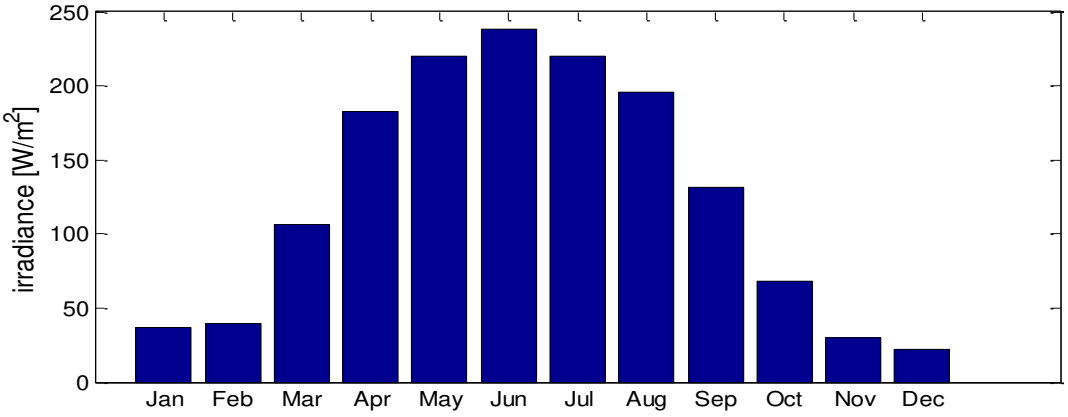

Figure 4.4 - Monthly average values of solar irradiance (2009)

From the Figure 4.4, it can be clearly seen that the greatest solar power can be produced during the months of May, June and July and the smallest in November, December and January. There is a large difference in the power production, as the same system produces just a small fraction of power (about 15%) of the capacity during the winter period. This is the major disadvantage of solar power.

Moreover, there is not a uniform power production during the day as well. There is no power production at night and there is a peak at noon. A positive point is that for different kinds of load demand (industries, households, transportation, etc.) most of the power is needed during the day. Unfortunately, the peak of the demand does not occur at 12.00, so it does not coincide with the peak of the solar irradiance.

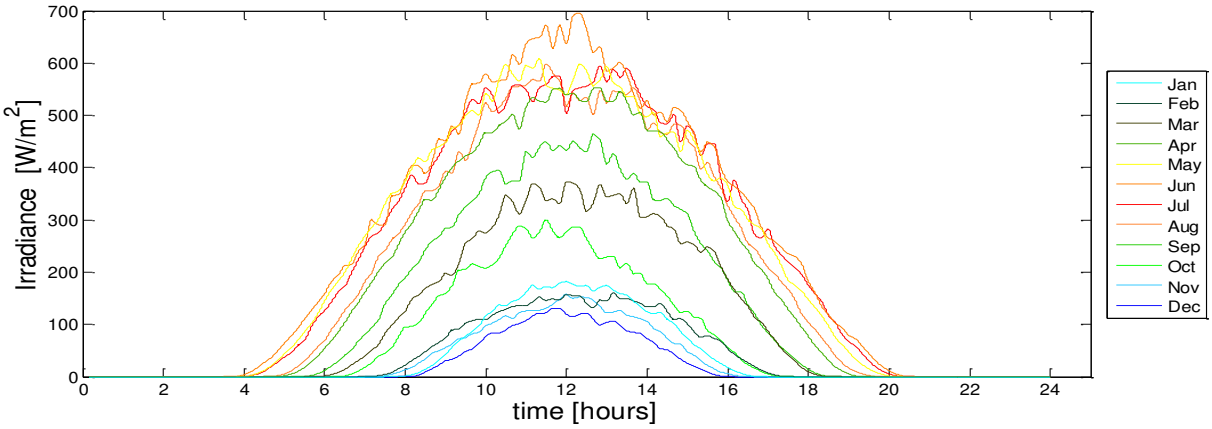

Figure 4.5 - Monthly daily average of solar irradiance (2009)

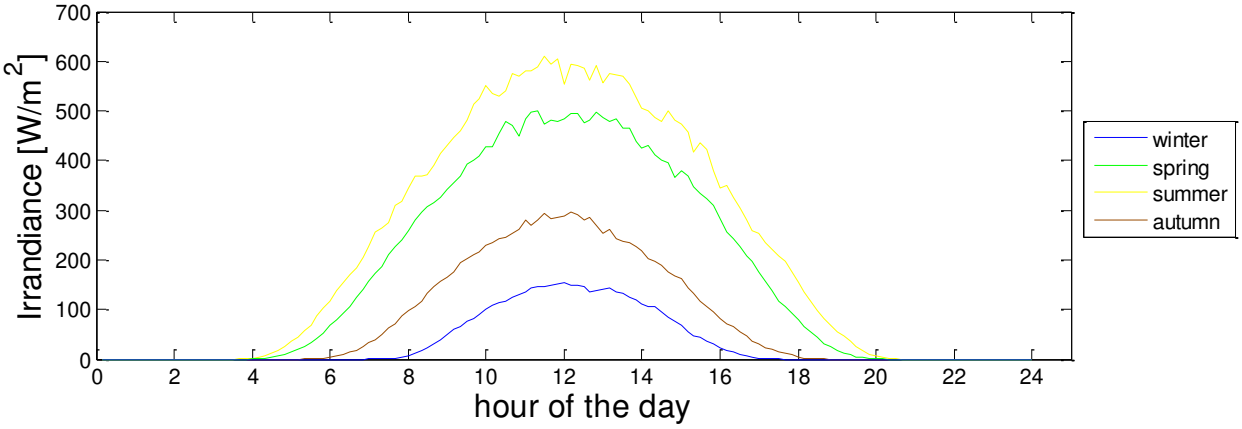

Figure 4.6 - Seasonal daily variations of solar irradiance

A measure to see how the energy production of solar systems varies through the years is the capacity factor.

$$capacity\ factor = \frac{Energy_{produced\ for\ one\ year}}{Power_{rated} \cdot 8760} = \frac{P_{average}}{P_{rated}}$$

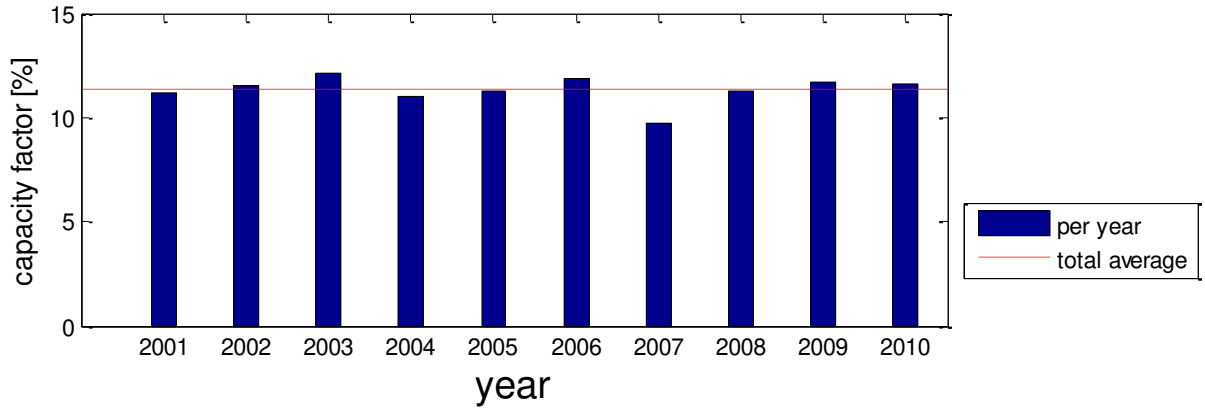

Figure 4.7 - Capacity factor for solar energy production

Depending on the solar irradiance the system produces more or less power. The variation between the years cannot be considered very significant and the average capacity factor for a solar system in the Netherlands was calculated at about 11.3%.

In order to get an overview of yearly production of power from a solar system, the figure below shows the results for the power produced by a solar system. The 1 per unit value equals the peak (maximum) production of the system.

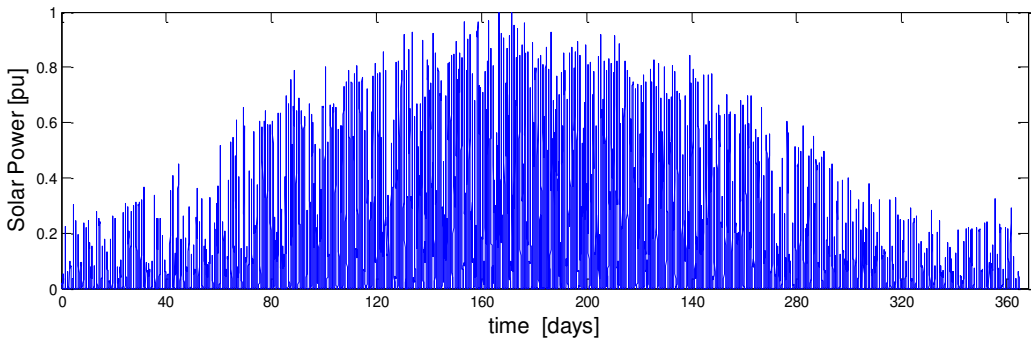

Figure 4.8 - Power produced from solar system (2009)

As during the night there no power production from the PV system, more than half of the time (about 5000 hours per year) the system produces zero power. The distribution of the solar power production for the rest of the time can be seen in the histogram below.

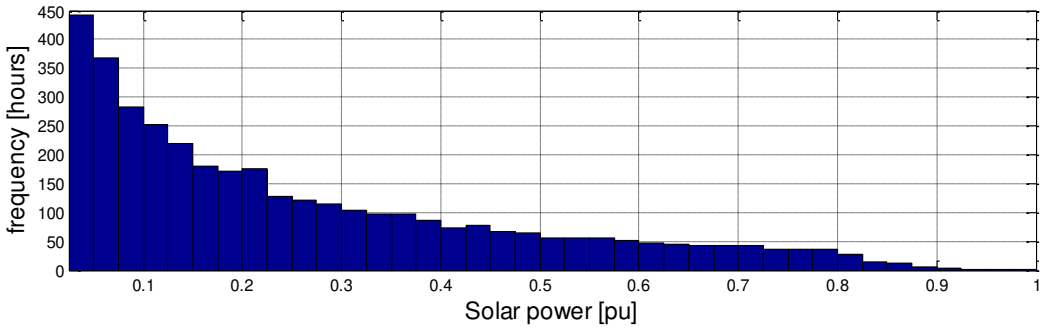

Figure 4.9 - Frequency of power produced from solar system (2009)

We can see that the maximum power (1pu) that be only produced just during a very small period of time. Most of the time there is no production (57% of the time) or up to 0.1 pu production (15% of the time).

In general, many solar systems have already been installed on a larger or on a smaller scale, grid-connected or stand-alone. As already mentioned implementation of solar panels next to the highway is not a new concept and some projects have already been completed with installing solar panels on sound barriers.

4.3.2 Wind Turbine Generators

In this sustainable microgrid wind turbines will also be included. The power produced from wind turbines greatly depends on the wind speed, so firstly some analysis concerning the data for the Netherlands will be presented [29]. The data are for altitude of 10m. Wind speed does not follow a precise pattern within the year as solar irradiance. However, it was observed that there are some periods of the year with stronger wind. To be specific, there is more wind during colder months (November-March) and less wind during warmer months (June-September).

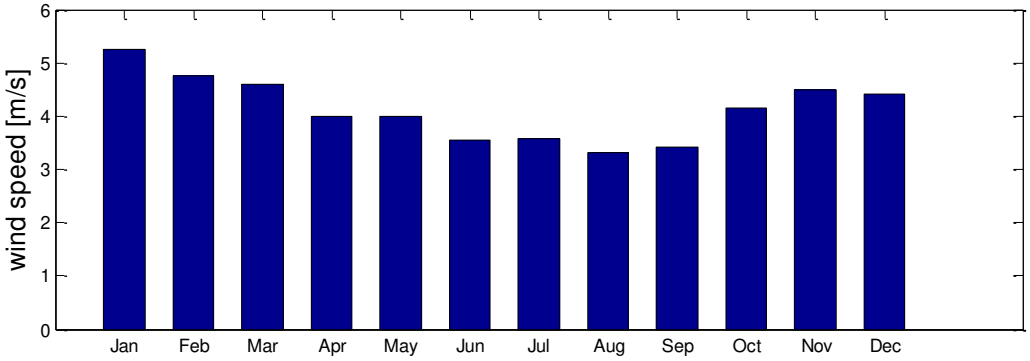

Figure 4.10 - Total average wind speeds per month (2001-2010)

However, within the years there are great variations. We can see that there are some peaks at specific years. For example, January is considered a month with high winds, although in years 2006 and 2010 this was not the case.

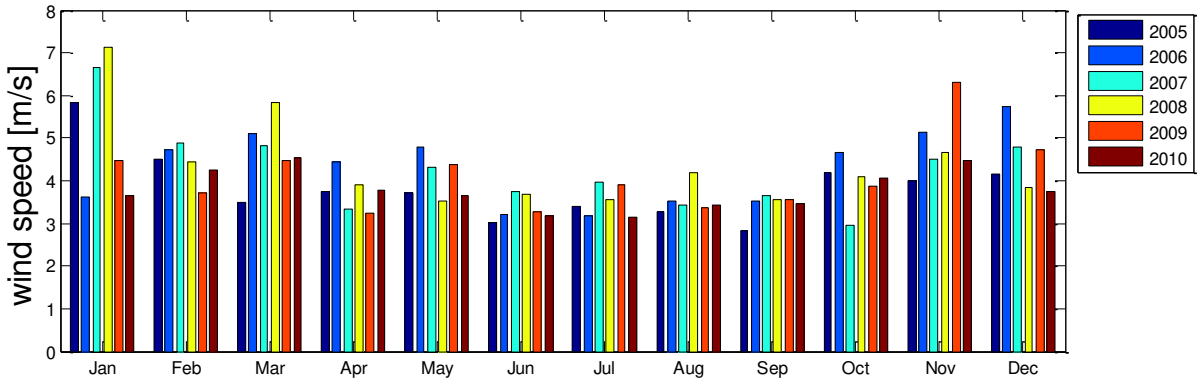

Figure 4.11 - Average wind speeds per month (2005-2010)

The wind speed variation during the day does not show such a precise pattern as in solar power; however there is also a trend of higher wind speeds between 12-16 pm. Also we can see that during winter the wind speed is more flat during the day, where during the other seasons and especially during the summer there are more variations during day and during the night. This figure is of the data of 2010. For other years the peak may be different, however the variations between maximum and minimum wind speed during the day remain similar.

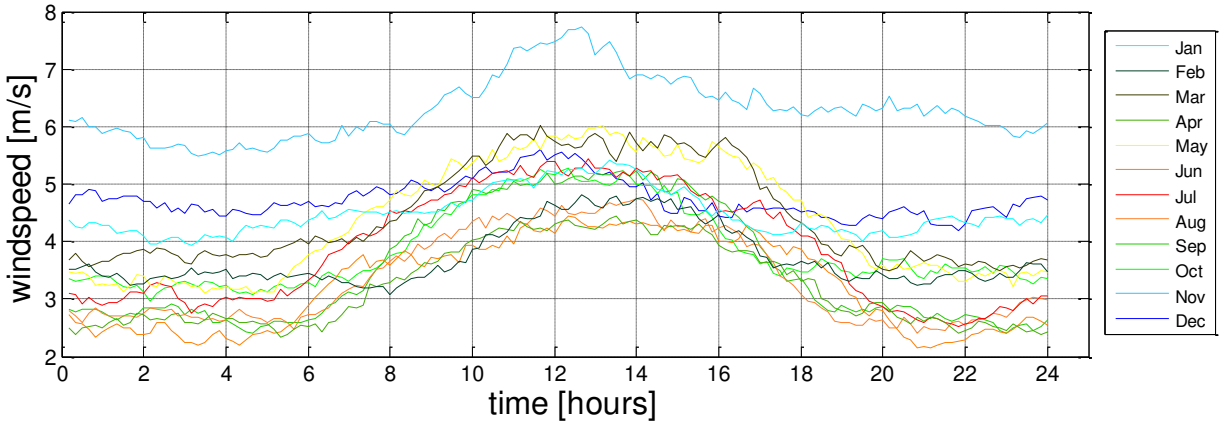

Figure 4.12 - Monthly daily variations of wind speed

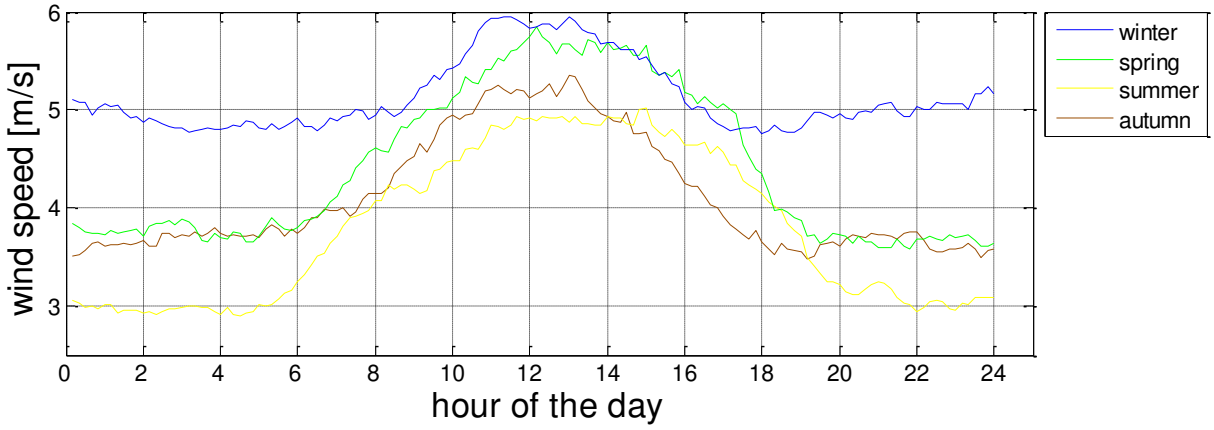

Figure 4.13 - Seasonal daily variations of wind speed

In order to calculate the power that is produced from the wind turbines that would be installed, first a correction of the wind speed for the altitude of the tower of the wind turbine. For this calculation the following formula will be used [30].

$$V(z)\Big/V(z_r) = \ln\left(\frac{z}{z_0}\right)\Big/\ln\left(\frac{z_r}{z_0}\right)$$

Where,

z_r, the reference altitude ($z_r = 10m$ for this thesis)

z, the new altitude

z_0, the surface roughness length ($z_0 = 0.075$, value that corresponds to areas with crops and few trees, typical landscape near Dutch highways)

$V(z)$, the wind speed at z altitude

$V(z_r)$, the wind speed at z_r reference altitude

Next, the power curve of the wind turbine has to be determined which shows the power produced depending on the wind speed. In this thesis the following power curve was used with a nominal power of 2MW.

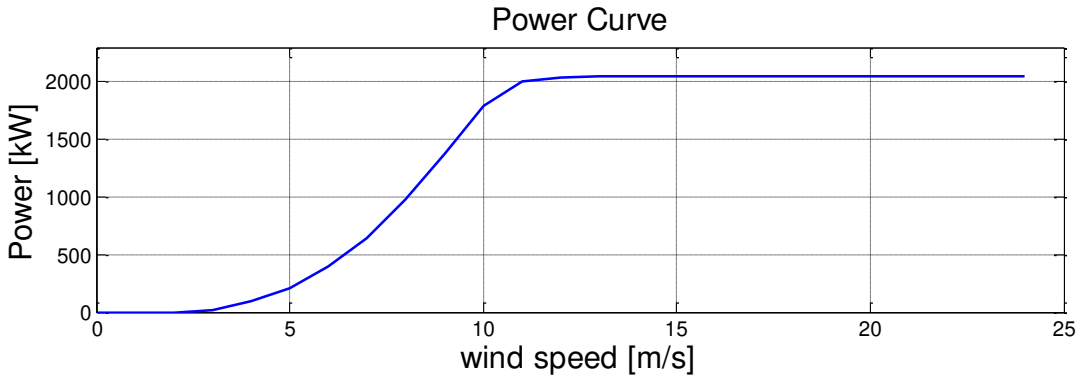

Figure 4.14 - Power curve of wind turbine

Table 4.1 - Characteristics of the simulated wind turbine

Rated power	2050 kW
Cut-in speed	3.5 m/s
Rated wind speed	14.5 m/s
Cut-out speed	25 m/s
Rotor diameter	82 m
Hub height	59/69/80/100 m

One way to estimate the yielding of the wind turbines is to calculate the capacity factor. By using the data for the Netherlands, the capacity factor for the years 2001 to 2010 is calculated in order to investigate the variation of wind power production the past 10 years.

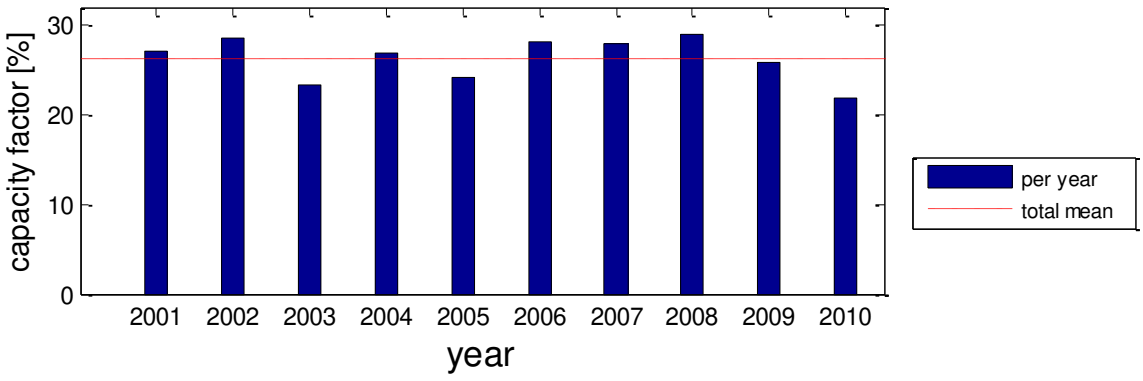

Figure 4.15 - Capacity factor for wind energy production

For the year 2009 the power production of a wind turbine is shown below where the great variations of the output power can be observed.

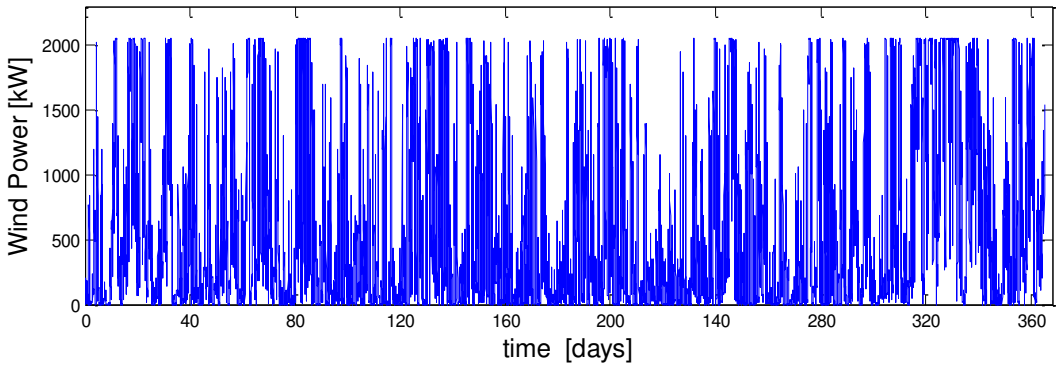

Figure 4.16 - Power produced by one wind turbine (data for 2009)

In order to get an idea of the frequency of every level of the produced power, the histogram of the previous graph is also presented.

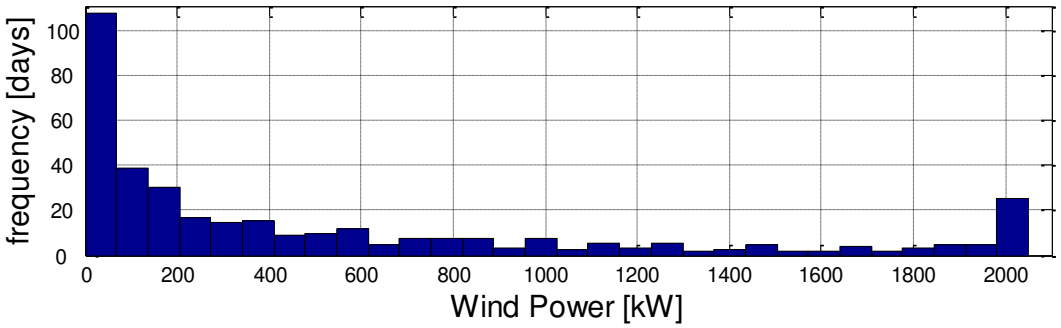

Figure 4.17 - Histogram of power produced by one wind turbine (data for 2009)

For placing the wind turbines next to highways, there are some guidelines to be met. The installation of wind turbines is allowed, provided that the distance to the road is half the rotor diameter and at least 30m in case the diameter is less than 60m. Additional safety measures are needed for placement next to interchanges or parking places (Rijkswaterstaat, Ministrie van Infrastructuur en Milieu).

For the space between the turbines, a typical rule is to have a 5 to 10 rotor diameters distance (NREL), which for the simulated wind turbine is about 400-800 m. It can be seen that the area near by the highways can be easily exploited for installing wind turbines. The density of these turbines will be found after the simulation of the microgrid.

4.4 Energy Storage System

The storage system is a very important component of a microgrid as it is used to store the excess energy produced and supply this energy when there is not enough power production from the renewable energy sources. As we saw from the previous sections of this report, solar and wind energy is produced depending on the weather conditions and cannot be controlled or predicted. Storage systems are

responsible for maintaining the power and energy balance between the load and the generation. Many possible systems for stationary storage have been reported in literature, with the most common to be batteries, hydro-power systems, flywheels and supercapacitors. In this thesis, a central battery storage system was assumed to be included to the microgrid. Battery systems are already widely-used and have a fast response to power variations which often occur in renewable energy production.

The most mature technology of battery storage systems for large scale application is Lead-Acid batteries and mostly the valve-regulated or sealed lead acid batteries (VRLA). A promising technology is the Sodium-Sulphur (NAS) batteries; however the high operating temperatures (greater than 300˚C) require a proper heating and insulation system. Li-ion batteries are a technology with a considerably high efficiency and better energy and power density, already well-established at the automotive industry. However, they are very expensive to be used for large scale applications. There are also some safety issues arising in case of overcharge or overdischarge. Another characteristic is that their lifetime significantly decreased with deep discharging.

To conclude, in this thesis Lead-Acid batteries were assumed to be used, as it is the technology mostly used in such applications. However, new technologies are emerging and maybe a better substitute in the near future, as Lead-acid batteries are very large in size and contain heavy toxic materials.

The specifications assumed for the simulation model considering the storage system are tabulated below.

Table 4.2 - Battery Storage system characteristics

Type	Lead Acid
Charging efficiency	0.90
Discharging efficiency	0.85
Round efficiency	0.77
Maximum SoC	95%
Minimum SoC	5%

The state of charge of the battery is limited to 5-95% in order to prevent overcharge/overdischarge. The same limitation for Li-ion batteries that are far more sensitive was taken 20-80%. A 5% margin from completely charged/discharged was considered a reasonable assumption for stationary lead-acid batteries.

The estimated lifetime depends greatly on

- The (dis)charge rate
- The DoD (depth of discharge) and the number of cycles at every DoD
- The operating temperature

Typical values of the battery lifetime are 8-12 years for shallow cycling and 2.5-5.5 years for deep daily cycling. An assumption of 10 years of lifetime will be made which is a typical value used for RES systems. However, it will be also validated when taking into account the simulation results. [31] & [32]

4.5 Power demand curve

The load curve of the microgrid follows the traffic pattern. Using data for the daily traffic and combining them with the power demand of every vehicle as well as the electric vehicle penetration, the total power demand can be derived.

To sum up, the power profile of the microgrid which will be simulated depends on the following factors

- The daily traffic of the road (number of cars per kilometer)
- Penetration of electric vehicles (percentage to the cars passing)
- The specifications of the CPT system (power & coverage), which depend on the driving range to be achieved and the size of the battery of the electric cars

The number electric vehicles that are passing on top of the CPT can be found as follows.

$$EVs_{on\ CPT} = \frac{(\%\ of\ EVs) \cdot (vehicle\ flow) \cdot (length\ of\ highway) \cdot (\%\ of\ coverage\ of\ CPT)}{(speed\ of\ vehicles)}$$

The total power required by the CPT system is the power required by every vehicle or the power of the CPT multiplied with the number of vehicles that are driving on top on the CPT system.

$$Power_{total} = (EVs_{on\ CPT}) \cdot (Power\ of\ CPT)$$

As far as the specifications of the CPT system is concerned, in Chapter 3 the combinations for achieving a certain driving range were found and can be also found in the Appendix A.

We can see that there are many combinations of the specifications CPT systems and in case the EV penetration is also taken as a variable, the resulting power curves are many.

For every combination of coverage and CPT power in order to achieve a specific driving range and EV battery size, the power demand curve is the same. However, there are many variations on driving range extension or battery size decrease that have to be investigated. In order to overcome this issue, a 'per unit' system for the power flows was introduced, so as to cover a broad range of cases rather than analyzing the microgrid for every percentage of EV penetration and every CPT system separately. The base of this per unit system is the average yearly demand. During the simulations, the power generation and all other power flows will be expressed as per unit of average demand. The per unit power demand curve represents all the possible combinations for driving range, EV battery size, EV penetration, as in all cases the demand curve follows the traffic density curve.

The average daily load profile expressed in per unit values is shown below. Note that the year maximum power was calculated 4.6 pu.

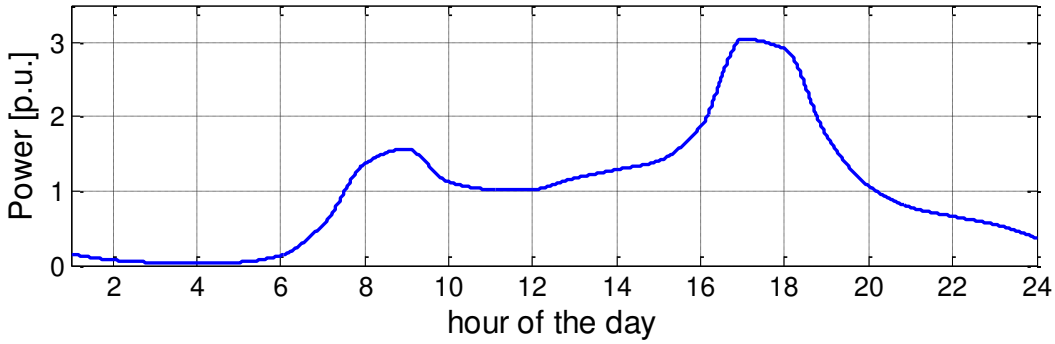

Figure 4.18 - Average Demand Curve

The absolute values of the demand curve for the specifications of the CPT system for 500km driving range are shown in the table below. The values concerning the power demand for other CPT systems can be found in the Appendix B.

Table 4.3 - Mean & maximum values of the demand for driving range of EV 500km [MW]

Length of Highway	Battery 100%		Battery 80%		Battery 50%		Battery 20%		Battery 10%	
	mean	*max*	*mean*	*max*	*mean*	*max*	*mean*	*max*	*mean*	*max*
10 km	1.4	6.4	1.5	6.8	1.6	7.4	1.8	8.2	2.0	9.4
20 km	2.8	12.7	2.9	13.6	3.2	14.7	3.5	16.3	4.1	18.7
30 km	4.1	19.1	4.4	20.4	4.8	22.1	5.3	24.5	6.1	28.1
40 km	5.5	25.5	5.9	27.3	6.4	29.4	7.1	32.7	8.1	37.5

The next figures show the variation of the demand throughout the year. For example, there is lower traffic during the winter period and this results in lower power demand.

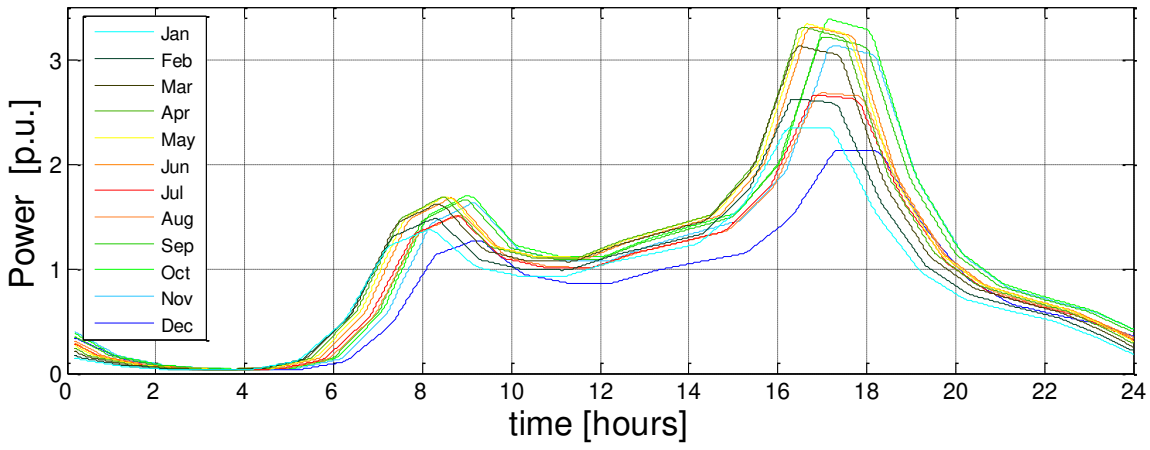

Figure 4.19 - Monthly daily variations of demand

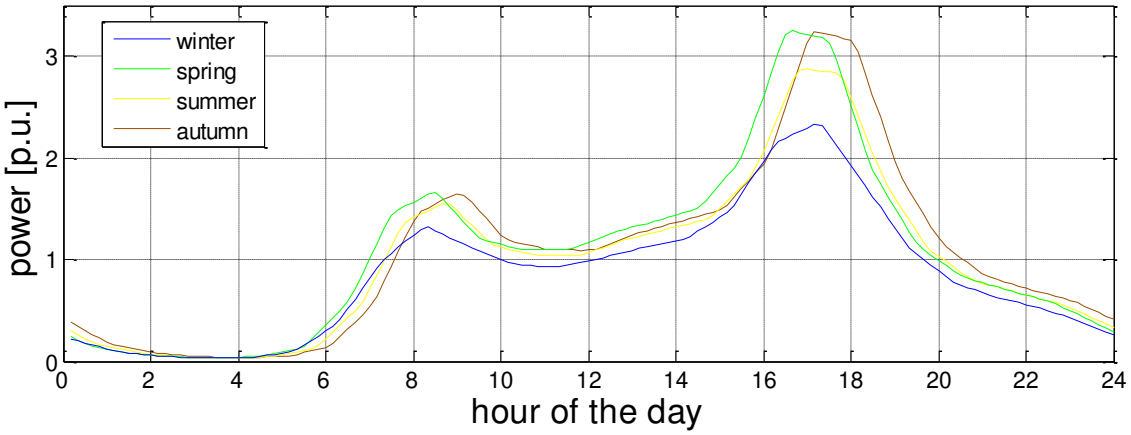

Figure 4.20 - Seasonal daily variations of demand

The average values per month of the power demand of the electric vehicles are shown below. During the months January, December, July and August the lowest demand occurs. Probably it is because these are considered 'holiday' months and less people need to commute.

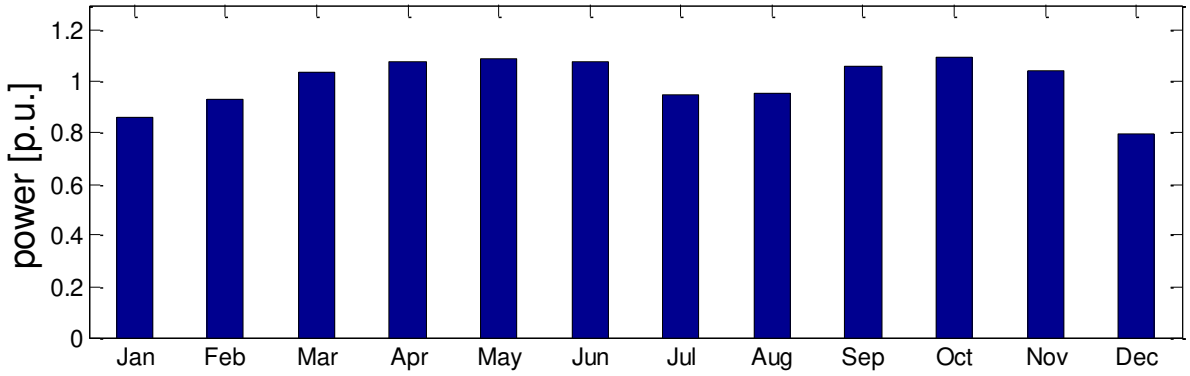

Figure 4.21 - Average demand per month

By plotting the histogram of the demand curve, we can see that most of the time there is low demand and the peak demand exists only for a few hours per year. We see that the average demand of 1 p.u. appears many times.

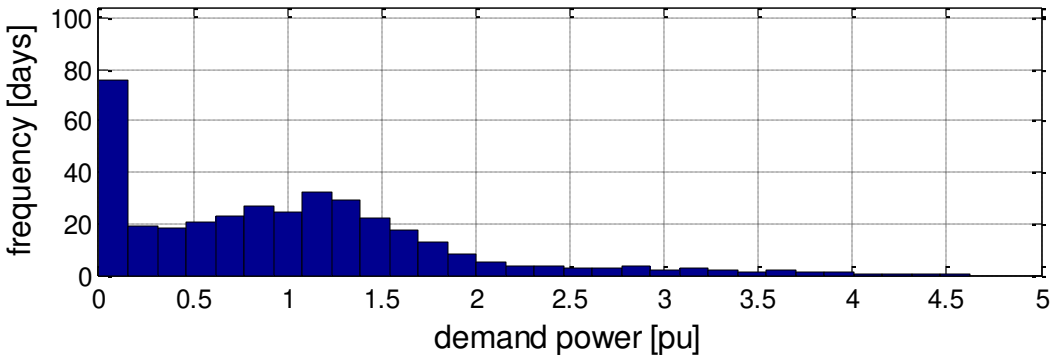

Figure 4.22 - Histogram of demand

4.6 Simulation model for sizing the microgrid

In this thesis a sustainable microgrid (wind & solar system) will be investigated in order to supply the electric vehicles via the CPT system.

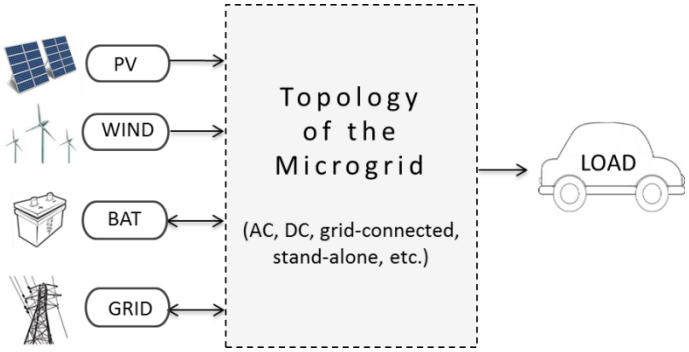

Figure 4.23 - Microgrid general overview

A simulation model was created in Matlab© in order to explore the possible sizing of the solar and wind power installed and the capacity of the storage. As shown in the flow chart of the model, iterations for all possible combinations of solar/wind/storage were made and those which could cover the load were saved. As a result, the output of the model consists of a data structure containing all the possible sizing combinations for the given system.

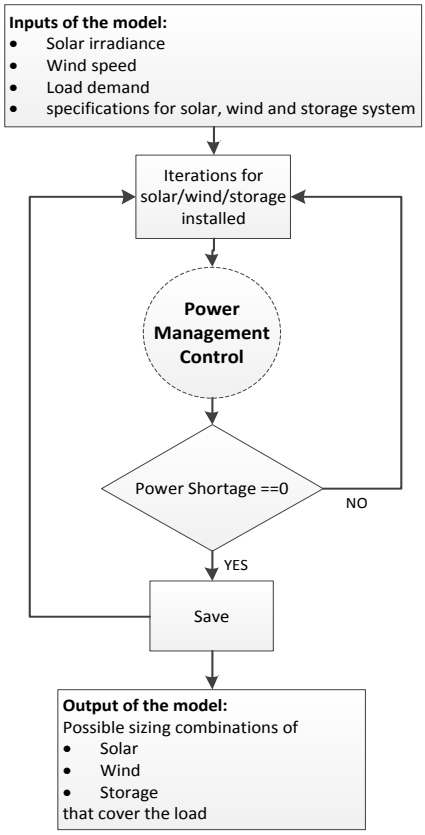

Figure 4.24 - Flow Chart of the simulation model for sizing

The output results of the model can be then analyzed. Different topologies and power management control strategies can be compared.

4.7 Cost Analysis of microgrid

4.7.1 Levelized Cost of Electricity

In this study a comparison between the different configurations of the system would be required. There are various approaches for optimizing the sizing of a microgrid [33]. In this thesis, a cost analysis optimization is proposed.

One parameter that is used in order to compare different technologies is the 'Levelized Cost of Electricity' or LCOE. The Levelized Cost of Electricity is measured in '€/kWh' and expresses the cost for every unit of energy produced by the system. In this case, the LCOE will be used to compare the different combinations concerning the energy mix of the system and the storage size. In this cost parameter, the investment/capital cost (materials & installation), the operation & maintenance costs and the lifetime of the system are taken into account. This analysis does not include financing issues, discount issues, future replacement or degradation costs. However, it was not considered essential as the goal of the analysis was use it as a comparison criterion.

The formula that is used in order to calculate the LCOE is shown below.

$$LCOE = \frac{\sum_{t=1}^{n}(Cost_t)}{\sum_{t=1}^{n}(Energy_t)}$$

$$Cost_t = {Investment}/{n} + Operation_t$$

Where,

t, the index representing the year
n, the lifetime of the system
$Cost_t$, the total cost (investment & operation) of the system for the year t
Investment, the total investment cost of the system
Operation $_t$, the O&M cost of the year t
Energy $_t$, energy required and used by the CPT system at the year t

4.7.2 Cost estimation of the microgrid components

In order to calculate the LCOE, estimations considering the investment cost, the maintenance cost and the lifetime of each component of the system had to be made. The investment, as well as the maintenance cost, greatly depends on the size of the system. For installations of a few kW there is a dramatic increase of the cost especially for wind systems. For solar system this difference is smaller.

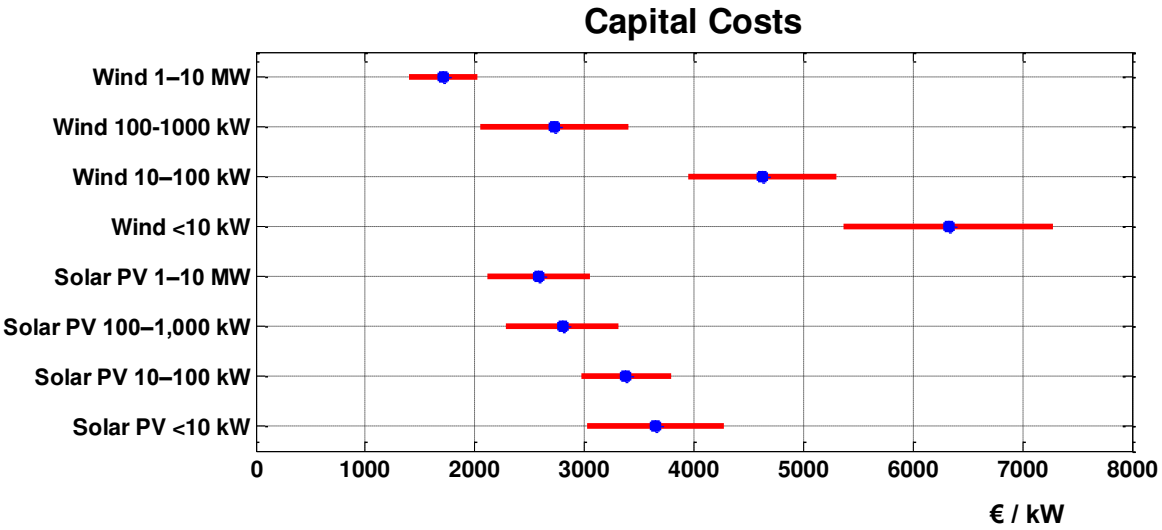

Figure 4.25 - Capital costs of Wind and Solar Systems

As far as the maintenance cost of the system in concerned, there is a wide range reported and it was also observed that O&M costs do not necessarily decrease when increasing the project size. Older installations tend to have higher yearly O&M costs. Newer installations are better designed and have lower installation and lifetime O&M costs. A comparison between solar and wind shows that solar systems require less yearly maintenance and so the O&M costs are lower in that case.

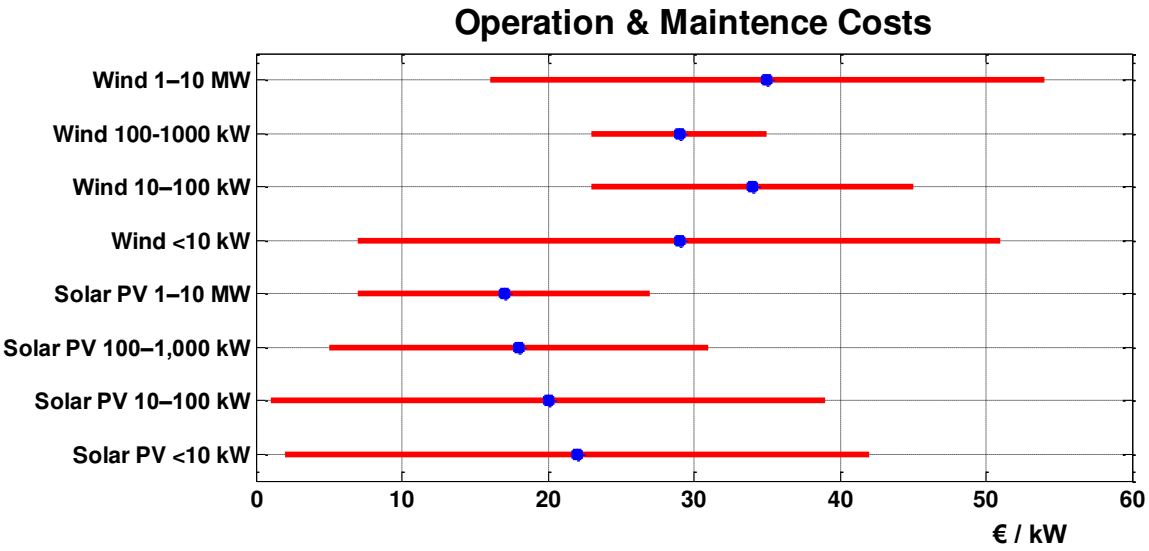

Figure 4.26 - O&M costs of Wind and Solar Systems

The presented data were found in [34] by NREL but also were crosschecked with reported values from the EWEA (European Wind Energy Association) and the IEA (International Energy agency).

The battery storage system cost should be also determined. As already mentioned, for large scale application mostly Lead-Acid batteries are used. The cost for these battery banks was found as 50-300 €/kWh and 200-450 €/kW [35], [36].

To sum up, all the assumptions used for the cost analysis in the simulation model are tabulated below.

Table 4.4 - Assumptions used in cost analysis

	Investment Cost	Maintenance Cost	Lifetime
Solar Energy	2500 €/kWp	18 €/kWp/year	20 years
Wind Energy	1700 €/kWp	35 €/kWp/year	20 years
Battery System	150 €/kWh, 300 €/kW	5 €/kWh/year	10 years
Converter DC/DC	120 €/kWp	10 €/kWp/year	15 years
Inverter DC/AC	400 €/kWp	10 €/kWp/year	15 years

Reference [37] was used for the PV and power electronics cost.

4.7.3 Simulation model for cost analysis of the microgrid

In order to perform the cost analysis, an additional model in Matlab© was created. The model uses the results obtained from the sizing model as an input and gives the most economical options for the simulated microgrid as an output.

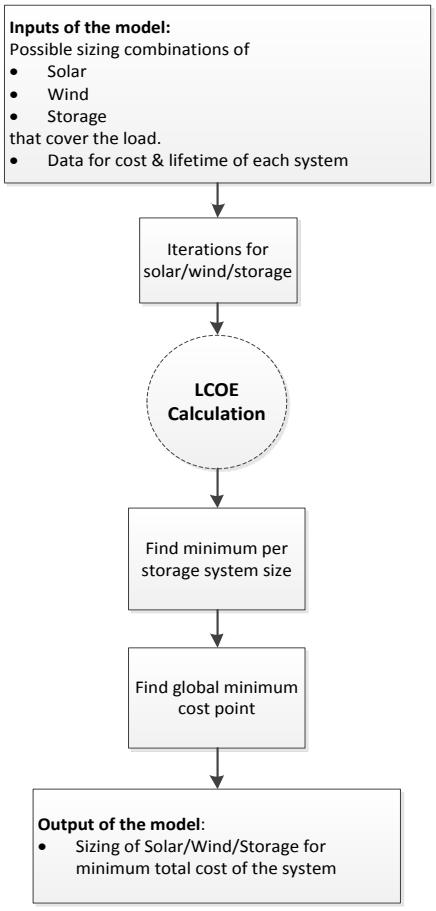

Figure 4.27 - Flow Chart of the simulation model for cost analysis

In the next chapters, the results from the model simulations will be presented and analyzed for the simulated microgrid topologies.

5 Stand-Alone Microgrid system

As mentioned before, a microgrid can be stand-alone or grid-connected. In this chapter the stand-alone operation mode will be studied in order to investigate the optimum configuration and find the optimum sizing of the stand-alone system for the wind power, the solar power and the storage. The power management strategy used for the model of the stand-alone operation will be presented and the results will be analyzed.

5.1 Configuration Topology

There are many possible configurations for the microgrid topology. There is the option of an AC microgrid, a DC microgrid, a hybrid microgrid with both an AC and DC bus and also a high frequency AC microgrid. The optimum topology for each system depends on the sources used (solar panels produce DC current where wind turbines produce AC) and the type of load (DC or AC) [38]. For the simulated microgrid the all the options are investigated next.

5.1.1 Stand-alone DC microgrid

If a DC microgrid is chosen as the topology, then the PV system which produces DC current can be directly connected with the DC bus. A DC/DC converter can achieve maximum power point tracking (MPPT) so the PV system operates at the voltage where the maximum power point exists and inject the corresponding value of current to the DC bus. The wind system which produces AC current needs to be connected to the DC bus via a rectifier. The power from the wind turbine is also controlled by yaw or pitch control methods of the blades; however, this control scheme is not analyzed is this study.

The battery is used in order to store the excess energy generation and provide this energy when the renewable power production is unable to cover the load. In this mode of operation the battery system is also responsible to provide voltage regulation at the DC bus. A converter is used for these purposes, which has to be bi-directional for power flow to or from the battery during charging or discharging respectively. [39]

The load, which in this microgrid is the CPT transformer, requires a high frequency AC. As a result, a high frequency inverter connects the CPT system with the DC bus.

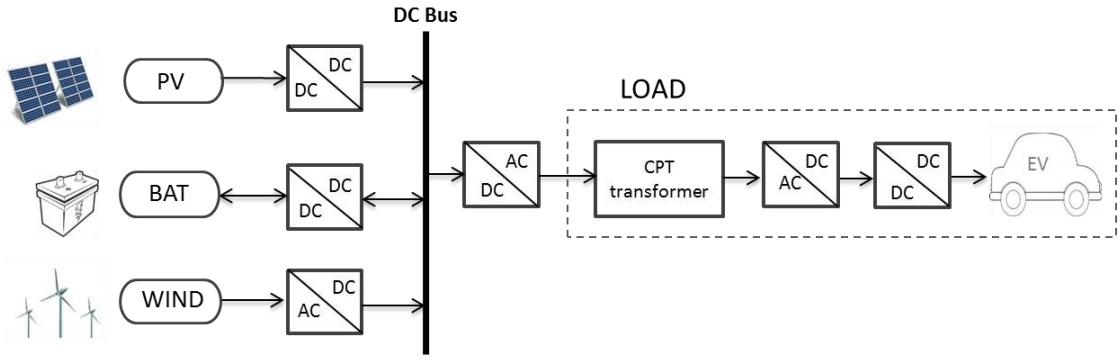

Figure 5.1 - Stand-Alone DC microgrid configuration

5.1.2 Stand-alone AC microgrid

The microgrid can be also built on an AC bus and the required power conversion steps will be explained briefly.

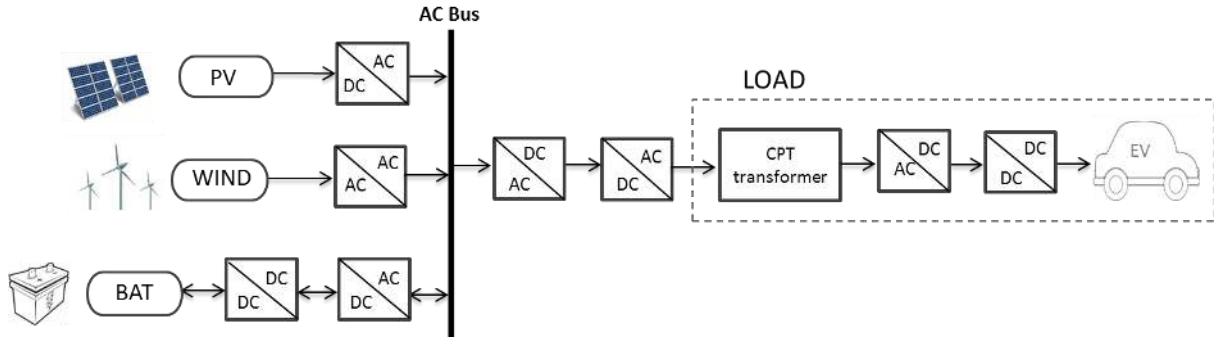

Figure 5.2 - Stand-Alone AC microgrid configuration

The PV system needs to be connected via an inverter to the AC bus. In literature it is found that the wind turbines can be connected directly, via a transformer (especially in large-scale systems) or via an AC/DC/AC conversion (especially for small wind turbines).

The battery system requires a bi-directional DC/DC and DC/AC conversion, where the direction of the power flow depends whether the battery is charging or discharging.

What has to be stated here is that in order to provide the load the very high frequency AC current (about 100kHz) an intermediate conversion of AC/DC/AC is required. This significantly increases the total losses of the system.

Together with the fact that for this stand-alone system, the battery storage is a very significant component, it is estimated that the AC microgrid is not the best option as far as the power conversion losses is concerned.

5.1.3 Stand-alone DC & AC hybrid microgrid

Moreover, a hybrid microgrid which consists of both an AC bus and a DC bus is also possible in order to interconnect the subsystems of the microgrid. In this case, only the wind energy system would be connected to the AC bus, as the CPT transformer is seen as a DC load from the microgrid. However,

there would still be losses from the AC to DC conversion at the interconnection of the two buses. For this reason, adding a complexity of two buses on the system does not provide any advantage and is not considered as an option for the studied microgrid.

5.1.4 High frequency AC microgrid

An option that should also be explored is the possibility of having a high frequency AC bus, to which the CPT system could directly be connected. However, these systems are characterized with high complexity in the design and the control. The main disadvantages are the higher power losses that cause system inefficiency and the voltage drop in the voltage delivered to the load. The most significant power losses caused by high frequency are the skin effect in the center of the conductors, the proximity effect and eddy currents. There is a limitation on the length of the cabling and general on the size of the microgrid. The limitation on the length depending on the frequency was also mentioned for the limitation on the length of the primary winding of the CPT transformer. In literature, frequency range of 400 Hz - 1 kHz is proposed and a single-phase microgrid operating at 500 Hz was built and tested. However, the CPT system has to operate at very high frequencies of 100 kHz and designing a bus with such high frequency is definitely a challenge. [40]

5.2 Power Control Management

From the previous analysis, it is concluded that for the stand-alone operation the DC microgrid configuration is the optimum topology for minimizing the conversion steps and the conversion losses. The simulation model was built in order to explore the possible sizing for the solar and wind power installed and the capacity of the storage, as presented in Chapter 4.6. The simulated topology is the DC microgrid topology shown in Figure 5.1.

The central controller checks the power flows and the SoC of the storage. Depending on the power production and the demand, the storage is charged or discharged. The controller is responsible in order the load to be covered by the microgrid energy sources and for the optimum operation of every component of the microgrid. [41]

A simplified diagram of the control scheme is shown below. In the model more details has been considered, such as the maximum charge/discharge rate, but are not shown in the figure in order to avoid complexity in the diagram.

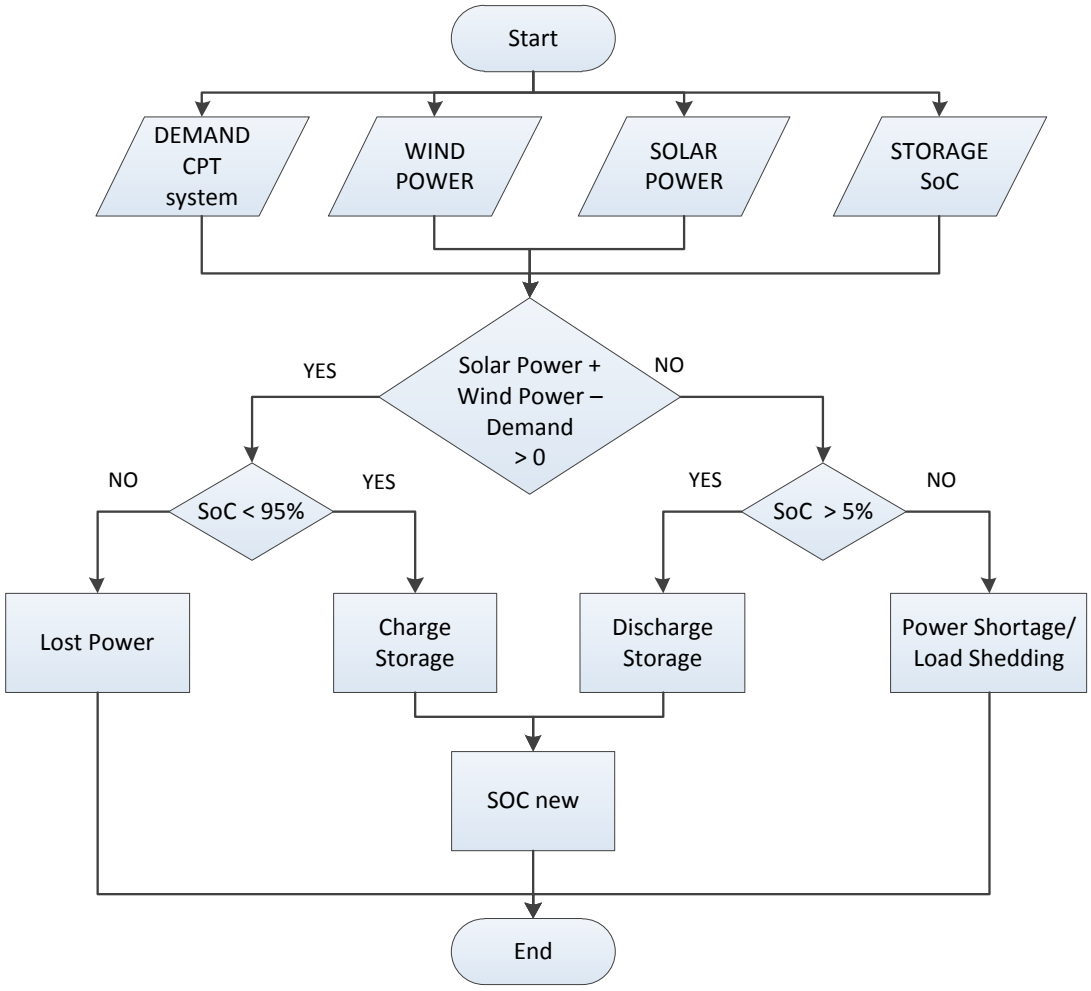

Figure 5.3 - Power Control Management, Stand-Alone mode

A list of the values used for the specifications and the efficiencies of the system components are shown in the Appendix C.

5.3 Sizing Results

After simulating the DC microgrid topology, the results are depicted below. On the Z-axis the total renewable power that should be installed is shown (solar peak power plus the rated power of the wind system). The total power is in per unit values, whereas the base of the 'per unit' system is the average yearly demand. On the Y-axis, the size of the storage is varied. The measuring unit of the storage is in reserve days, so for example 2 days reserve means that the storage has the capacity to cover the load for 2 days. The X-axis shows the solar power installed as a percentage of the total power installed. In this way the axis starts from an only wind system (0% of solar power) and gradually ends to an only solar system (100% solar power).

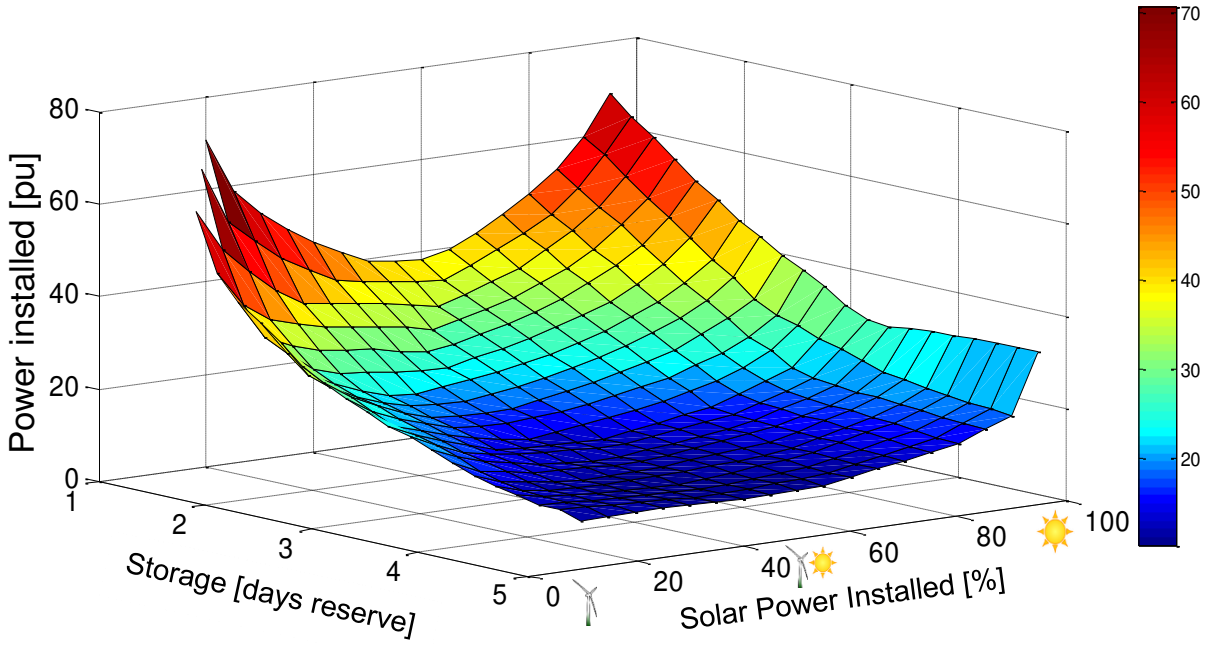

Figure 5.4 - Sizing of stand-alone DC microgrid

We can easily see that when increasing the storage of the system, the total power installed decreases. This decrease is more significant for smaller storage sizes and the power curve becomes more flat for greater storage capacity.

We can also see that for every storage size, the point where the minimum installed power is required lies somewhere near the system with both wind and solar power installed. This shows the main advantage of microgrids. The power that should be installed for an only wind or an only solar system is significantly greater than if a combined solar and wind system is used. This is the reason why on the top left of the plot there are some edges. It is because the power installed at these points was too large that is was considered useless to be included in the plot and as a result some points for storage sizes 1-1.4 and small percentages are missing.

A diagram that shown in 'slices' the above figure for storage sizes 1,2,3,4 and 5 reserve days is shown separately for better understanding of the aforementioned observations.

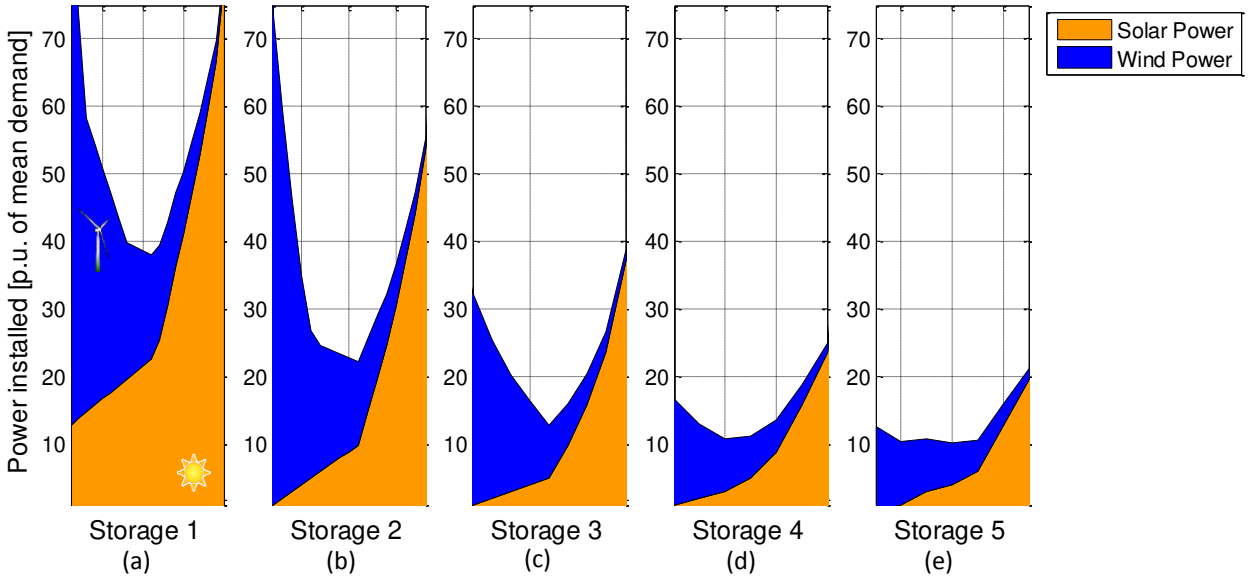

Figure 5.5 - Sizing of Solar & Wind system for storage 1 – 5 reserve days

From the above figure we can clearly see that the minimum of the total power installed exists for a combination of solar and wind system.

The greater efficiency of the wind system in comparison to a solar system is also shown in the figure. The total power that needs to be installed for an only solar system is greater that for an only wind system, due to the difference of the capacity factor of the two technologies. We can see that for a large size an only solar system requires a great amount of installed power for an only solar system in comparison to an only wind system.

However, even for the points for minimum power installed, the power system should be oversized in order to have a fully renewable microgrid. This is because of the low capacity factors of the solar and wind energy generation. For example, for 1 day of reserve storage seen in Figure 5.5 (a), total power of 38 p.u. (22 p.u. from solar and 16 p.u. from wind) needs to be installed. This means that power 38 times the average daily demand should be installed. If we take into account that the capacity factor is about 11% for a solar system and 25% for a wind system, the average power produced of such system is 2.4 p.u. of solar and 4 p.u. of wind power. We see that the system produces about 6 times more energy than what is required by the load because of the time mismatch of the renewable generation and the load. This is the reason why the same plot with the average produced power is shown as well.

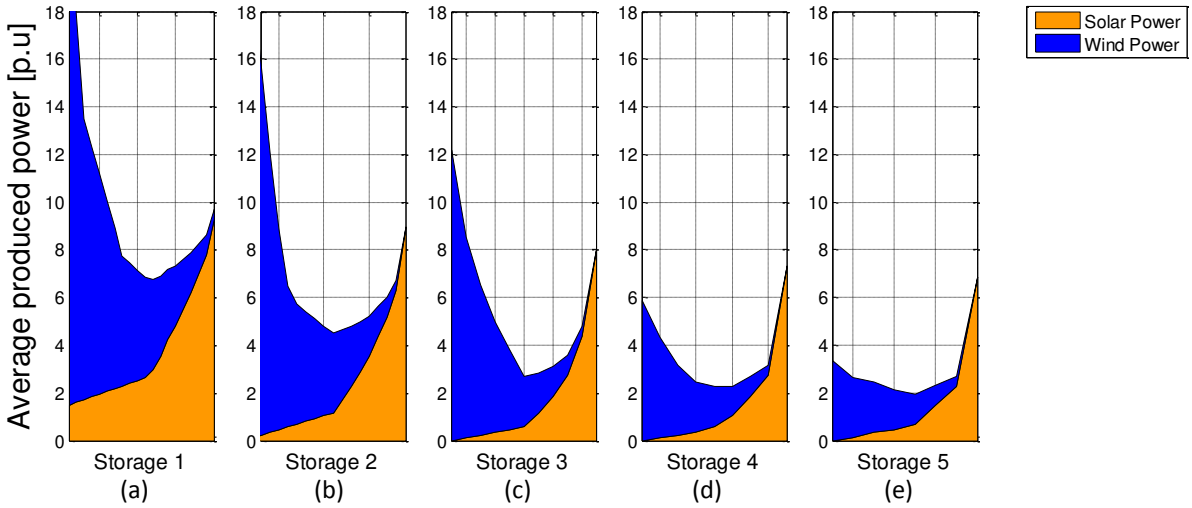

Figure 5.6 - Average power produced of possible MG systems for storage 1 – 5 reserve days

We can see that in order to cover the load the system should be oversized, meaning that there is more power produced than required. The average power produced even for large storage facilities needs to be more than 2 pu. Keeping in mind that only an average of 1 pu is required by the load, the excess power represents actually the lost power of the system.

5.4 Optimization for minimum cost

5.4.1 Results of cost analysis

From the previous analysis, it cannot be derived which sizing of the microgrid is more beneficial. When choosing a system where the lowest peak power needs to be installed, the requirements for storage become large. We should always keep in mind that the storage adds a significant cost in RES systems.

Therefore, an optimization criterion is required in order to draw conclusions on the combinations of sizing shown before. In Chapter 4.7, the 'Levelized Cost of Electricity' was introduced and will be now used as the optimization parameter of the system.

The results from the cost analysis are shown next. The axes of the 3D plot are similar to the one presented in the previous chapter. However, now the LCOE is plotted instead of the power installed. The X and Y-axis remain the same, with the storage size in reserve days and the solar power as a percentage of total power respectively.

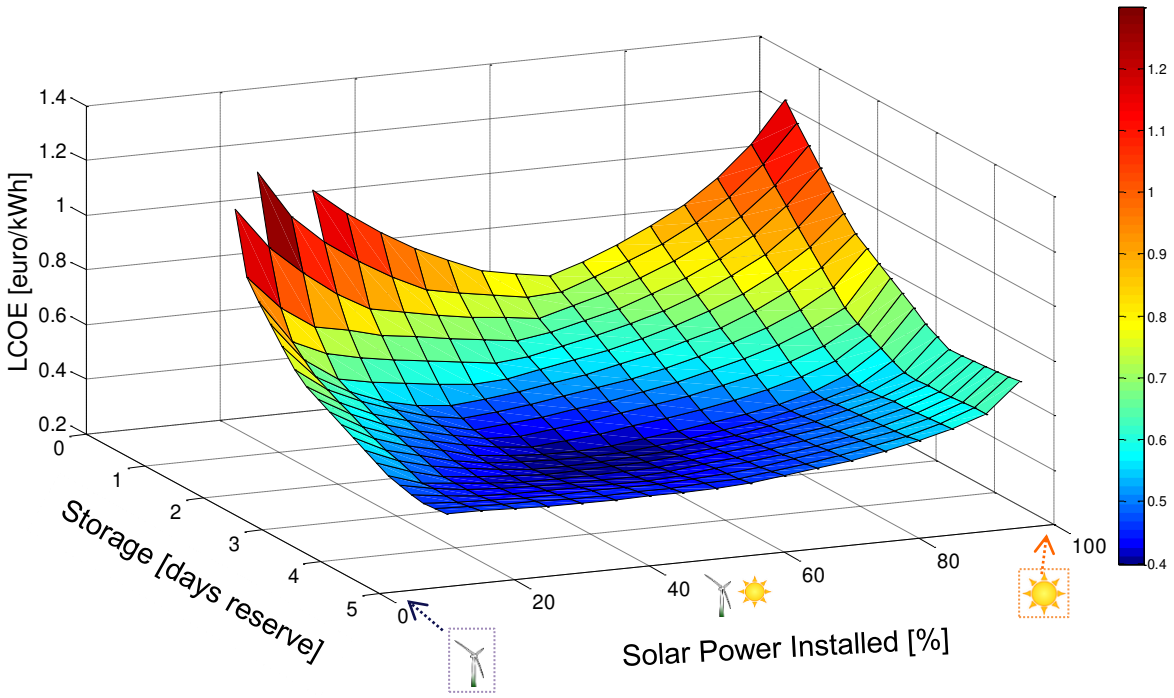

Figure 5.7 - LCOE of energy consumed by EVs

The area with the minimum cost of the system is colored with very dark blue. We can see that installing more storage decreases the LCOE initially until a storage size of about 3 reserve days. After this threshold, increasing the storage size of the system is not beneficial as the cost of the storage is much greater than the cost saved by installing smaller solar and wind system.

Next, the points that give the minimum cost for every storage size (1-5 days) are presented in a bar diagram. In this figure it can be seen that the optimum sizing is for 3.2 days storage capacity.

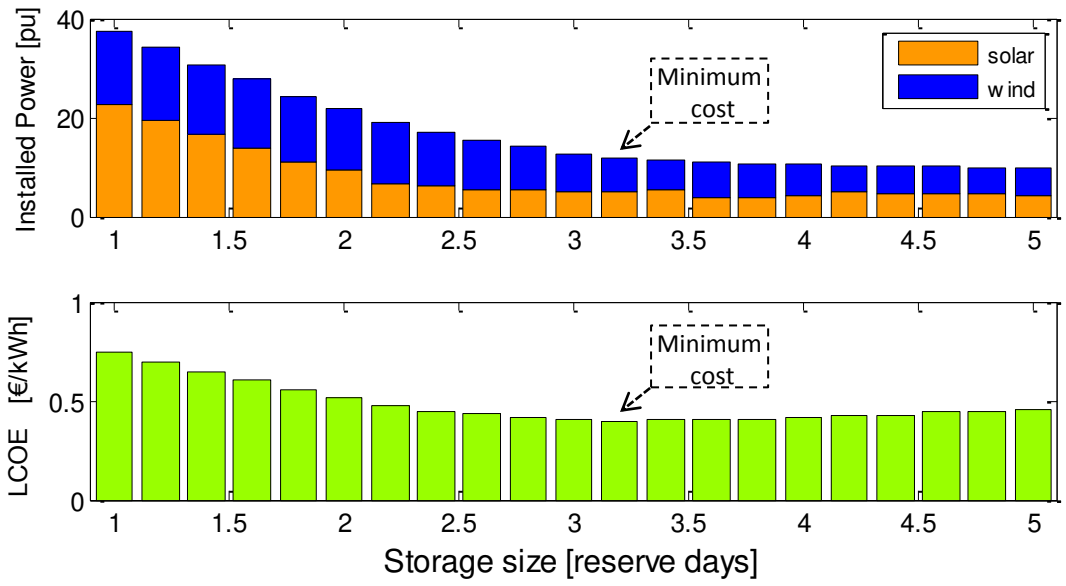

Figure 5.8 - Minimum Cost Points for different storage sizes

Overall, the sizing with the minimum cost consists of about 3 days of storage and the renewable energy sources should be 40% of solar and 60% of wind system, in total 12p.u. power installed.

5.4.2 Sensitivity analysis of cost estimation

A sensitivity analysis will be carried out considering the assumptions for the cost of the components of the system. The cost of the storage system, as well as for the wind and solar system, was varied in order to see how the optimum configuration of the system changes. During the cost estimation of each component in Chapter 4.7.2, the variations found in the market concerning the cost were presented. As result, the optimum sizing was found (storage size and the percentage of wind/solar) for each component cost range. The results from the sensitivity analysis of the storage system cost are shown in the following graphs.

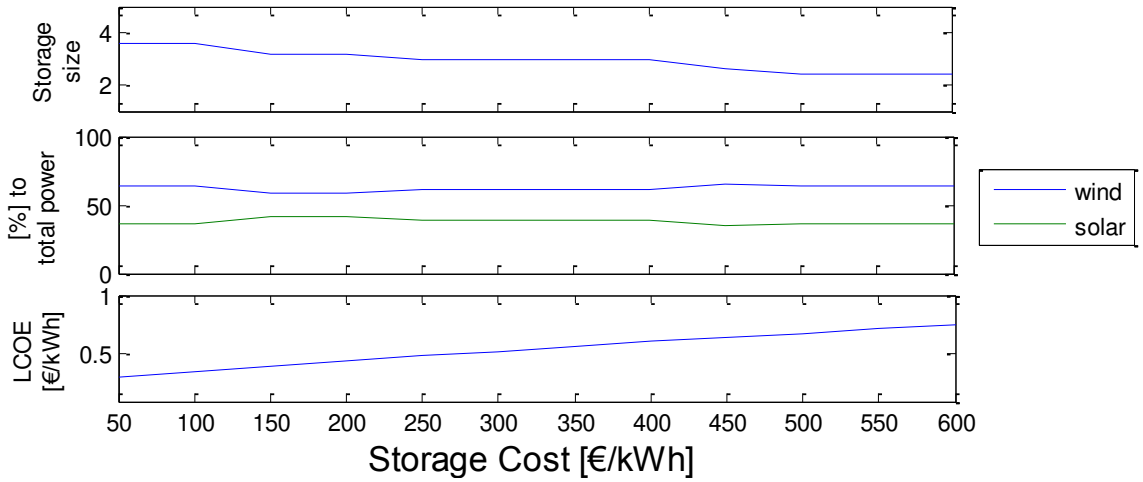

Figure 5.9 - Sensitivity Analysis for Storage Cost

In case the storage cost is lower, there is a slight increase in optimum storage size of the system to 3.5 days. If the storage becomes more expensive, the optimum size decreases to 2.5 days. However, for a wide range and reasonable values of storage cost the optimum size remains close to 3 days reserve, as estimated. The percentage of wind and solar system is not dependent on the storage cost remains about 60% and 40%. The LCOE increases if the storage cost increases.

The results from the sensitivity analysis of the solar system cost are shown next.

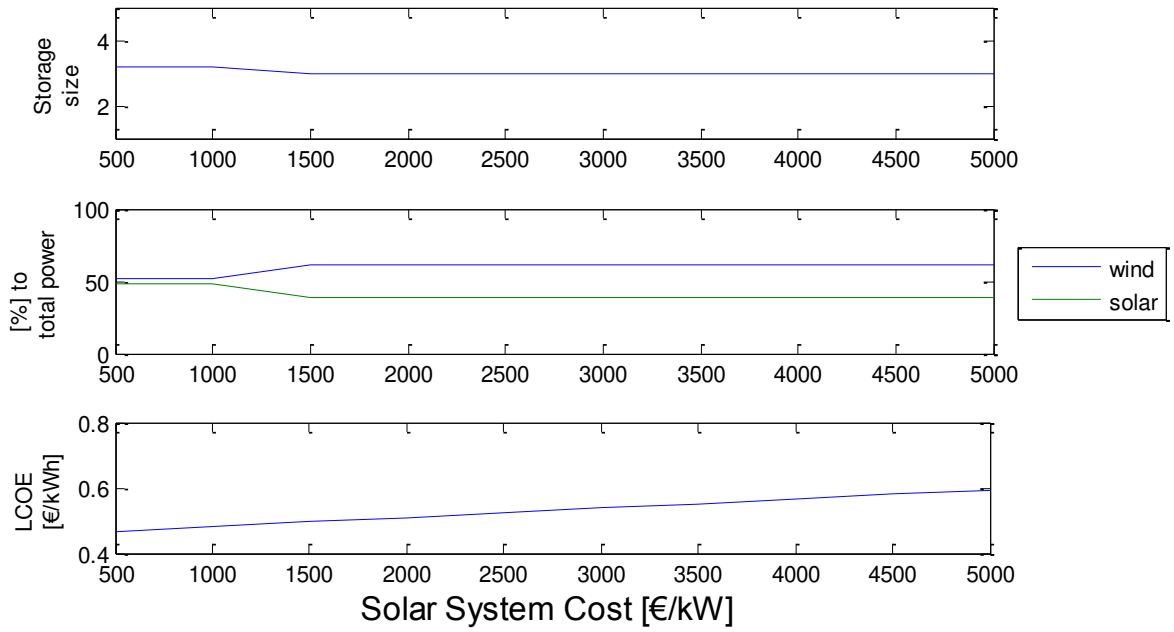

Figure 5.10 - Sensitivity Analysis for Solar System Cost

In case the solar energy becomes cheaper, which is the trend nowadays, the solar system would have an optimum size of 50% in the energy mix of the microgrid. For very high costs up to 5000 €/kW, the distribution remains 40% solar - 60% wind the same as the proposed system.

The results from the sensitivity analysis of the wind system presented in Figure 5.11 show that if a high cost of wind turbines is considered, which is realistic for small scale wind turbines, then the wind system should have a smaller fraction of the installed power. Especially, for cost more than 6000 €/kW, it would be beneficial to install more solar than wind.

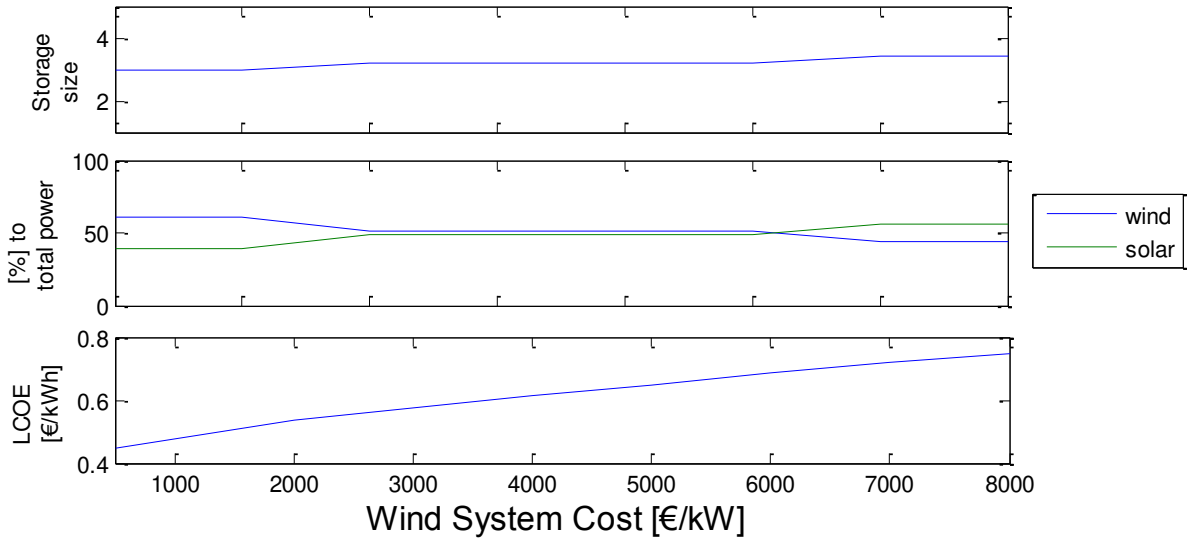

Figure 5.11 - Sensitivity Analysis for Wind System Cost

Overall, it was observed that increase the cost of a system component, increases the total LCOE; this effect is stronger for the cost of the storage.

To conclude, now it can be safely stated that a system of 3 days reserve and 60% wind - 40% solar, represents the optimum configuration for a stand-alone microgrid. In the case of a decrease in the solar system costs, then a 50-50% system is also possible. From the sensitivity analysis, we can assume that this result remains the same for the range of cost found currently in the market.

5.5 Power Flow Analysis of minimum cost point

From the previous analysis, the sizing with the minimum cost consists of about 3 days of storage and the renewable energy sources should be 40% of solar and 60% of wind system, in total 12p.u. power installed.

Table 5.1 - Optimum sizing of stand-alone system

Grid connection capacity	0 pu
Storage System size	3 day
Solar peak power	4.8 pu (40%)
Wind power installed	7.2 pu (60%)

An overview of the average power of each component for the minimum cost point is depicted in the bar figure below.

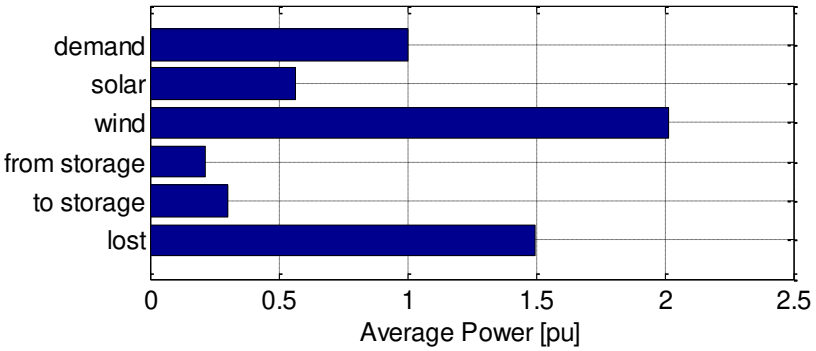

Figure 5.12 - Average Power of each system component [pu]

The average power of the demand, the solar & wind production, the storage and the lost power that are shown above, which corresponds also with the distribution of the energy of the system. The larger capacity factor of the wind energy can be seen, as the installed power the distribution is 40% to 60% for solar and wind respectively and the average produced power is 20% to 80%. The amount of lost power is also significant for the stand-alone system, as the generation should be oversized in order to cover the load in all cases. We see that the amount of lost power is 1.5 times greater than the actual demand of the system.

The power flows for some weeks of the simulated year will be now presented. In this way a better overview will be gained concerning the usage of every component and its capability in covering the load.

In Figure 5.13, the power flow during a week low renewable power production is shown. In this case, during the peak hours there is almost no power produced. Within 4 days, the storage reaches its minimum state of charge.

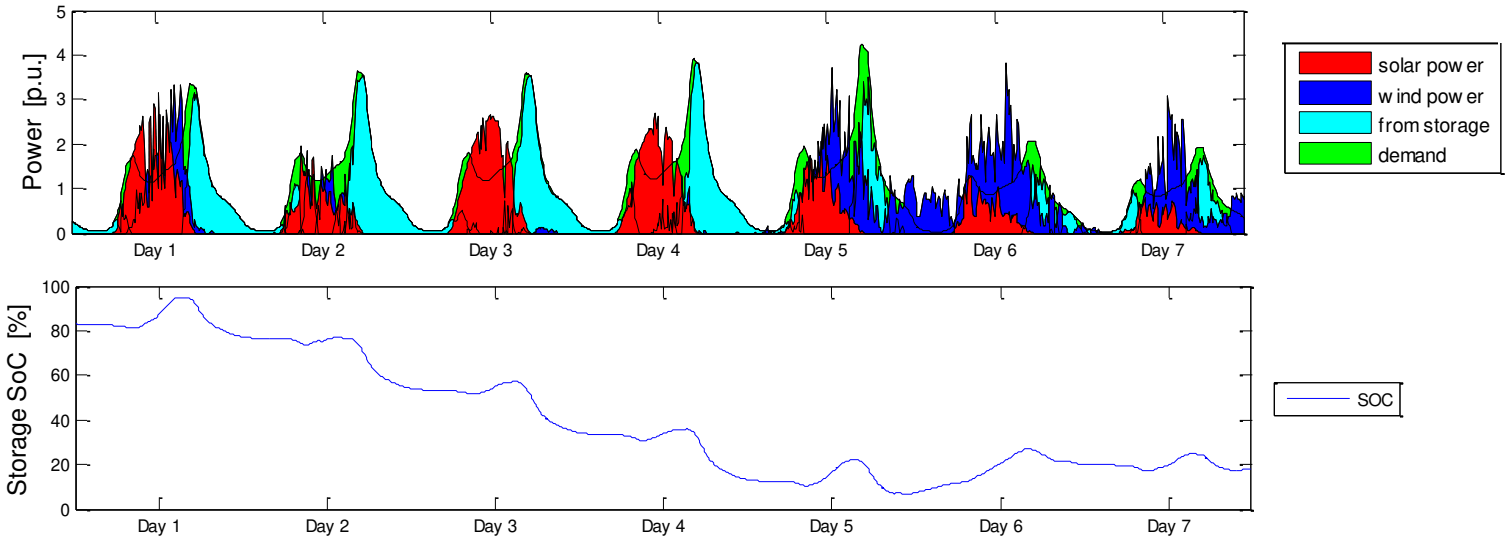

Figure 5.13 - Week with low RE production, (a) Power Flows, (b) SoC

In Figure 5.14, a week with high wind speeds is shown. It can be seen that the storage is used just for a few hours, only when the demand reaches its peak. An only wind system would be sufficient in this case. Most of the wind power is lost as just a fraction of it is used to cover the load. The low solar power produced is therefore not needed.

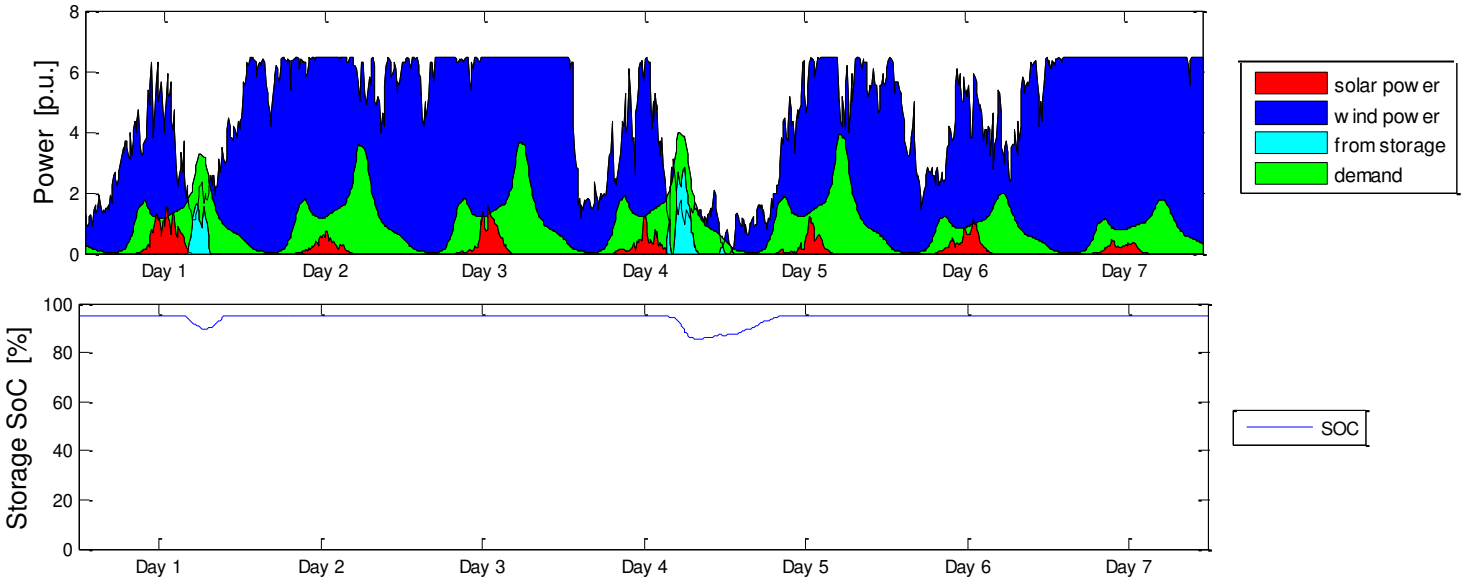

Figure 5.14 - Week with high Wind Power production, (a) Power Flows, (b) SoC

In Figure 5.14, the 21st calendar week is shown. In this case the solar system produces the year maximum power. This maximum power is produced at about 12.00. The storage is again barely used and about half of the power produced during the period 09.00 – 16.00 is lost.

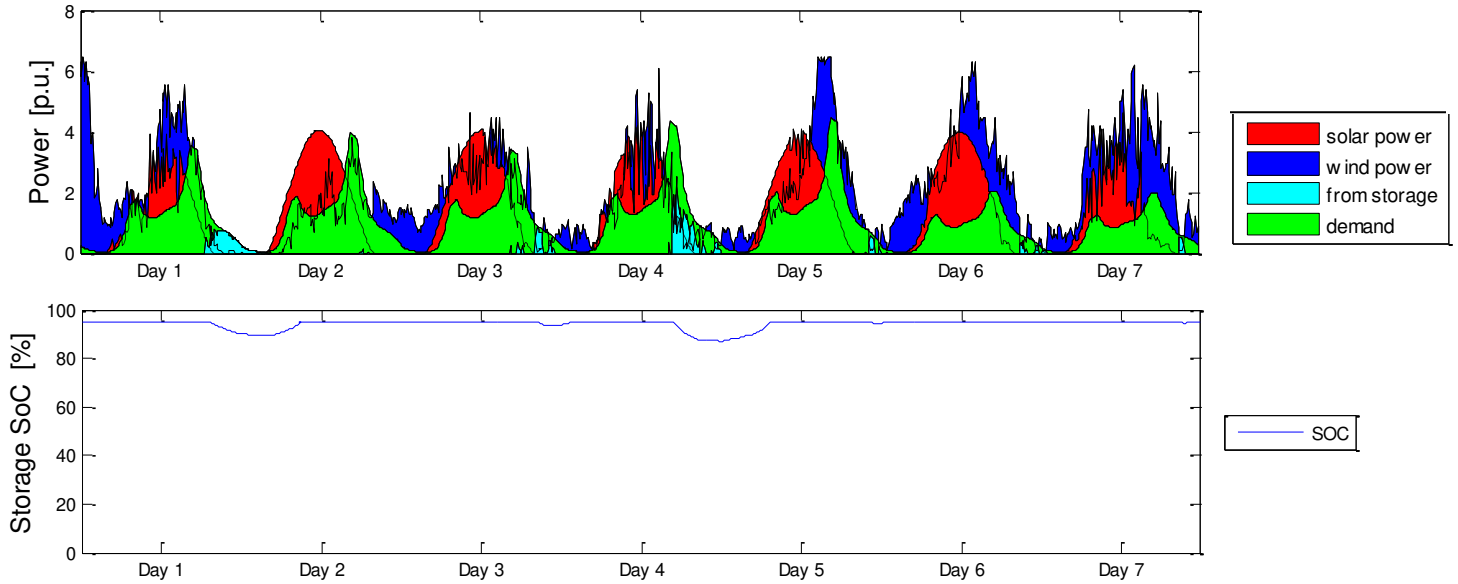

Figure 5.15 - Week with high Solar Power production, (a) Power Flows, (b) SoC

The above figures plotted separately for each component with additional information on the power to storage and the lost power can be found in the Appendix D.

In order to have a year overview of the power (produced or consumed), a bar diagram which shows the average power per month is shown below.

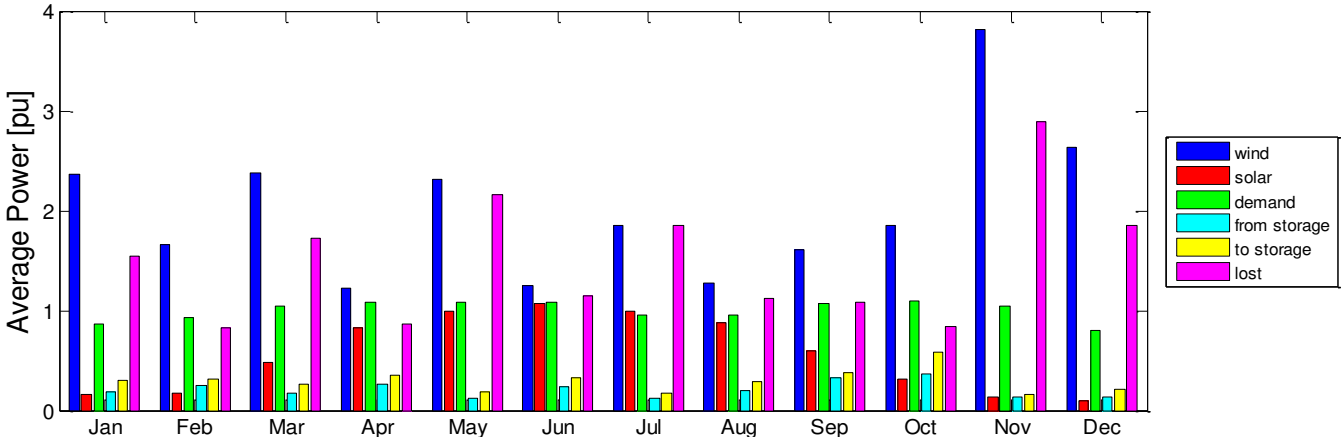

Figure 5.16 - Average power flow per month

As it was expected, during months with higher wind speeds there is also more power lost. The average power to or from the storage depends greatly on the renewable energy production. For example during September and October where there is low renewable power produced, there is much power from the storage. The power to charge the storage depends whether there is excess power produced and also whether the storage capacity has been used and the state of charged has dropped.

5.6 Analysis of the storage of the microgrid

The storage system of the microgrid is an important component. It is interesting to make a brief analysis and see the state of charge of the storage of the system throughout the year.

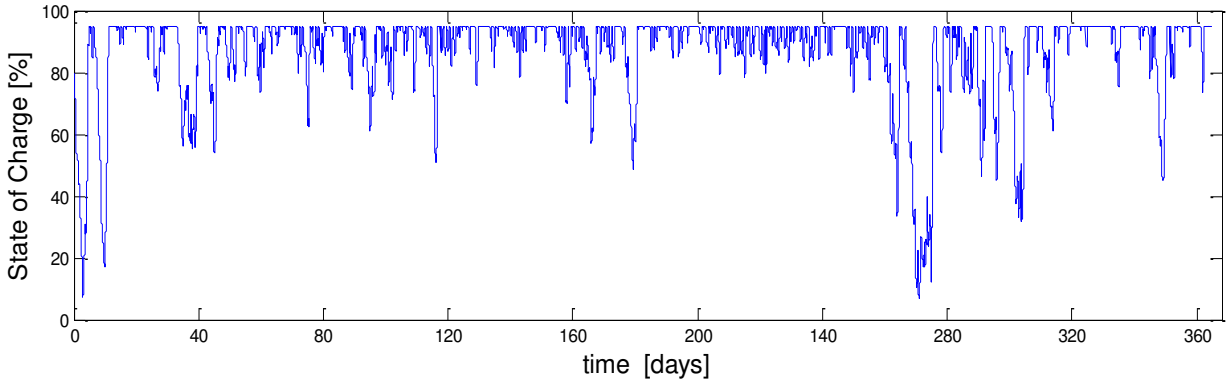

Figure 5.17 - State of Charge of storage system

We can see that most of the time the SoC fluctuates on values above 50%. This saves the battery life of the storage systems. Deep cycling is far more harmful than shallow cycling. However, if shallow cycling occurs only several times it shows that the stored capacity is barely used to the fullest.

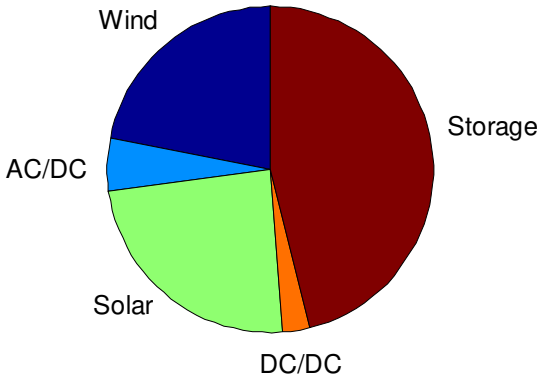

Figure 5.18 - Cost distribution

When seeing the distribution cost, the storage is responsible for about the half of the total cost. Therefore, it can be concluded that the storage is the most costly component, although its full storage capacity is required only in extensive low wind and low sun conditions (like in Figure 5.13).

5.7 Sizing of microgrid storage depending on system availability

From the previous analysis, it was shown that the storage becomes empty only several times per year. Therefore, it is interesting to estimate the sizing of the microgrid in case the availability of the system is not 100%.

Microgrids are systems that are intended to operate continuously and may be considered operational even when one or more components fail to perform their function. Availability of the microgrid system can be defined as the probability that the microgrid is able to supply the load at any given time. In other words, it is the percentage of time that the microgrid is able to power the load [42]. Mathematically, it can be described from the following formula.

$$Availability = \frac{T_U}{T_U + T_D}$$

Where,

T_U, is the average up time of the system

T_D, is the average down time of the system

For the microgrid described in the previous section, the availability was 100% during the simulated period. Keeping the sizing of the renewable energy system constant, the storage size can be decreased and the availability can be calculated.

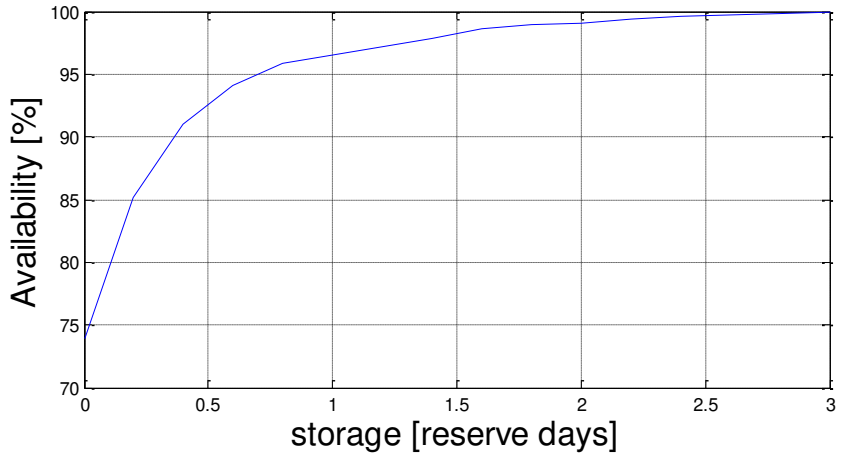

Figure 5.19 - Availability of microgrid depending on storage size

We can see that by decreasing the storage size to half (1.5 days reserve), the availability is decreased to 98.25%. This means that 1.25% of the time or 6.4 days (154 hours) per year the microgrid is not able to supply the load.

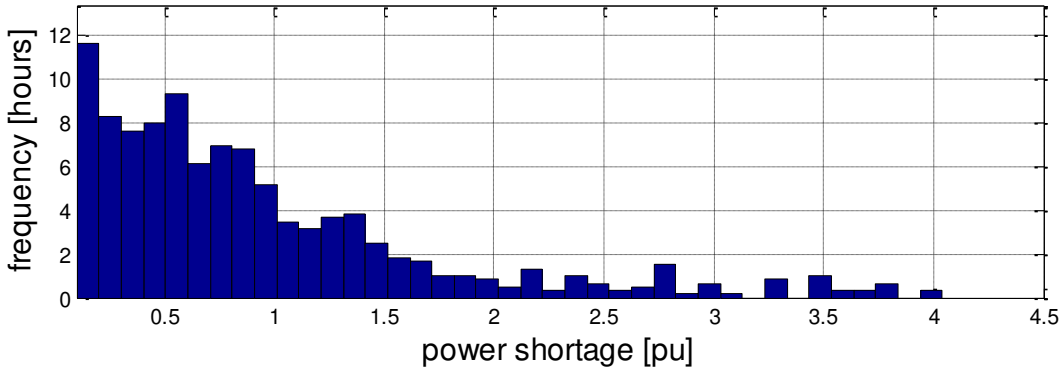

Figure 5.20 - Histogram of the year power shortage (storage size 1.5 days reserve)

In order to conclude if o load shedding scheme is acceptable or not, the amplitude and the duration of the power shortage during the time the system experiences unavailability has to be studied. From the histogram, we can see that in most of the cases the power shortage is less than 1 pu.

One case where there is extensive power shortage can be seen in Figure 5.21. No load can be supplied after 5pm for 2 days in a row. This includes the high peak occurring at around 6 pm.

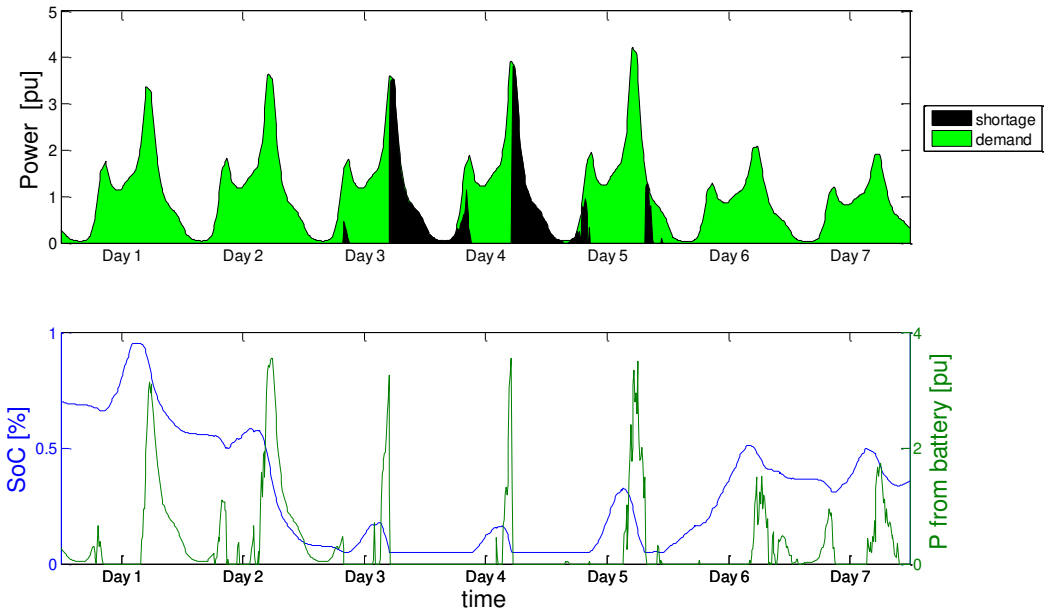

Figure 5.21 - Week with high power Shortage (storage size 1.5 days reserve)

A better option could be to have partial load shedding for an extended period of time whenever the SoC becomes low, rather than have total power shortage during a smaller period of time.

5.8 Comparison of microgrid storage with storage removed from the EVs

While implementing the CPT system, the decrease of the battery of the electric vehicle was investigated. The power requirements for the electric vehicles via the CPT system for various EV battery sizes have already been calculated (see Appendix A). Depending on this EV battery decrease and on the driving range that needs to be achieved, the different power curves were also calculated (see Appendix B). As a result, for EV each battery size and driving range, a different sizing of the microgrid is required. In this section, a comparison between the storage size of the microgrid and the storage capacity saved from the electric vehicles' battery decrease will take place. The main goal is to reduce the total storage capacity of the overall system which consists of the electric vehicles as well as the microgrids that power these vehicles. Now, we can see in which case this goal is achieved.

5.8.1 Microgrid storage size

As the storage needed for a stand-alone system is significant, it is interesting to compare this storage capacity with the storage capacity that can be removed from the electric vehicles.

As far as the microgrid storage is concerned, from the previous analysis it was found that 3 days reserve capacity is the optimum configuration. Depending on the CPT system specifications and the length of the highway, the demand was estimated. Then, the storage can be estimated as well.

$$Storage_{microgrid} = 3 \cdot (average\ demand) \cdot 8760 \ \rightarrow [kWh]$$

5.8.2 Storage capacity removed from the EVs

The next step is to find the number of different vehicles that use this highway, in order to estimate the storage capacity that is removed from these vehicles. The average daily vehicle flow is known for the simulated highway. So, the average number of cars driving on that highway can be derived. From the data of the simulated highway it is known that 36963 cars are passing per day for one direction (2 lanes) [20].

An important value that has to be taken into account, derived from the Dutch mobility analysis is that every vehicle in the Netherlands drives on average 36km per day [18], [21].

Combining the above information, it is assumed that about 37000 individual (different) cars use 36 km of highway (one direction) per day. In other words, about 1000 different cars 'correspond' to 1 km of highway. For other lengths of highway a linear interpolation can be used for the estimation of the individual cars that use it per day. For example, in case a large length of highway is considered, it means that 37000 have covered the whole distance, but in the meanwhile there are some cars that would exit the highway and other ones entering. The estimated number of individual cars driving (or using) on the simulated highway for various highway lengths is shown below.

Table 5.2 - Number of individual vehicles using the highway per day

Length of highway	Number of cars
10 km	10268
20 km	20535
30 km	30803
40 km	41070
50 km	51338

Depending on the scenario for the battery decrease of each electric car, the total amount of the storage removed from the EVs can be estimated. The size of the electric vehicle battery nowadays was considered 24kWh.

Table 5.3 - EV battery sizes [kW]

Battery Size	Storage remaining at the EV	Storage removed from the EV
0.2	4.8 kWh	19.2 kWh
0.4	9.6 kWh	14.4 kWh
0.5	12 kWh	12 kWh
0.8	19.2 kWh	4.8 kWh
1	24 kWh	0 kWh

Combing the above tables, the total storage capacity 'saved' from the decrease of EV battery size can be calculated.

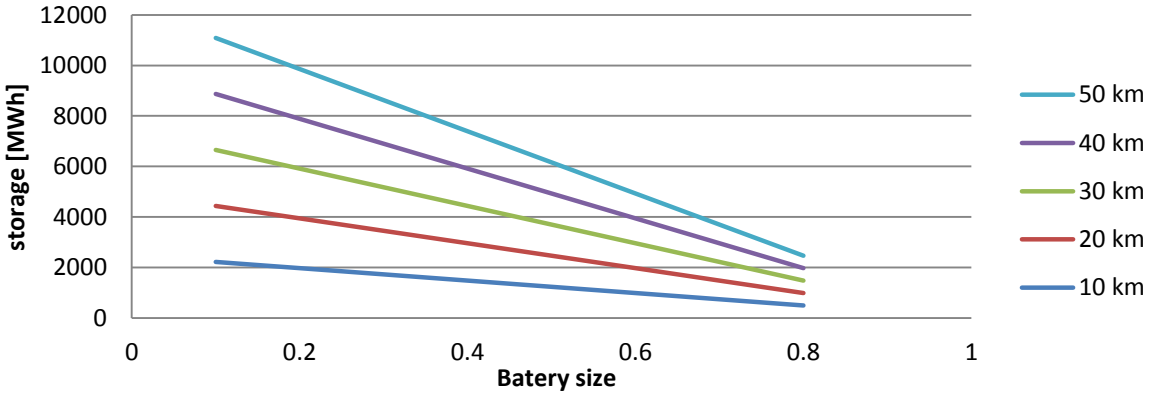

Figure 5.22 - Storage capacity removed from EVs depending on highway length

5.8.3 Comparison for different EV battery size reduction

In order to compare the storage capacity of the microgrid to the capacity removed from the electric vehicles, a part of 10km of highway is assumed with 100% of the cars being electric. The specifications (average and maximum value) of the demand curve for each case of EV battery decrease and driving range extension can be found in Appendix B. In this way for every battery size of the EV from 0.1 (2.4kWh) to 1 (24kWh), the needed storage of the microgrid can be plotted. As this analysis has been made for driving ranges of 140, 300 and 500km, the three curves are included in the figure.

The total storage capacity removed from the electric vehicles by decreasing their battery size is also plotted and is represented by the dashed curve.

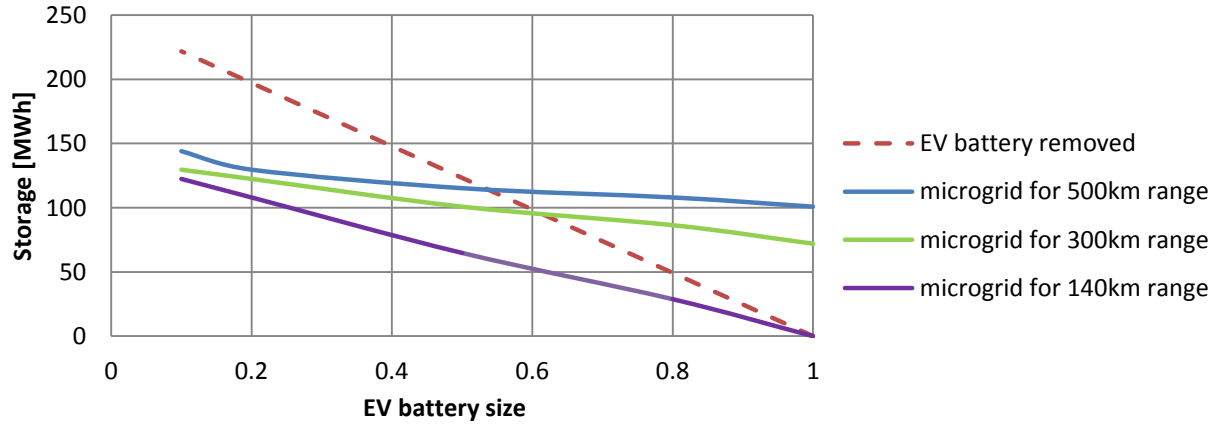

Figure 5.23 - Storage comparison for different EV battery sizes & driving range extension

From the difference of the dashed curve with one of the rest, we can see if storage capacity is saved or not after by implemented the CPT system and the sustainable microgrid. To be specific, we can see that in order to achieve the range that electric vehicles have today (140km) with a smaller battery, the storage needed for the microgrid is almost half the capacity that can be removed from the EVs

(comparison between purple and dashed line). As a result, the other half of the storage removed from the EVs is actually saved.

In order to extent the driving range, the microgrid components to supply the on-road systems should be greater in size and so is the storage capacity of the microgrid. However, for a great decrease in the EV battery size (e.g. more than 50%), the microgrid requires again less storage than the storage removed by the electric vehicles and overall there is still battery storage capacity saved.

5.8.4 Comparison for different EV penetration

The previous graph is for 100% of electric vehicles penetration. Now, different percentages of electric vehicles will be investigated and the graph for battery size of electric vehicles 0.2 (4.8kWh), 0.5 (12 kWh) and 0.8 (19.2 kWh) will be presented.

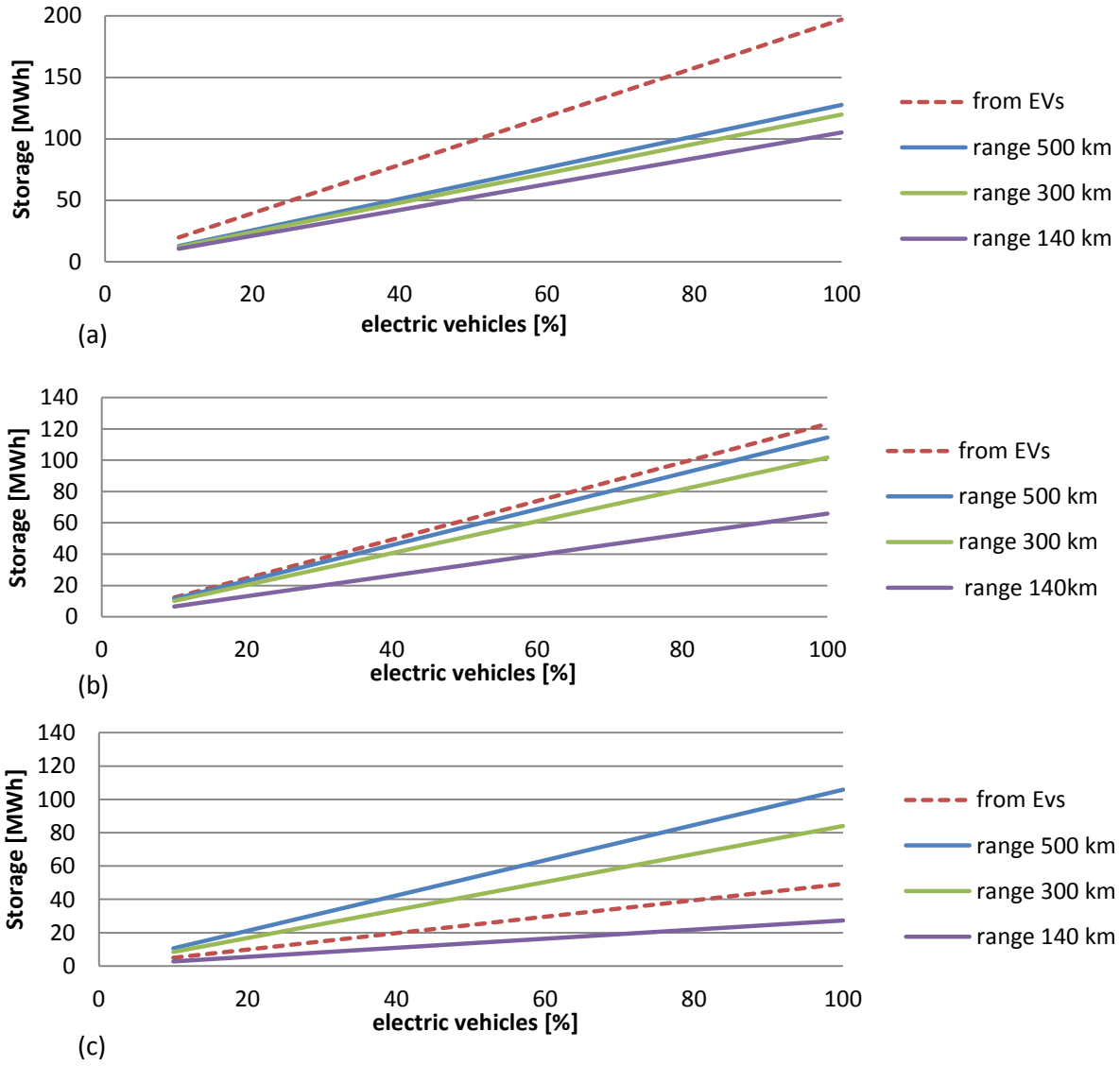

Figure 5.24 - Storage comparison for different percentage of EV penetration
(a) EV battery size 0.2, (b) EV battery size 0.5, (c) EV battery size 0.8

As it has been already mentioned, greater decrease in EV battery is more beneficial from the scope of saving storage capacity. As for the dependence on the EV penetration, the relative (%) difference between the storage removed from the EV and the storage of the microgrid remains more or less constant. For smaller EV penetration, the absolute difference (MWh) between the storage removed from the EVs and the storage needed for the microgrid is much smaller. The absolute difference gradually increases for greater EV penetration.

5.8.5 Comparison for different vehicle flow

Now, the storage will be compared for highways with different vehicle flows. If the vehicle flow varies, then the speed especially during the peak hours will be different as well. The relation between vehicle flow and vehicle speed was previously explained in Figure 2.14. As a result, the power demand is also different in every case. Becoming more flat for the cases where there is lower vehicle flow and having greater peaks when the speed decreases during peak hours. The demand curves were needed to be estimated and the corresponding simulations needed to be run again, based on the simulation model described before. The results showed that 3 days reserve is again the optimum sizing of storage.

The following figures show the comparison of storage capacities as a function of the average daily vehicle flow per direction (in this thesis 2 lanes were assumed per direction). The figures do not include values more than an average flow of 2500 veh/h because this is the limit case where in peak hours great instant vehicle flow occurs. In the speed-flow analysis in Chapter 2.3.2, it has been shown that there is a threshold in the vehicle flow where the highway has a Level of Service (LOS) reaches category F (flow is forced, with frequent drops in speed to nearly zero). As a result, there should be a realistic consideration on the amplitude of peak vehicle flow and how many times per year this occurs. It can be also seen that the simulated highway can be considered a busy highway, however still with reasonable times per year of very high vehicle flow.

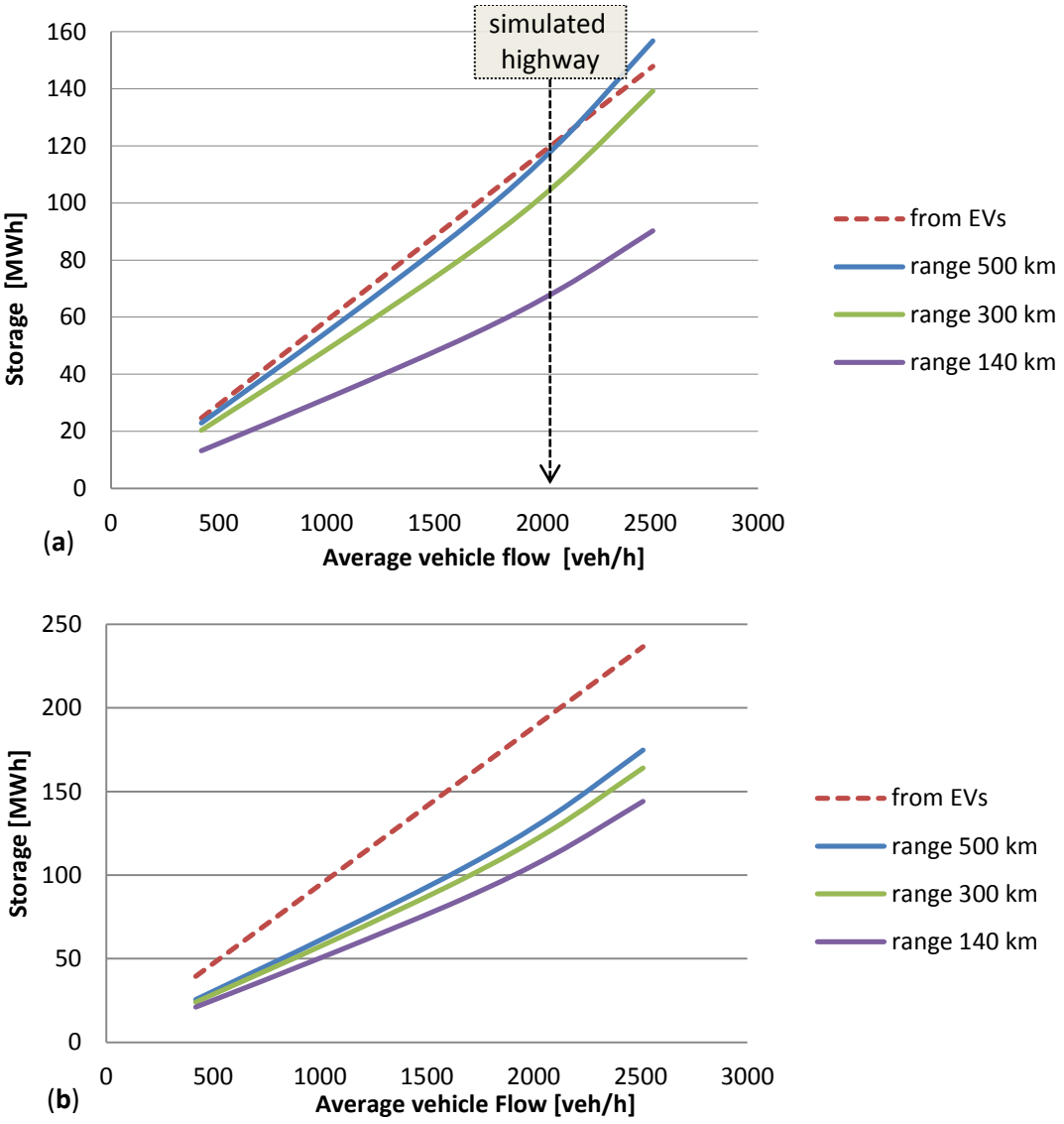

Figure 5.25 - Storage comparison for varying vehicle flow (a) EV battery 0.5, (b) EV battery 0.2

We can see that the increase in the microgrid storage is not linear but has more the exponential form for greater values of vehicles' flow. For significant vehicle flow, the demand during peak hours is large which results in need of a bigger storage capacity. Congestion increases the peak load significantly and as a result the required storage. For every CPT system (range extension & battery decrease) there is an optimum value as far as the vehicle flow of the highway is concerned. However load shedding during extremely high traffic conditions can be a solution.

5.9 Discussion on Stand-alone mode of the microgrid

During the previous analysis, the DC stand-alone microgrid was investigated as an option for powering the electric vehicles via the CPT system. It was found that the storage should have a size of 3 days

reserve and that the system should consist of 40% solar power and 60% wind power. In total the installed power should be 12 times the average power demand and average produced power is twice the size of the average demand.

The LCOE was about 0.40€/kWh which is high in comparison with the cost of power from the grid which in Netherlands is about 0.23€/kWh. Note that, this is the selling price where the production cost is much lower. In the simulated system optimized for the minimum cost, the storage has the major contribution in the investment cost.

The size of the storage might be significant; however it was proven that in case the battery of the electric vehicle is decreased, then the storage capacity removed from the EVs is much greater than the storage of the microgrid. This is true for all EV battery sizes for a driving range of 140km, or for decrease of the EV battery size more than 50% for driving ranges 300km or more. An advantage of having a central storage system of the microgrid in comparison to the distributed storage systems of the electric vehicles is that the central storage can be controlled better and also has most of the time shallow cycles. In this way the lifetime increases. Also, the central storage would be a stationary system and as a result major issues like the mass or the volume of the storage are not crucial in comparison to the battery placed in cars. On the other hand, a smaller battery on the electric vehicle would mean a limitation on driving on roads without CPT systems installed. The cycles within a smaller battery would be deeper with negative effect on the EV battery's life.

From the energy distribution bar graph (Figure 5.12), it was derived that there is a lot of power lost that cannot be used by the system. Considering the great cost of storage and the great amount of energy lost, the grid-connected option has to be also studied as a possible configuration for the microgrid. Most of the highways are not located in isolated areas and as a result the need for connection with the existing transmission lines would probably not be an issue.

Moreover, another issue that has not been investigated is the length of the highway that the microgrid could cover. The CPT systems are distributed along the road, and so are the renewable energy generation systems. There can be a variation of the number of the wind turbines and PV arrays that can be interconnected to form a microgrid. Meaning that along the highway separate microgrid systems can be installed. Smaller systems are easier to control and they have shorter interconnection cables and as a result less power losses. However, every system needs to have its control unit. So, the total cost of electrifying the highways increases if the energy sources are distributed in more microgrids. The flexibility for expendability of the system should also be considered. The penetration of electric vehicles in transport system will come gradually. Also, the number of cars is increasing year by year. As a result, easily expandable systems are surely a good solution for powering electric vehicles.

6 Grid-Connected Microgrid System

In the previous chapter the stand-alone configuration of the microgrid was studied. As the results showed that a considerable capacity of storage is required, in the following chapter the grid-connected microgrid option will be investigated. In case a grid connection is established, then the storage can become smaller in size and the excess power produced can be also sold to the grid.

6.1 Configuration Topology

As there were options for the stand-alone microgrid configurations, also for the grid-connected microgrid a configuration with a DC bus, an AC bus or a hybrid system with both an AC and a DC bus is possible. What is different for this case is that the power exchange between the microgrid and the grid has to be AC with the voltage and frequency level defined by the utility grid. The renewable energy sources are expected to work in the maximum power point (MPPT) and deliver the maximum available power to the grid. The utility grid is responsible to balance the power within the microgrid.

6.1.1 Grid-connected DC microgrid

In the DC configuration, the power from/to the grid has to pass through an AC/DC conversion step. The utility grid should keep the power balance of the system and regulate the DC voltage.

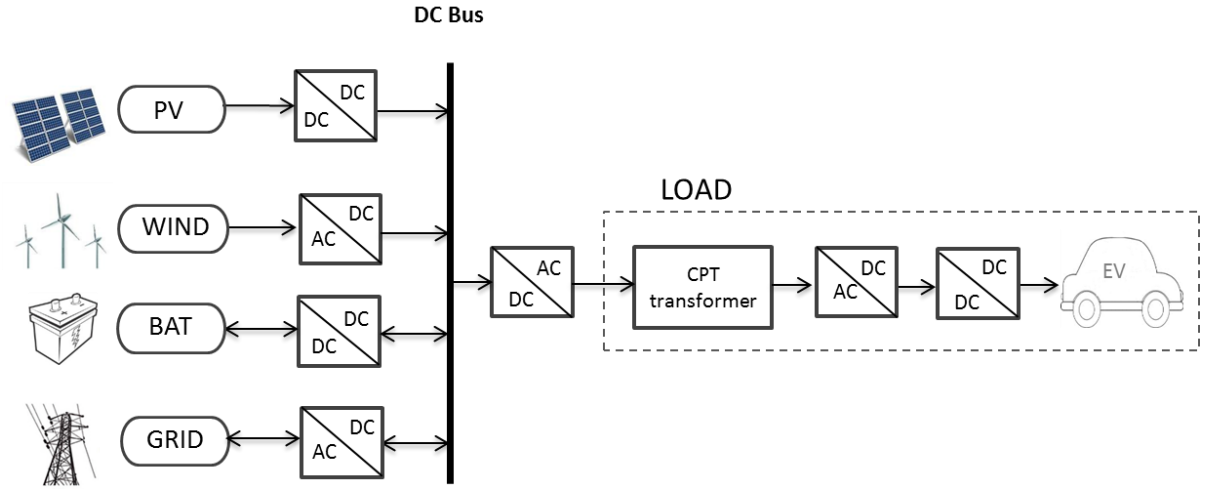

Figure 6.1 - Grid-connected DC microgrid configuration

The battery storage system is connected to the DC bus via a DC/DC converter which regulates also the charging process. The solar and the wind system are also connected to the DC bus with the required components (the connection was also discussed during the stand-alone operation mode in Chapter 5.1.1). A high frequency inverter is used to deliver the power to the CPT transformers. [43]

6.1.2 Grid-connected AC microgrid

In case of a grid-connected AC microgrid, the grid can be connected via a transformer to the main grid. The grid has a specific value of voltage and frequency at the point of common coupling with the sustainable microgrid which might not be the same as the operating values of the AC microgrid and this is the reason why they should be coupled. The remaining configuration remains the same as for the stand-alone operation mode.

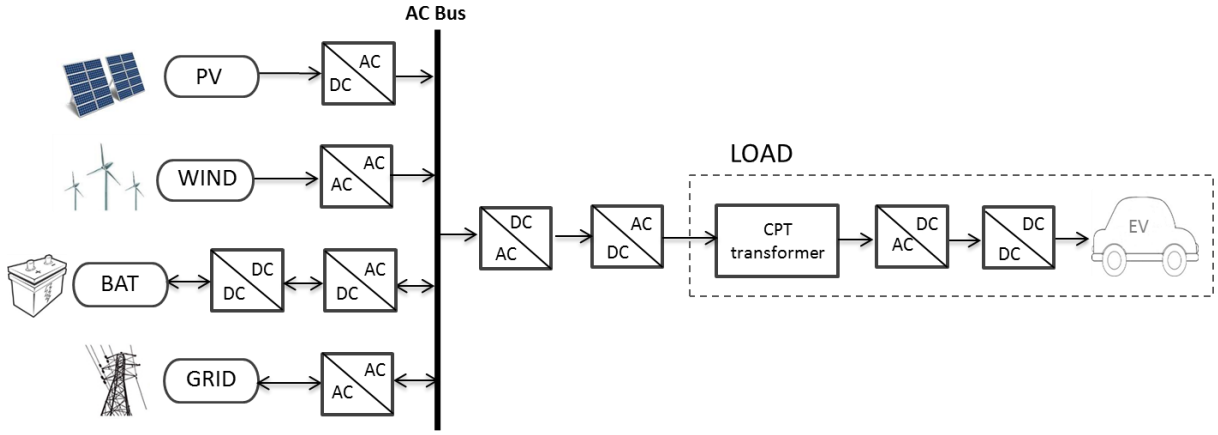

Figure 6.2 - Grid-connected AC microgrid configuration

For the stand-alone operation mode the DC microgrid was considered to be the most appropriate topology for minimizing the power conversion losses. A DC microgrid will be also studied for the grid-connection operation. The main benefit of having an AC microgrid is for the injected the excess wind power to the grid. For supplying the load from the grid, an AC/DC conversion is in any case also needed. As the main goal is to efficiently supply the load and the power flow to grid would be considered a secondary process. This benefit of an AC grid-connected microgrid is not considered of high significance.

The hybrid microgrid and the high frequency AC microgrid are also possible options. However, cannot be proposed for the same reason described in the stand-alone operation section.

6.2 Power Control Management

The power control management in the grid-connection system is more complex compared to the stand-alone as far as the power flows is concerned. This is because the unbalance of the power demand and supply could be covered from both the battery and grid in the most beneficial way.

Firstly, a control strategy where the battery had the first priority was simulated (for storing the excess power or providing power in case of shortage). The goal was to achieve maximum independence of the microgrid from the main grid and to use the grid connection as an auxiliary back-up source.

However, in that case the battery would become empty and then the power connection to the grid should be large enough to cover the maximum demand. As a result a significant power connection was required which made the goal of independence from the utility grid not valid.

Therefore, a new control strategy was implemented which provided a cooperative function of both the storage and the grid. Within this control, the goal is to use the storage for covering the load while keeping it on a high state of charge. If the state of charge becomes lower, then the power needed to supply the load comes from both the storage and the grid. A simplified diagram of the control strategy is shown below.

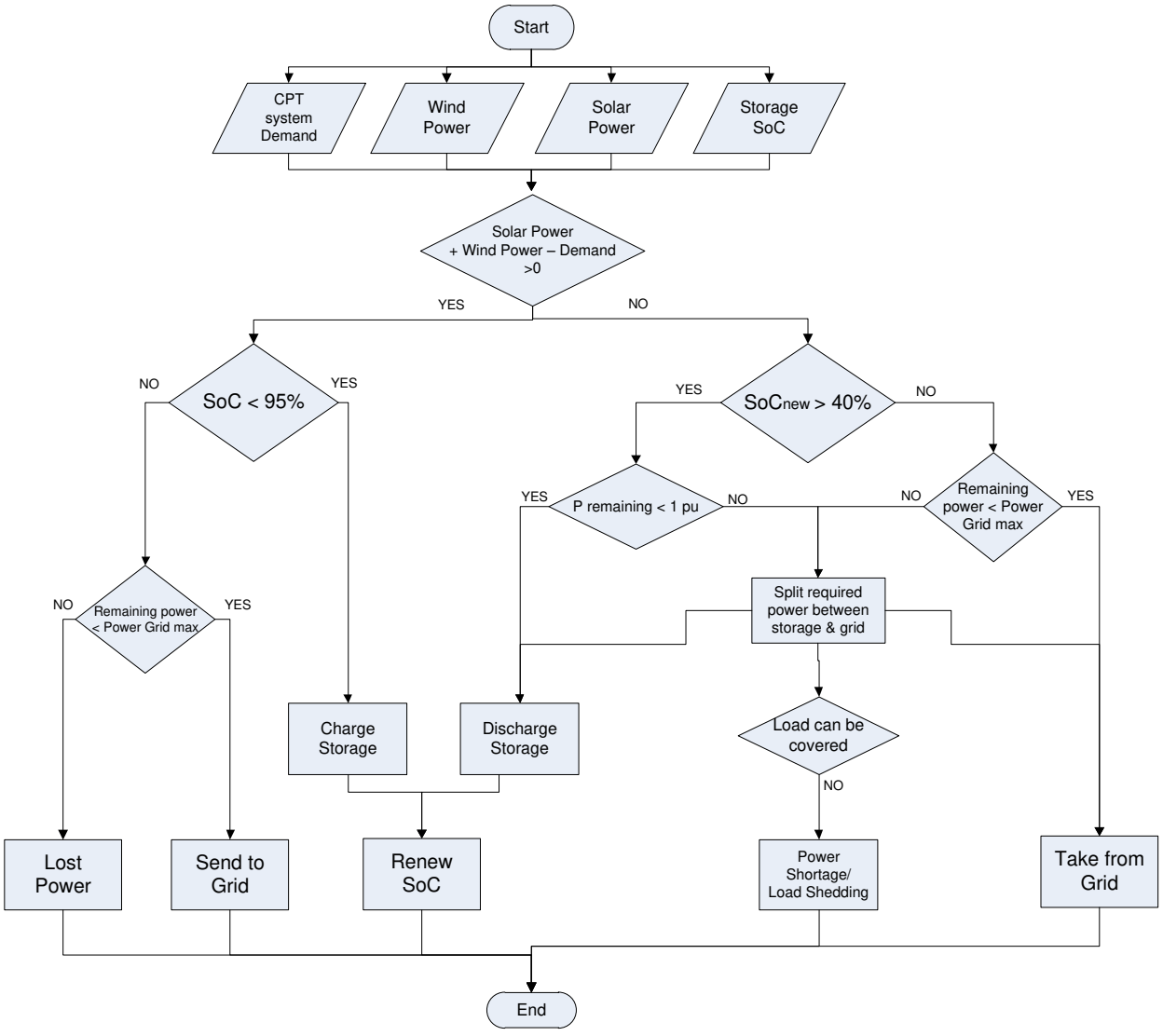

Figure 6.3 - Power Control Management, Grid-connected mode

6.3 Sizing Results

In the simulation model, the control strategy described above was used and the results of the sizing are presented below. The 3D figures show the total power that should be installed as a function of the grid connection capacity and the energy mix of wind and solar system. The storage size during these simulations is kept constant. The first two figures are for storage size of 1 day reserve. Then, results for storage of 2 days are presented.

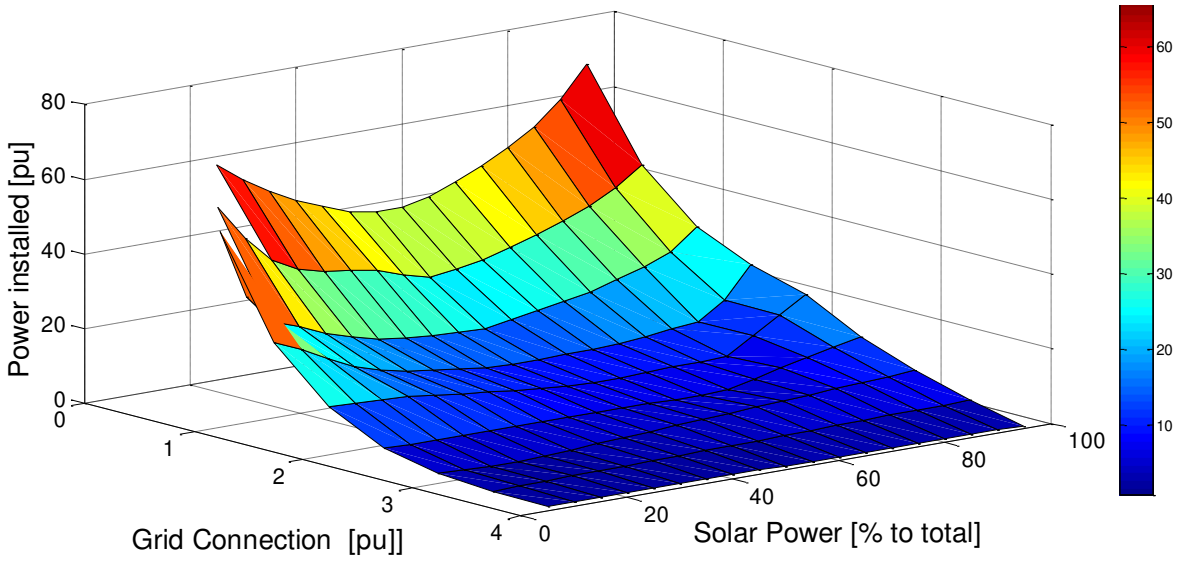

Figure 6.4 - Sizing of grid-connected microgrid (storage size 1 day reserve)

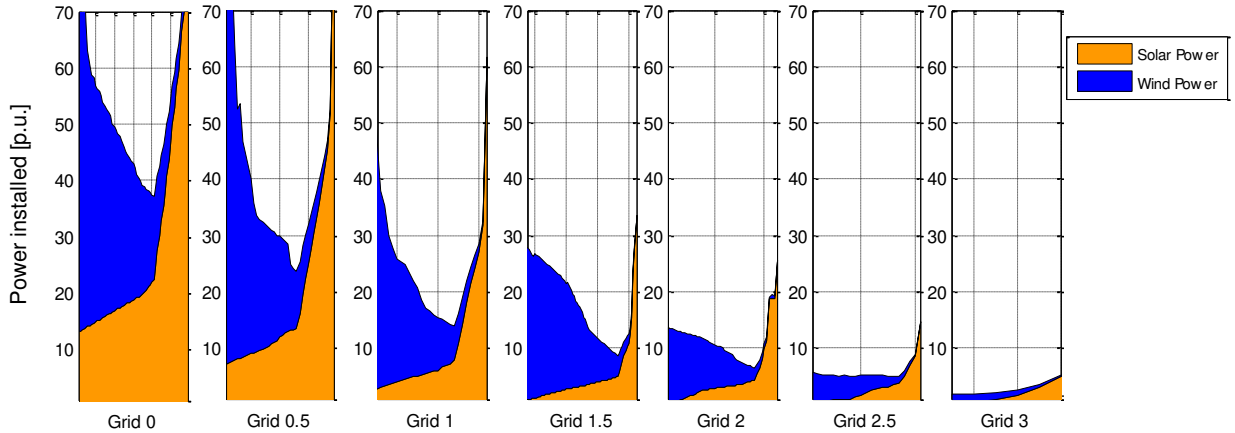

Figure 6.5 - Sizing of Solar & Wind system for grid connection 0-3 pu (storage size 1 day)

It can be observed that by introducing a grid connection, the total power that should be installed decreases. Without a grid-connection about 38 pu RES is needed. However, with grid-connection of 0.5 pu, the power installed decreases to 24 pu and with a grid-connection of 1 pu it decreases to 13pu. The curve on Figure 6.4 becomes more flat for a large grid-connection, meaning that the benefit of the grid connection decreases by increasing further the capacity of this connection.

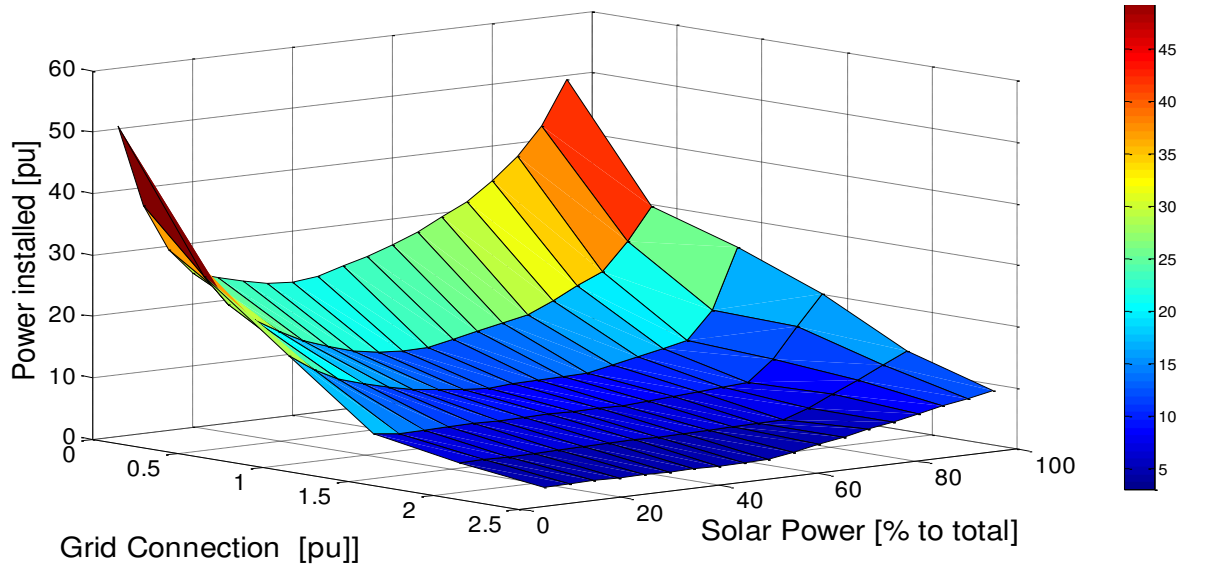

Figure 6.6 - Sizing of grid-connected microgrid (storage size 2 days reserve)

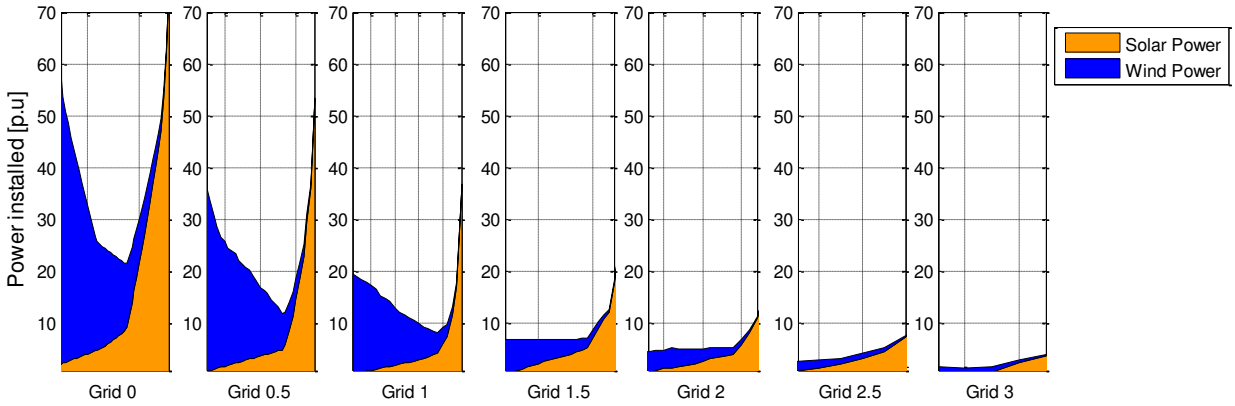

Figure 6.7 - Sizing of Solar & Wind system for grid connection 0-3 pu (storage size 2 day)

The same is true also for a storage size of 2 days. In this case apparently the total renewable power installed is even less and the total curve is flatter, meaning that the benefit from extra grid connection capacity is lower than in the cases with smaller storage.

6.4 Economic Analysis of grid-connected microgrid

For the grid-connected operation mode the basic cost analysis based on the 'Levelized Cost of Electricity' remains the same as in the stand-alone operation mode. However, in this case the prices for buying power from the grid and sell power to the grid should be taken into account.

In the Netherlands there is a liberalized energy market where there are two related power markets in which power can be sold. The Amsterdam Power Exchange (APX) is the so called spot market where power is traded. The producers offer the power and bid for the amount of power they are willing to

produce and the price they require, on an hourly basis. This power exchange is a day-ahead market, so the prices reflect the real conditions such as the load demand or the weather conditions.

The power can also be sold via bilateral contracts with a fixed price. These long-term contracts have more uniform prices which depend on the annual supply. Typical values are shown in Table 6.1.

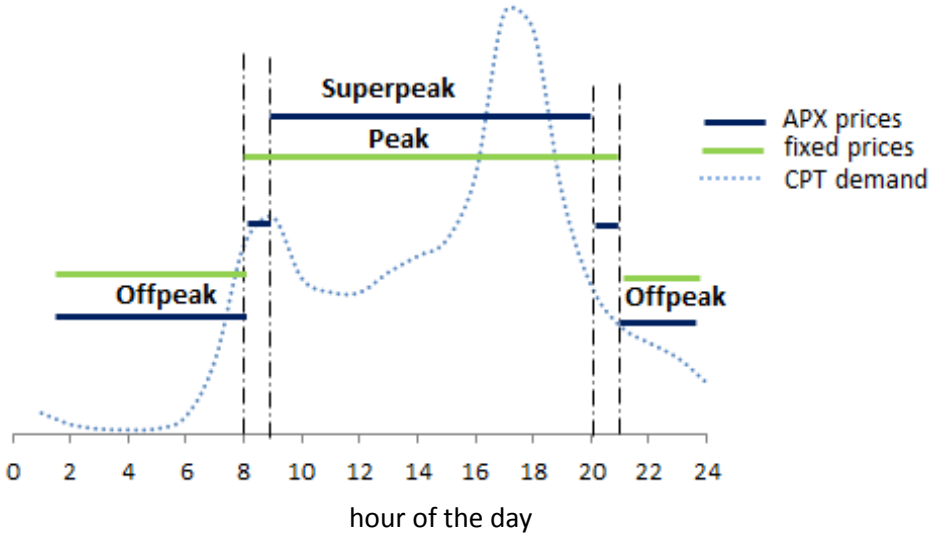

Figure 6.8 - Daily distribution of electricity market prices

Table 6.1 - Fixed pricing of power

Annual Supply	Selling Price
< 3MWh	Off-peak: 160 €/MWh Peak: 214 €/MWh
3MWh - 5MWh	82 €/MWh
> 5MWh	60 €/MWh

Data for the prices of electricity are difficult to find as the terms of bilateral contracts are confidential. Also, the APX prices are very sensitive to external conditions and might significantly change during the day or the year. The above prices assumed for the model are found in [44], based on average APX prices for 2006.

We can see that the super-peak prices unfortunately coincide with the evening peak of the demand of the CPT system. However, the morning peak which has smaller amplitude exists during the morning off-peak hours.

In energy markets there is also the balancing market where the producer should resort to when he has a contract of selling power that he was unable to produce. The cost for buying balancing power can be considered also as a penalty to the producer and the prices are quite high. As these mechanisms are quite complex and go out of the scope of this thesis, the balancing market was not taken into account when the electricity was sold to the grid.

Moreover, the cost for grid connection should be estimated. Data for many European countries provided by the EWEA [45] showed that the estimated cost for grid-connection is about 45-160 €/kWh. For the Netherlands a range of 60-110 €/kW was stated. In extreme cases values up to 400€/kW are found. In this study an average value of 85 €/kW was assumed [46]. Cost of the extension of transmission lines is also mentioned in literature. However, in this study the microgrid is placed near highways, so it is assumed that not significant extension of the transmission line is required, like in the implementation of microgrids in remote areas.

All in all, the LCOE for the grid connected mode can be calculated by the following formula.

$$LCOE = \frac{\sum_{t=1}^{n}(Cost_t - Revenue_t)}{\sum_{t=1}^{n}(Energy_t)}$$

$$Cost_t = {Investment}/{n} + Operation_t$$

Where,

t, the index representing the year
n, the lifetime of the system
$Cost_t$, the total cost (investment & operation) of the system for the year t
$Investment$, the total investment cost of the system
$Operation_t$, the O&M cost of the year t
$Revenue_t$, revenues from selling electricity for year t
$Energy_t$, energy required and used by the CPT system at the year t

6.5 Optimization for minimum cost

6.5.1 Results of cost analysis

For all the sizing combinations shown above, the LCOE is calculated in order to draw conclusions on the optimal configuration from the point of view of minimum cost.

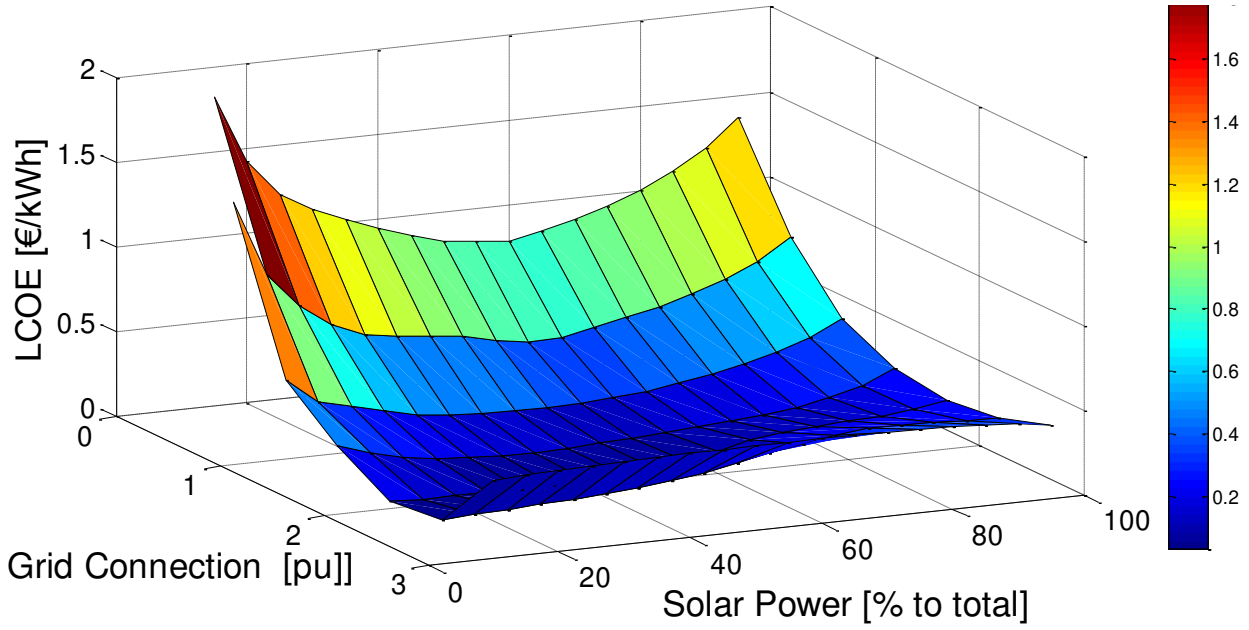

Figure 6.9 - LCOE considering the microgrid revenues vs. grid connection and (%) solar power

The above figure was made with the assumption that the excess power is sold to the grid, taking into account the limitation of the grid connection capacity. The assumed prices were mentioned in the previous section and are also listed in Appendix C.

It can be clearly seen that for a storage of 1 day reserve, there is an optimum that lies around a grid connection of 2 pu capacity. Then, increasing the grid-connection increases the total cost of the system.

It is important to also see the optimum point with minimum cost when taking into account only the investment cost of the system, without taking into consideration the revenues from sold power.

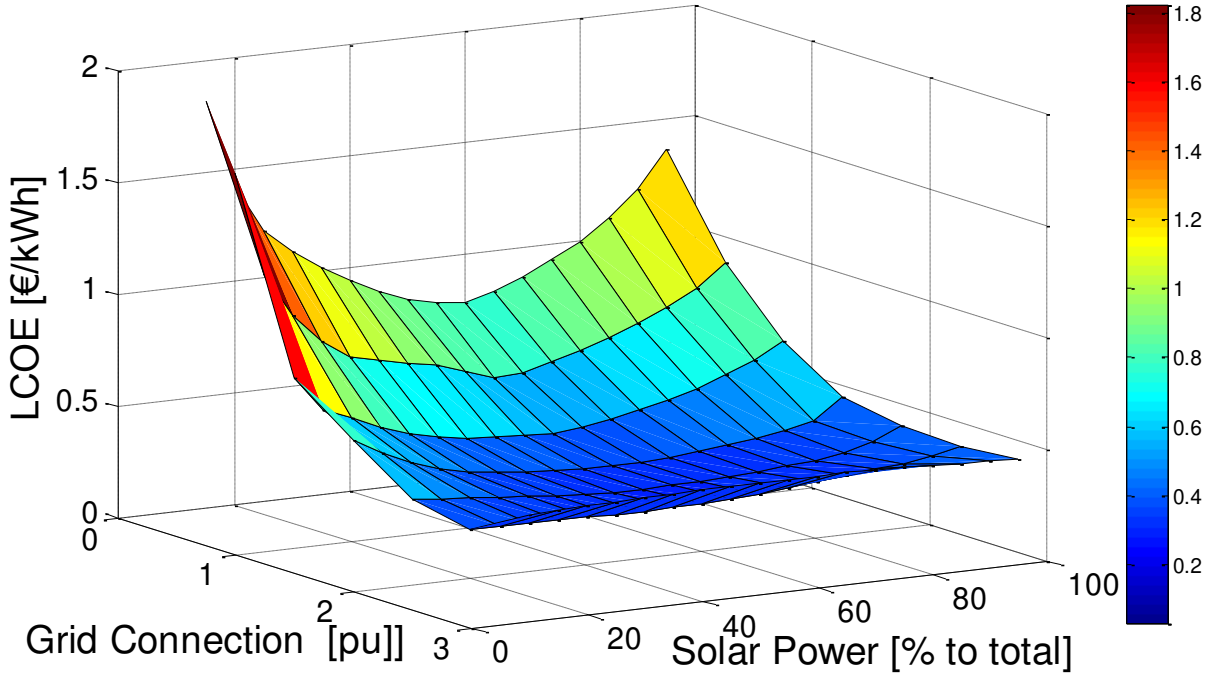

Figure 6.10 - LCOE considering only investment cost vs. grid connection and (%) solar power

The curve in this case is more flat but shows still that the optimum grid-connection capacity lies near the 2 pu grid exchange capacity.

Next, the combinations of storage and grid interconnection are shown. The combination with the minimum LCOE can be concluded as the optimum configuration of the system. First, the curve for the investment cost is shown and next the curves when the energy is sold are presented.

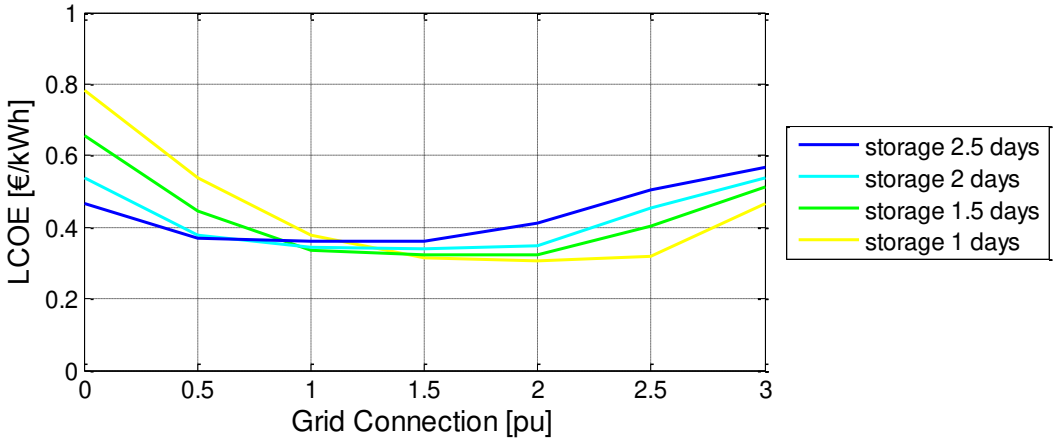

Figure 6.11 - LCOE considering only investment cost vs. grid connection & storage size

It is observed that there is some trading-off between the grid connection capacity and the storage size, as these are the two back-up sources which provide auxiliary power to the load.

For the stand-alone operation, it was found that 3 days of storage are required and the LCOE was about 0.40 €/kWh. When a grid connection is introduced to the system, for the same cost there is an alternative to reduce the storage to 2 days with 0.5 pu grid connection or for a storage size of 1 day the grid connection should be about 1 pu. The above values are for the investment cost only (Figure 6.11). Considering the excess power (limited by the interconnection capacity) is sold and the microgrid has the corresponding revenues, then the storage could be decreased to 1 day reserve with 0.5 pu grid connection (with the same investment cost as the stand alone system).

As far as the investment cost is considered, the LCOE for the microgrid can reach a minimum value of 0.30 €/kWh. However, much lower LCOE can be achieved when the excess power is sold to the utility grid.

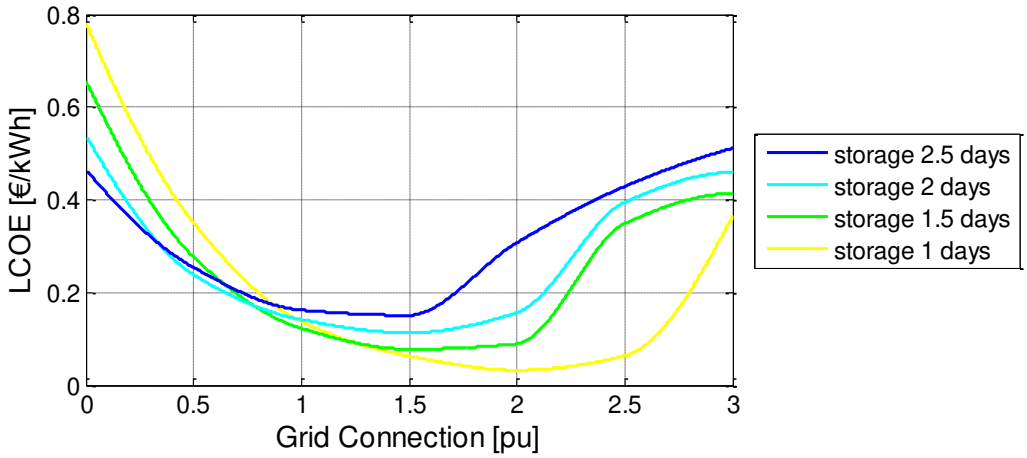

Figure 6.12 - LCOE considering the revenues from selling power vs. grid connection & storage size

The optimum sizing in this case is to have a storage size of 1 day (yellow line) and a grid-connection capacity of about 2 pu. The large interconnection capacity offers a greater capability of selling electricity. We can see that for grid connection of 1 pu and storage of 1 day, the LCOE when selling power reaches the 0.14€/kWh. For grid connection of 2 pu and storage of 1 day, the LCOE is just a few eurocents.

Here, to remind that power of 1 pu, means the average demand and that the peak demand over the year is about 4.5 p.u.

6.5.2 Sensitivity analysis of cost estimation

A sensitivity analysis for the assumptions of the solar/wind system cost and the storage cost was performed in the stand-alone system. In this chapter, the sensitivity analysis will be focused on the electricity market prices and on the cost of the grid connection.

The cost of the grid connection is in general considered low in respect to the cost of the other system components. We can see that it does not change the results that were already presented (Figure 6.13 - Sensitivity analysis for grid-connection cost). The storage system and the installed renewable power have the main share in determining the LCOE.

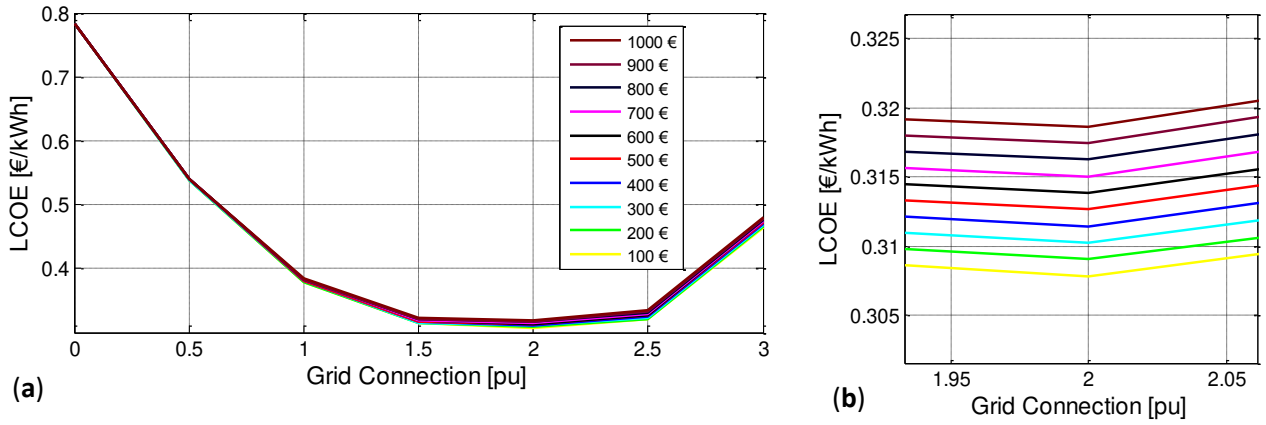

Figure 6.13 - Sensitivity analysis for grid-connection cost (a) grid connection 0-3 pu, (b) grid connection 2 pu

However, this is valid under the assumption that the transmission lines already exist and no significant extension is needed. In order to extend the transmission lines, the total cost is higher depending on voltage level. In a microgrid implemented in the Netherlands or in other heavily populated countries, extension of transmission line is not considered an issue.

It is important to also see how the selling prices of the power to the grid affect the LCOE.

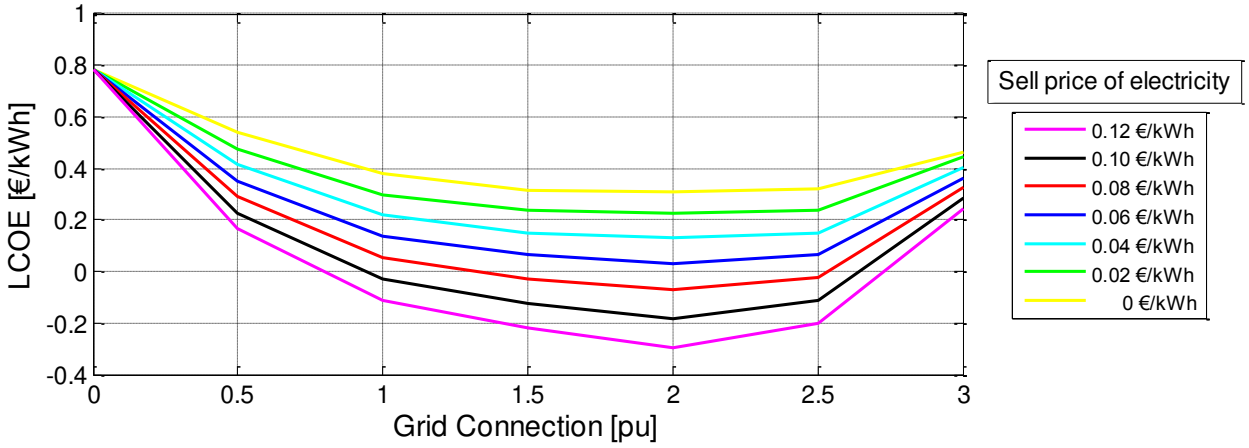

Figure 6.14 - Sensitivity analysis for selling price of electricity

The analysis shows that the LCOE changes significantly if the selling price of electricity changes. However, the minimum cost sizing remains the same and only the absolute value of the cost changes. We know that energy markets have a special structure that was not studied in detail in this thesis. The optimum size of the grid connection can be safely estimated to 2 pu which comes from the form of the curves and remains the same even for zero prices.

All the above are results for a grid-connected system with a storage capacity of 1 day reserve.

6.6 Power Flow Analysis of minimum cost point

In this section the minimum cost point from the previous analysis will be presented and analyzed. The sizing of each system is tabulated below.

Table 6.2 - Optimum sizing of grid-connected system

Max grid connection capacity	2 pu
Storage System size	1 day
Solar peak power	3.3 pu (35%)
Wind power installed	6.2 pu (65%)

In order to get an overview of the power flow, the average year power of each component has been calculated. The major difference from the stand-alone system is the lost power. However, we can see that even with a grid-connection there is significant power lost. This is because there is a limitation of the capacity of the interconnection to 2 pu. The solar system provides a maximum power of 3.3 pu and the wind system a maximum of 6.2 per unit. As a result the grid interconnection should be roughly more than 6 pu in order to deliver to the grid all the excess renewable power produced during the time with low demand from the electric vehicles. However, the goal of this microgrid is to cover the load of the electric vehicles and not produce power to be sold to the utility grid.

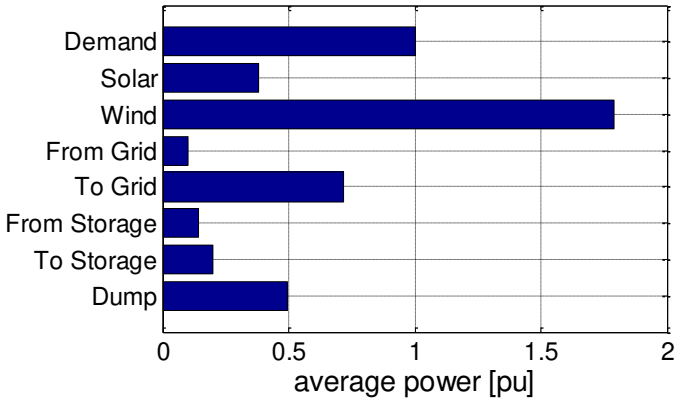

Figure 6.15 - Average power of each system component [pu]

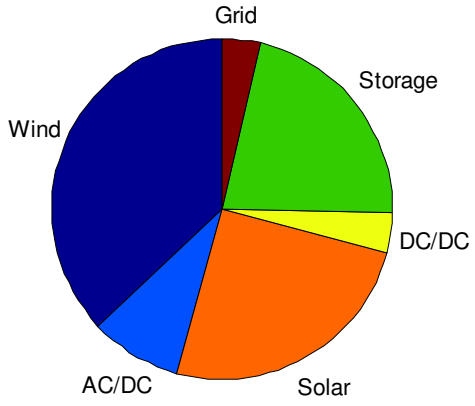

Figure 6.16 - Investment cost distribution

The investment cost in the grid-connected system is distributed more evenly within the different components. The grid connection has a small share in the cost, however now the storage is 3 times smaller and has a share of 20% of the cost, in comparison to 50% for the stand-alone mode.

The state of charge of the storage is plotted below. We can see that there are deeper cycles in comparison with the 3-day storage of the stand-alone system. However, the SoC barely goes below 30% as the control is set to keep it to a safety level of charge in order to be able to cover the load at all times.

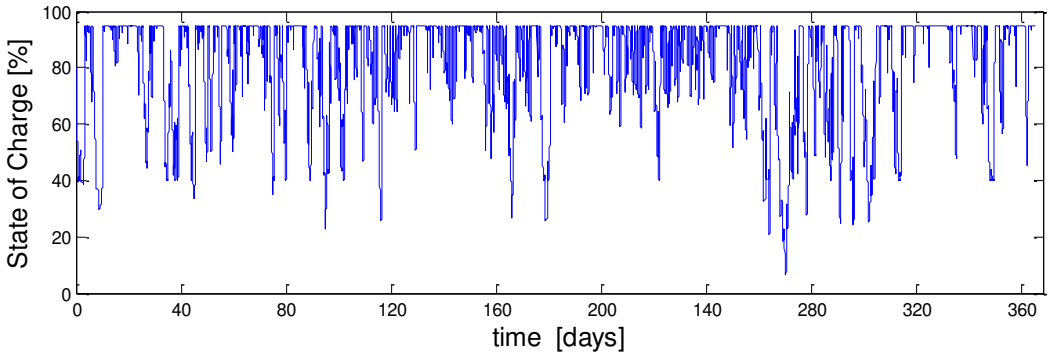

Figure 6.17 - State of Charge of storage system

To get an overview of the average power of each component throughout the year, data for the average power flow per month are plotted. Months with high renewable power generation have high power sent to the grid and high amount of power lost.

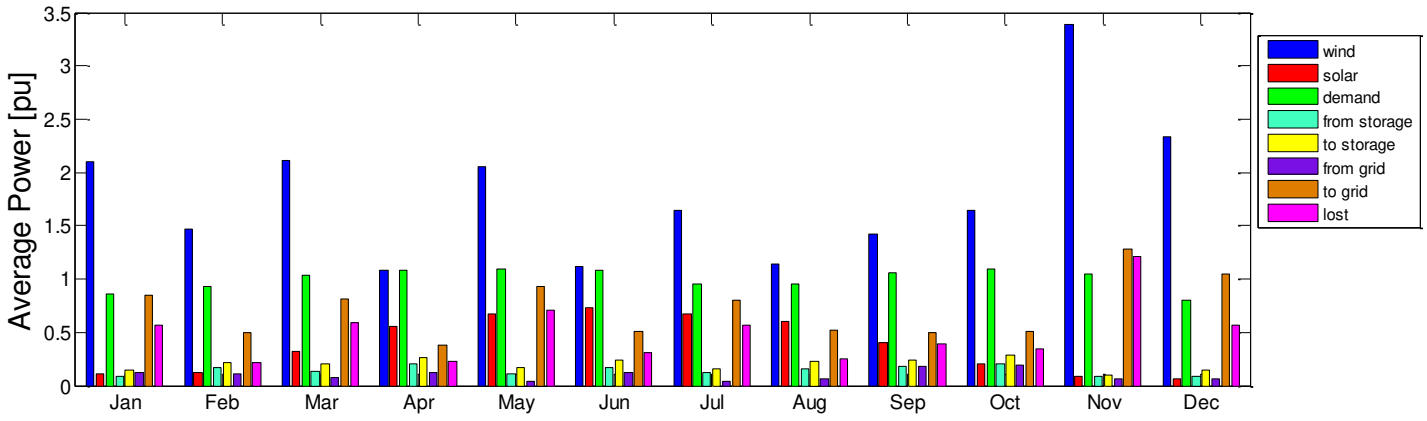

Figure 6.18 - Average power flow per month

Next, some figures will be presented in order to get an idea of the power exchange between the utility grid and the sustainable microgrid. As the prices of the power vary during peak and off peak hours it is important to see when power should be bought from the grid (preferably during off-peak hours) and when power can be sold to the grid (preferably during peak hours).

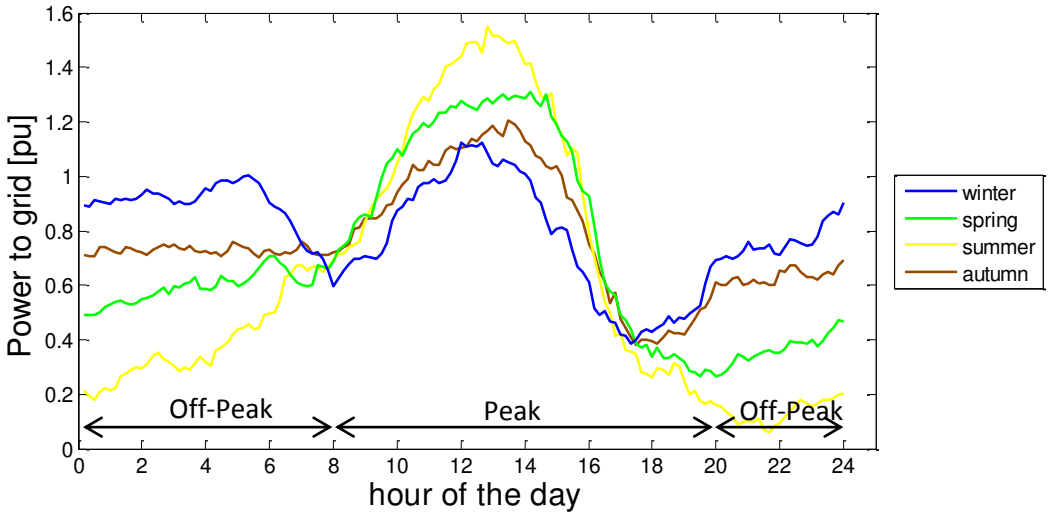

Figure 6.19 - Average power to the grid during the day

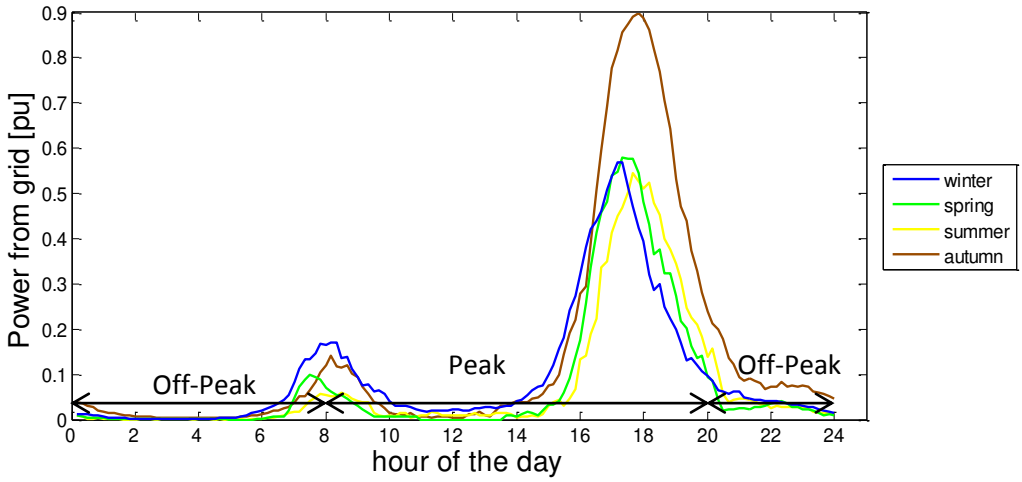

Figure 6.20 - Average power from the grid during the day

It can be seen that the 2 peaks of the demand affect a lot the power flow from/to the grid. We can see that power is required from the grid basically during the time the 2 peak of the demand at around 8:00 and 18:00. At this time, the power to the grid is of course limited. Autumn is a period with low renewable energy production and this is the reason why there is high demand of power from the grid and at the same time there is low power sold to the grid. The curve of the power to the grid follows the solar power production for the time between 8.00 and 18.00 and has often a peak at 12.00. During the night hours, the power to the grid comes from the wind energy system.

The curve of the lost power is similar with the power to grid, as both depend on the excess renewable power produced. The lost power is the amount of power that cannot be transferred to the grid due to the limited capability of the grid interconnection.

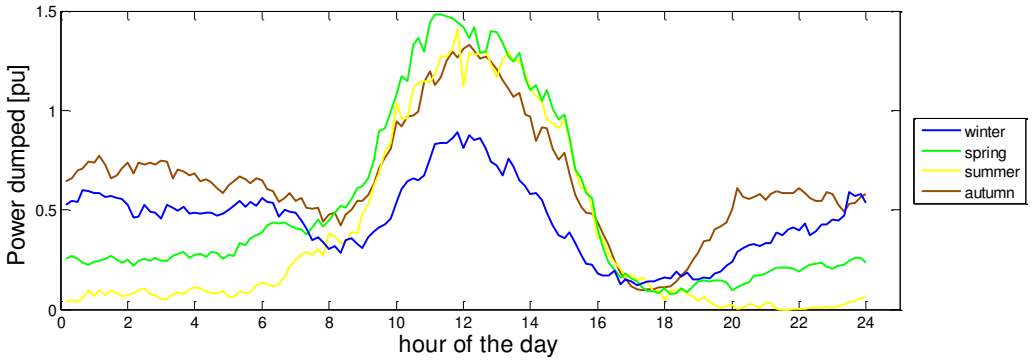

Figure 6.21 - Average Power lost during the day

6.7 Discussion on Grid-Connected mode of the microgrid

Introducing a grid-connection to the system decreases significantly the required capacity for storage. As the cost for a grid interconnection is much lower than the cost of the storage, total investment cost of the system is decreased significantly. For the stand-alone microgrid, the optimum configuration of the system was considered to have 3 days reserve of storage. For the grid-connected microgrid the storage could decrease, but it cannot become smaller than the energy required for 1 average day. Even with a small grid connection the total cost of the system decreases significantly, as both the amount of renewable power installed and the storage capacity become smaller.

When optimizing for the minimum cost of the system, a grid connection of 2 pu is required. In other words, the interconnection capacity should be twice the average demand or less than half of the maximum demand (maximum demand is 4.6 pu). Having a larger interconnection, decreases the power that is lost which is injected to the main grid and in this way the system gains additional revenues. The total revenues greatly depend on the electricity pricing. Electricity prices are quite sensitive and volatile, so it is difficult to make a correct estimation.

In the above study, it was assumed that the main grid would be able to supply the power needed until reaching the maximum power capability of the interconnection. Also, it would be able to accept the excess power produced until reaching again the maximum power capability. These results are under the assumption that the extension of the transmission lines for the grid-connection is not significant.

7 Conclusions

The transition from petrol-fueled mobility to electric mobility could be enhanced by installing on-road charging systems for powering electric vehicles while driving. The road transport system would become really sustainable in case the on-road chargers are supplied by renewable energy sources.

In this thesis, Contactless Power Transfer for powering electric vehicles while driving was studied. As described, the concept of CPT on-road charging system is similar to a transformer where the primary winding is installed on the road and the secondary winding below the vehicle's chassis.

For the primary winding's specifications, the operating frequency, the power transferred and its length are the main parameters. High frequency and resonant mode coupling are necessary for transferring power efficiently. There are many advantages and disadvantages concerning these parameters and in many cases the benefits come in opposition to each other (see Table 1.3). An operating frequency of 100 kHz is a realistic value which provides quite high transfer efficiency. The maximum length of the primary winding in such case can be up to 300m.

The primary windings which are placed one next to the other create a CPT segment. The segments can be distributed in many ways, with longer or shorter distances in between. The length of each CPT segment should be small and the segments should be well distributed over the road in order to optimize the efficiency of the system. For the battery of the vehicle, small shallow cycles are better than deep cycles, so smaller segments are more beneficial for the health and lifetime of the battery. It was also shown that in order to maximize the driving range, there should be a balance between the energy produced by a CPT segment and the energy consumed by the EV while driving in between the segments. In case the CPT segments are distributed over the highway and are not densely placed, the usefulness of the overall system can be maximized.

The major benefits of installing CPT system are the significant driving range extension and decrease of the battery size of the EV that can be achieved. To be specific, the driving range can be increased to 500 km (similar to the one of petrol-fueled vehicles) with 50% of the highway covered with primary windings with power transfer capability of 20 kW. By keeping the driving range to 140 km, the battery of the EV can be decreased to 50% by installing a CPT system of 50% coverage and 14 kW power. For increasing the driving range to 500km while decreasing the battery to 50%, a CPT system of 50% coverage and 24kW is needed. All the possible combinations for different driving ranges and battery sizes can be found in the Appendix A.

The proposed location for installing CPT systems is the highways. The main reason is that most of the distance driven by a car is covered on highways (result based on NL mobility data [18]). Moreover, highways cover only 4% of the total road system in the Netherlands. As a result, implementation of CPT systems in segments on highways is proposed within this research.

The CPT systems installed at highways would be powered from wind turbines and solar arrays which would be installed next to the road. These renewable energy sources will form a sustainable microgrid. Due to the uncontrollable nature of the RES systems, a stationary storage system would be essential. A

DC sustainable microgrid is proposed in this thesis. The power demand curve for charging EVs was estimated and the average and maximum values for different scenarios can be found in the Appendix B.

As far as the stand-alone microgrid configuration is concerned, storage of 3 days reserve capacity is required in order to supply the demand during low renewable energy production periods. The renewable power system of the microgrid should have installed peak power of 12 pu or 12 times more than the average power which is 2.6 times the maximum power demand. A system of 40% solar and 60% wind is proposed as it offers the required power with the minimum possible cost.

Due to the fact that storage with high capacity is required for the stand-alone microgrid, which is fully used only few times per year, the grid-connected system was also introduced. With a grid-connection the storage size can be decreased to 1 day reserve. The optimum size of the grid-connection was found to be 2 times the average demand, which is less than half of the maximum load. The renewable power that should be installed is also decreased by a factor of 1/4.

The investment cost has decreased from 0.40 €/kWh for the stand-alone system to 0.30 €/kWh for the grid-connected. The LCOE (€/kWh) can decrease down to a few eurocents, when the revenues for selling the excess power to the grid are taken into account.

All in all, the grid-connected option is proposed for a microgrid used to power electric vehicles while driving via Contactless Power Transfer systems. These microgrids would be placed at the roadside of highways and the extension of transmission lines for the grid-connection would not be considered an issue.

If the CPT system is implemented in busy highways, then more vehicles use the system. Therefore, the payback time of the investment decreases. However, it was found that during peak hours the maximum power demand increases significantly when there is extreme vehicle flow. As a result, the demand curve has high spikes and the microgrid should be oversized in order to cover the load in such conditions. A load shedding scheme could be applied in such cases in order to supply the vehicles with lower power. The driving range in case of very high traffic would decrease. However, drivers already experience a decrease in driving range during extreme traffic when driving with combustion engine vehicles.

8 Recommendations & Further Research

A combined research on on-road charging and on the sustainable microgrid supplying the charging systems was conducted in this thesis.

As far as the on-road charging system, further work could be made on a comparison of CPT with fast charging and battery swap which are the technologies that are planned to be extensively used for electric mobility. Home charging is always considered a convenient option for consumers. However, in case of implementation of CPT systems there might be no need of public fast charging stations. The feasibility of fast chargers and CPT chargers can be compared.

A thorough study on the material and installation cost of CPT systems is missing in literature. This is also necessary for the aforementioned feasibility study for the comparison with the other charging options. The implementation of CPT on vehicles that have supercapacitors, as main or auxiliary energy source, can be also a topic for further investigation.

As far as the microgrid sizing is concerned, a typical highway was modeled and data for the wind speed and the solar irradiance for the Netherlands were used. Moreover, weather data for other geographical regions could be used. A step further could be to investigate the overall road system infrastructure of other countries and model highways with different driving patterns. In this way, the resulting sizing of the microgrid (e.g. the percentage of the solar and wind energy system) might differentiate from the proposed one.

In case of extensive implementation of CPT charging systems supplied by a grid-connected microgrid, it is necessary to research whether the main grid would be able to support the power needs during low RES production. The effect on the stability of the main grid might be an issue.

More intelligent and complicate systems, as far as the installation and the control, could be also investigated. The concept of having variable length and distribution of the CPT segments on the highways has already been introduced. This can be studied for a specific road depending for example on its inclination and the entry/exit parts of the highway. A more complex power management control scheme could also increase the efficiency of the system. For example, a variable load scheme for load shedding during extreme traffic conditions could decrease the energy storage and the energy bought from the main grid. The amount of power transferred to the cars could also depend on the renewable energy production and on the estimated trip range specified by each driver.

Bibliography

[1] O. H. Stielau, G. A. Covic, C. Wang, "Design Considerations for a Contactless Electric Vehicle Battery Charger," *IEEE Transactions on Industrial Electronics*, vol. 52, no. 5, pp. 1308-1314, Oct. 2005.

[2] S. Chopra, P. Bauer, "Analysis and Design Considerations for a Contactless Power Transfer System," in *Telecommunications Energy Conference (INTELEC), 2011 IEEE 33rd International* , Oct. 2011.

[3] C. Rathge, U. Jumar, D. Kurschner, "Design Methodology for High Efficient Inductive Power Transfer Systems With High Coil Positioning Flexibility," *IEEE Transactions on Industrial Electronics*, vol. 60, no. 1, pp. 372-381, Jan 3013.

[4] P. Venugopal, "Wireless Power Transfer for E-Mobility," TU Delft, Master Thesis, 2012.

[5] S. Chopra, P. Bauer, "Driving Range Extension of EV With On-Road Contactless Power Transfer - A Case Study," *IEEE Transactions on Industrial Electronics*, vol. 60, no. 1, Jan. 2013.

[6] Y. Gao, M. Ehsan, A. Emadi, *Modern Electric, Hybrid Electric and Fuel Cell Vehicles*.: CRC Press, 2009.

[7] M. Castilla, P. Bauer, F. A. van der Pijl, "Adaptive Sliding-Mode Control for a Multiple-User Inductive Power Transfer System Without Need for Communication," *IEEE Transactions on Industrial Electronics*, vol. 60, no. 1, pp. 271-279.

[8] L. Lam, "A Practical Circuit based Model for State of Health Estimation of Li-ion Battery Cells in Electric Vehicles," TU Delft, Master thesis, 2011.

[9] Electropaedia, 2012, [Online]. http://www.mpoweruk.com/

[10] M. Saunders, Z. Pantic, S. Hung, J. Taiber, S.M. Lukic, "Use of inductive power transfer for electric vehicles," in *Power and Energy Society General Meeting, IEEE*, 2010.

[11] A. Cruden, P. J. Hall, R. Carter, "Optimizing for Efficiency or Battery Life in a Battery/Supercapacitor Electric Vehicle," *IEEE Transactions on Vehicular Technology*, vol. 61, no. 4, pp. 1526-1533, May 2012.

[12] M. E. Ortuzar, "Design, Implemetation and ebaluation of an auxiliary energy system for electric vehicles, based on ultracapacitor and buck-boost converter," Santiago de Chile, PhD Thesis, 2011.

[13] Centraal Bureau voor de Statistiek Statline, "Lengte van wegen; naar wegkenmerken en gemeente", 2012, [Online]. http://statline.cbs.nl/StatWeb/publication/?DM=SLNL&PA=70806ned&D1=0,2,8,14&D2=0&D3=l&HDR=T,G2&STB=G1&CHARTTYPE=1&VW=T

[14] Eurostat European Commision, "Regions with the highest motorway density (km 100 km2)", 2010, Dec., [Online]. http://epp.eurostat.ec.europa.eu/statistics_explained/index.php?title=File:Motorway_density_(km_1000_km2)_by_regions.PNG&filetimestamp=20110518121016

[15] Eurostat European Comission, "Motorway density (km 1000 km2) by regions", 2009, [Online]. http://epp.eurostat.ec.europa.eu/statistics_explained/index.php?title=File:Motorway_density_(km_1000_km2)_by_regions.PNG&filetimestamp=20110518121016

[16] Statline, C.B.S. Centraal Bureau voor de Statistiek. 2011. [Online]. http://statline.cbs.nl

[17] WegenWiki. 2012 [Online]. http://www.wegenwiki.nl/Nederland

[18] Ministerie van Verkeer en Waterstaat/Rijkswaterstaat, "Mobiliteitsonderzoek Nederland," Research Survey 2009.

[19] A. Brooker, M. Thornton, J. Rugh, NREL, "Technology Improvement Pathways to Cost-Effective Vehicle Electrification," in *SAE 2010 World Congress*, Detroit, Michigan, 2010.

[20] Ministerie van Verkeer en Waterstaat Rijkswaterstaat. 2010. Oost Nederland. [Online]. http://rws-oostnederland.verkeersgegevens.nl

[21] J. Harikumaran, "Sizing and Charge Control Strategies for a Grid-Connected Micro-grid with Electric Vehicles," TU Delft, Master Thesis, 2012.

[22] M. Vandehey, L. Elefteriadou, P. Ryus, Transportation Research Board, "Highway Capacity Manual," United States, 2010.

[23] S. Bai, S. M. Lukic, Z.Pantic, "Inductively coupled power transfer for continuously powered electric vehicles," in *Vehicle Power and Propulsion Conference, IEEE*, 2009.

[24] T. Loix. leonardo ENERGY initiative. 2009, Feb. [Online]. http://www.leonardo-energy.org/files/root/pdf/2009/article2.pdf

[25] KEMA. PowerMatching City: a living Smart Grid demonstration. 2011 [Online]. http://www.kema.com/Images/Results%20PowerMatching%20City_Brochure.pdf

[26] TNO. Solar energy from roads. [Online]. http://www.tno.nl/downloads/solar_energy_from_roads2.pdf

[27] M. Zeman, *Solar Cells*. Delft: Delft University of Technology, 2010.

[28] Drie keer groener, Duurzame Energiesnelweg A15. 2012, Jun. [Online]. http://www.energie-snelweg.nl

[29] Royal Netherlands Meteorological Instititute (KNMI), "Wind speed and solar irradiance data set for Cabauw Netherlands," 2001-2010.

[30] J.G. McGowan, A.L. Rogers J.F. Manwell, *Wind Energy Explained*: John Wiley & Sons Ltd, 2002.

[31] B. A. Sanden, C. R. Rydh, "Energy analysis of batteries in photovoltaic systems. Part I: Performance and energy requirements," *Energy Conversion and Management 46*, pp. 1957-1979, 2005.

[32] J. Østergaard, K.C. Divya, "Battery energy storage technology for power systems-An overview," *Electric Power Systems Research 79*, pp. 511–520, 2009.

[33] A. Kaas, P. Bauer, "Design approaches for a sustainable off-grid power system," in *37th Annual conference of the IEEE industrial electronics society, IECON*, Melbourne, 2011.

[34] NREL, "Distributed Generation Renewable Energy Estimate of Costs," 2012.

[35] www.batteryuniversity.com. http://batteryuniversity.com/learn/article/batteries_for_stationary_grid_storage.

[36] G. L. Soloveichik, "Battery Technologies for Large-Scale Stationary Energy Storage," *The Annual Review of Chemical and Biomolecular Engineering*, pp. 503-521, 2011.

[37] Solarbuzz Retail Pricing.

[38] P. Bauer, L.E. Weldermariam, E. Raijen, P. Kumar, "Connecting Topologies of Stand-Alone Micro Hybrid Power Systems," in *PCIM*, 2011, pp. 304-310.

[39] D. Chen, L. Xu, "Control and Operation of a DC Microgrid With Variable Generation and Energy Storage," *IEEE Transaction on Power Delivery*, vol. 26, no. 4, pp. 2513-2522, Oct. 2011.

[40] M. G. Simões, S. Chakraborty, "Experimental Evaluation of Active Filtering in a Single-Phase High-Frequency AC Microgrid," *IEEE Transactions on Energy Conversion*, vol. 24, no. 3, pp. 673-682, Sep. 2009.

[41] M.H. Nehri, C.M. Colson, "A Review of Challenges to Real-Time Power Management of Microgrids," in *IEEE Power & Energy Society General Meeting*, 2009.

[42] A. Kwasinski, "Quantitative Evaluation of DC Microgrids Availability: Effects of System Architecture Converter Topology Design Choices," *IEEE Transactions on Power Electronics*, vol. 26, no. 3, Mar. 2011.

[43] E. Farjah, N. Eghtedarpour, "Control strategy for distributed integration of photovoltaic and energy storage systems in DC microgrids," *Renewable Energy 45*, pp. 96-110, 2012.

[44] J. Frunt, J.M.A. Myrzik, D.T. Ho, "Photovoltaic Energy in Power Market," *European Energy Markets Conference* , 2009.

[45] S.Krohn, P.Morthorst, S. Awerbuch EWEA, "The Economics of Wind Energy," Denmark, 2009.

[46] F. Steinke , P. Muhlich, T. Hamache,r K. Schaber, "Parametric study of variable renewable energy integration in Europe: Advantages and cost so ftransmission grid extensions," *Energy Policy*, pp. 498–508, 2012.

Appendix A

CPT system specifications for different battery size & driving range

Coverage (%)	Power of CPT needed [kW] – range 140 km					
	Battery 80%	***Battery 60%***	***Battery 50%***	***Battery 40%***	***Battery 20%***	***Battery 10%***
10	26	48	-	-	-	-
20	13	26	32	39	57	-
30	9	18	22	27	37	45
40	7	14	17	20	27	33
50	6	11	14	17	22	26
60	5	9	12	14	19	21
70	4	8	10	12	16	18
80	4	7	9	11	14	16
90	3	6	8	9	13	14
100	3	6	7	9	11	13

Coverage (%)	Power of CPT needed [kW] – range 300 km				
	Battery 100%	***Battery 80%***	***Battery 50%***	***Battery 20%***	***Battery 10%***
10	-	-	-	-	-
20	36	42	53	-	-
30	25	29	35	43	49
40	19	22	26	32	35
50	16	18	21	25	28
60	13	15	18	21	23
70	11	13	16	18	19
80	10	11	14	16	17
90	9	10	12	14	15
100	8	9	11	13	14

Coverage (%)	Power of CPT needed [kW] – range 500 km				
	Battery 100%	***Battery 80%***	***Battery 50%***	***Battery 20%***	***Battery 10%***
10	-	-	-	-	-
20	50	55	60	-	-
30	34	36.5	40	46	-
40	25.5	28	30	33.5	40
50	20	22	24	27	32
60	17.5	19	20	22.5	26
70	15	16	17.5	19.5	22
80	13.5	14	15.5	17	18.5
90	12	12.5	13.5	15	17
100	11	11.7	12.5	13.5	15.5

Coverage (%)	Power of CPT needed [kW] – range inf.	
	Battery 100%	***Battery 80%***
10	-	-
20	-	-
30	48	48.5
40	36	36.5
50	29	29.5
60	24	24.5
70	20.5	21
80	18	18.5
90	16	16.5
100	15	15

Appendix B

Average and maximum value of the demand curve for different CPT systems and lengths of highway, 100% of cars are assumed to be electric (2 lanes, one direction)

For driving range 500km:

Length of Highway	Battery 100%		Battery 80%		Battery 50%		Battery 20%		Battery 10%	
	mean	*max*	*mean*	*max*	*mean*	*max*	*mean*	*max*	*mean*	*max*
10 km	1.4	6.4	1.5	6.8	1.6	7.4	1.8	8.2	2.0	9.4
20 km	2.8	12.7	2.9	13.6	3.2	14.7	3.5	16.3	4.1	18.7
30 km	4.1	19.1	4.4	20.4	4.8	22.1	5.3	24.5	6.1	28.1
40 km	5.5	25.5	5.9	27.3	6.4	29.4	7.1	32.7	8.1	37.5

For driving range 300km:

Length of Highway	Battery 100%		Battery 80%		Battery 50%		Battery 20%		Battery 10%	
	mean	*max*	*mean*	*max*	*mean*	*max*	*mean*	*max*	*mean*	*max*
10 km	1.0	4.7	1.2	5.4	1.4	6.5	1.7	7.7	1.8	8.4
20 km	2.0	9.4	2.3	10.7	2.8	13.0	3.3	15.4	3.6	16.7
30 km	3.0	14.1	3.5	16.1	4.2	19.5	5.0	23.1	5.4	25.1
40 km	4.1	18.8	4.6	21.4	5.6	26.0	6.7	30.7	7.3	33.5

For driving range 140km:

Length of Highway	Battery 100%		Battery 80%		Battery 50%		Battery 20%		Battery 10%	
	mean	*max*	*mean*	*max*	*mean*	*max*	*mean*	*max*	*mean*	*max*
10 km	-	-	0.4	1.8	0.9	4.3	1.5	6.8	1.7	7.7
20 km	-	-	0.8	3.5	1.8	8.5	2.9	13.5	3.4	15.5
30 km	-	-	1.1	5.3	2.8	12.8	4.4	20.3	5.0	23.2
40 km	-	-	1.5	7.1	3.7	17.1	5.9	27.0	6.7	31.0

Appendix C

Specifications of the microgrid's system components

Battery System	
Type	Lead Acid
Round efficiency	0.77
Charging efficiency	0.90
Discharging efficiency	0.85
Maximum SoC	95%
Minimum SoC	5%
Initial SoC	95%
Investment Cost	150 €/kWh, 300 €/kWh
Maintenance Cost	5 €/kWh/year
Lifetime	10 years
Solar System	
Efficiency	12%
Investment Cost	2500 €/kWp
Maintenance Cost	18 €/kWp/year
Lifetime	20 years
Wind System	
Power curve	MM92
Investment Cost	1700 €/kWp
Maintenance Cost	35 €/kWp/year
Lifetime	20 years
DC/AC conversion	
Efficiency	94%
Investment Cost	400 €/kWp
Maintenance Cost	10 €/kWp/year
Lifetime	15 years
DC/DC conversion	
Efficiency	98%
Investment Cost	120 €/kWp
Maintenance Cost	7 €/kWp/year
Lifetime	15 years
AC/DC conversion	
Efficiency	94%
Investment Cost	400 €/kWp
Maintenance Cost	10 €/kWp/year
Lifetime	15 years
Grid Connection	
Investment Cost	85 €/kW
Maintenance Cost	5 €/kW
Lifetime	30 €/kW
Price buy power	0.21 €/kWh
Price sell power (<3000kWh)	0.1870€/kWh
Price sell power (3000-5000kWh)	0.0820€/kWh
Price sell power (>5000kWh)	0.0588€/kWh

Per unit system of microgrid sizing

Base of per unit system: average demand

$$\text{demand}_{\text{pu}} = \text{demand} \Big/ (\text{average demand})$$

$$\text{Solar Power}_{\text{pu}} = (\text{Solar Power}) \Big/ (\text{average demand})$$

$$\text{Wind Power}_{\text{pu}} = (\text{Wind Power}) \Big/ (\text{average demand})$$

Appendix D

Power Flows for different weeks, Stand-Alone Microgrid

Calendar week 38, low RE production:

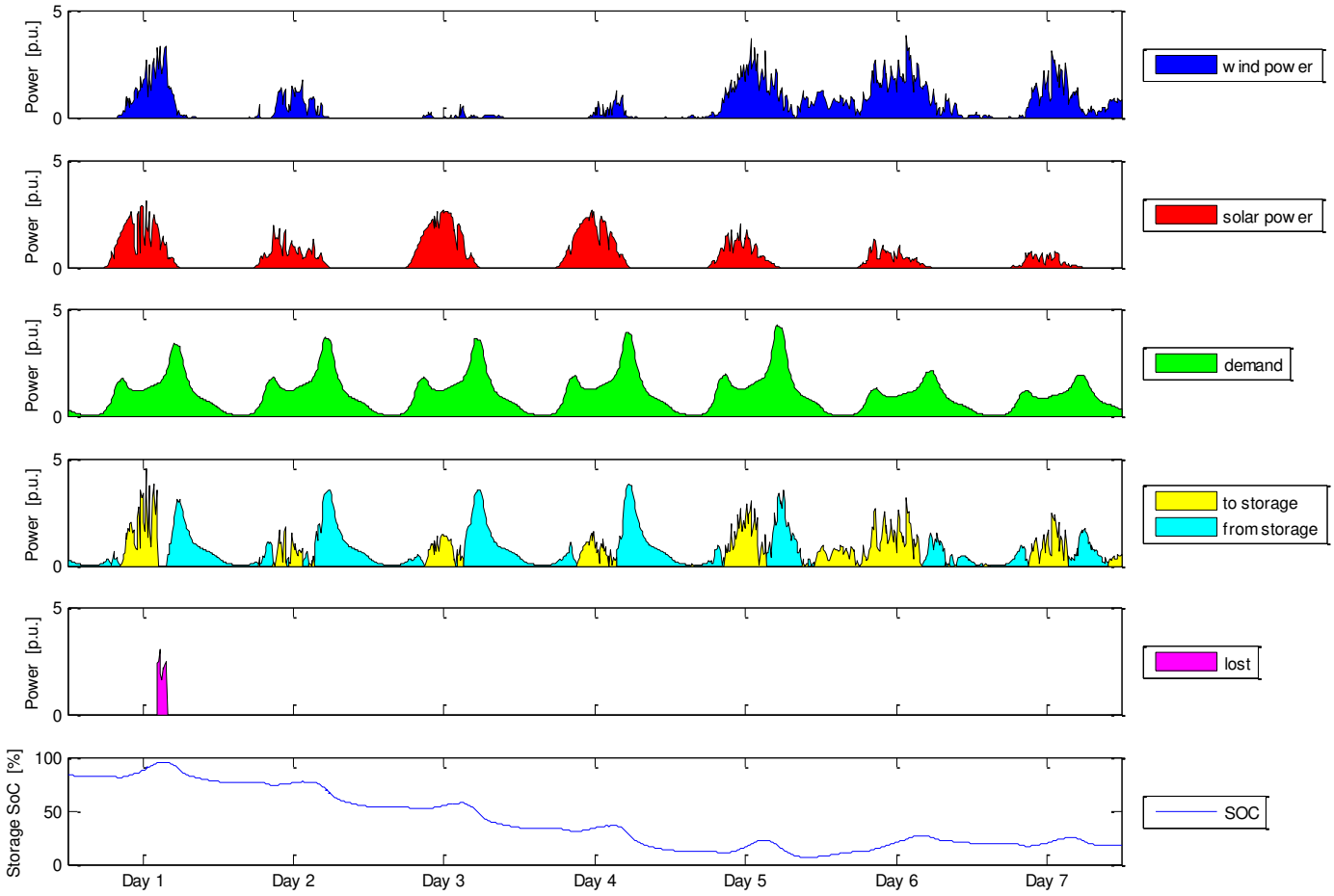

Calendar week 45, high wind power production:

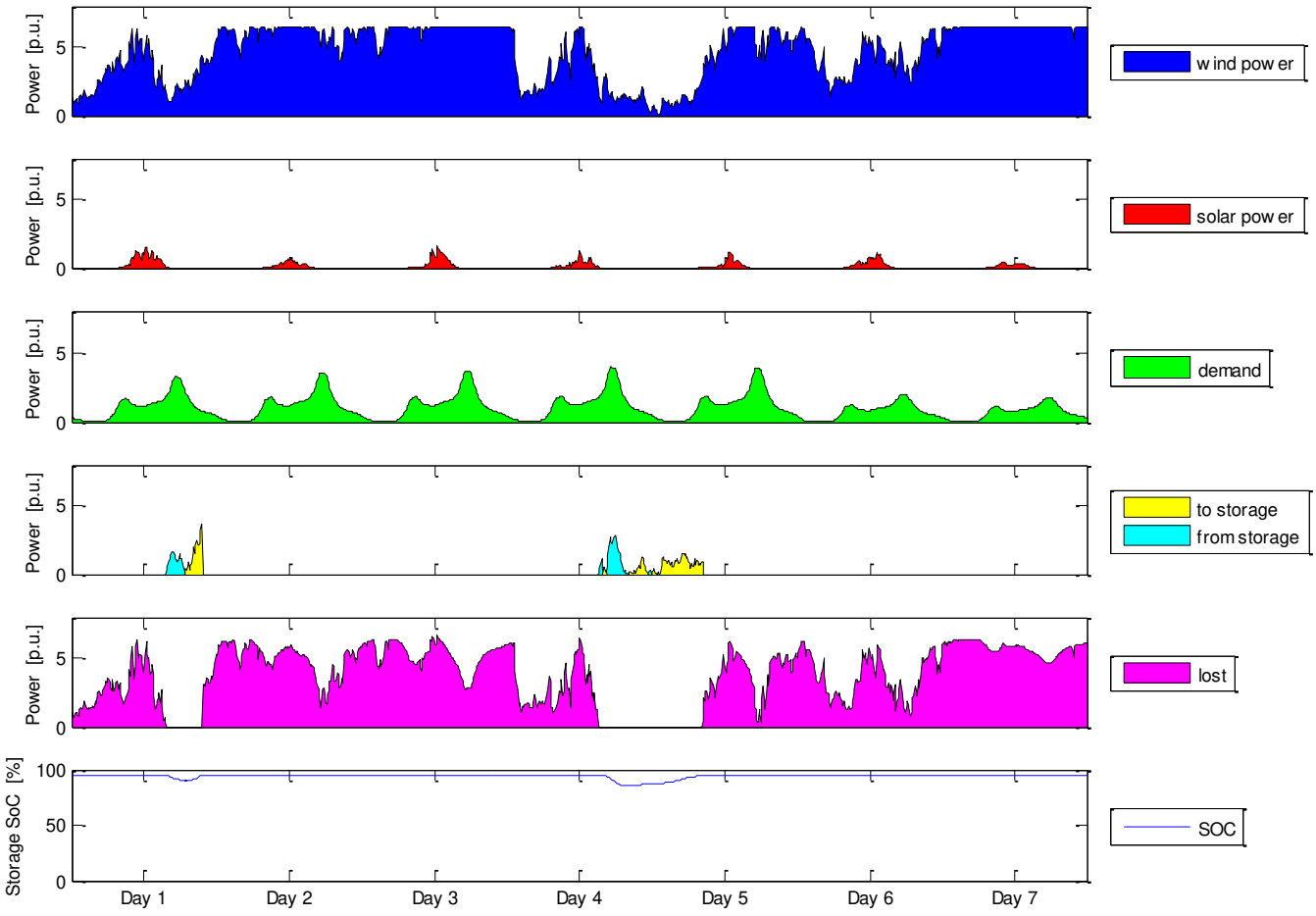

Calendar week 21, high solar power production:

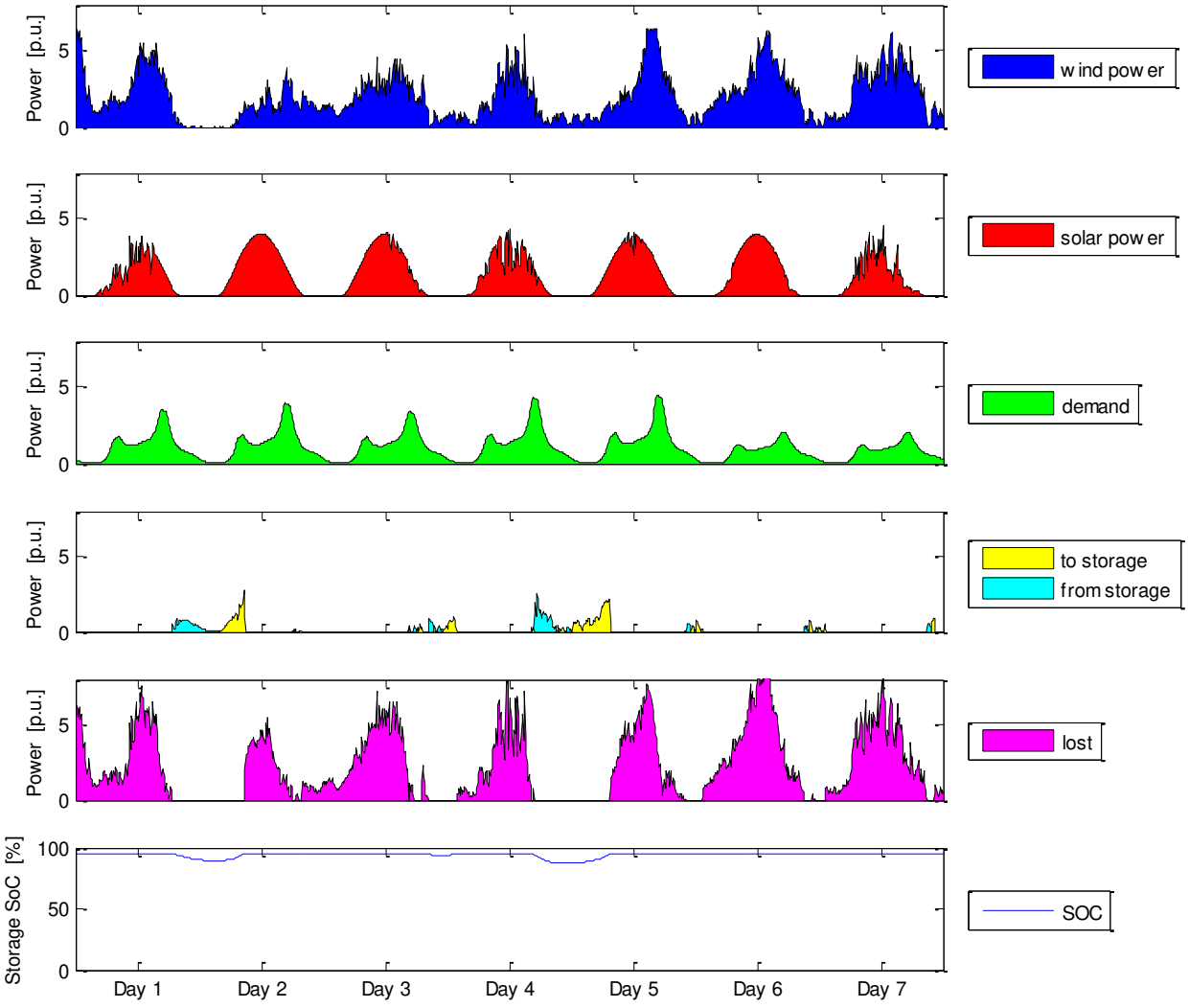

Appendix E

Paper title: Green Energy for On-road Charging of Electric Vehicles

Authors: Theodora-Elli Stamati, Pavol Bauer

Conference: 15th International Conference on Mechatronics – Mechatronika 2012, December 2012, Prague, Czech Republic.